NOVEL THERAPEUTIC AGENTS FOR THE TREATMENT OF HEAD AND NECK SQUAMOUS CELL CARCINOMA:

PRECLINICAL FEASIBILITY AND VETERINARY CLINICAL APPLICATION

A dissertation submitted by

Diane E. Peters

In partial fulfillment of the requirements for the degree of

Doctor of Philosophy

in

Pharmacology and Experimental Therapeutics

TUFTS UNIVERSITY

Sackler School of Graduate Biomedical Sciences

August 2014

Advisor: Thomas H. Bugge, Ph.D.
Faculty Advisor: David J. Greenblatt, M.D.

ABSTRACT

Head and neck squamous cell carcinoma (HNSCC) is a debilitating disease, with more than 630,000 new cases diagnosed worldwide each year. Greater than 60% of these patients are diagnosed at a locally advanced disease-stage where prognosis remains poor despite aggressive multi-modal treatments involving radical surgery, radiation and chemotherapy. Novel therapeutic agents are therefore warranted that will have efficacy in this vulnerable patient population.

My dissertation work has focused on characterizing engineered, tumor-targeted versions of anthrax lethal toxin with potential therapeutic utility in HNSCC. Previously, three separate versions of anthrax protective antigen (PrAg) had been designed, which required activation by the tumor-overexpressed proteases, matrix metalloproteinases (MMPs) and/or urokinase plasminogen activator (uPA). When these engineered PrAg variants were co-administered with various cytotoxins, they were selectively activated within the tumor microenvironment and they exhibited potent anti-tumor activity in multiple preclinical models of cancer. However, simultaneously with reports of dramatic anti-tumor efficacy, toxicities of varying severity had been reported with their use.

To address toxicity concerns and evaluate the feasibility of further developing these engineered anthrax lethal toxins, I performed in-depth toxicological and efficacy profiling. I identified that an engineered variant requiring co-localized activation by both MMPs and uPA, IC-PrAg + LF, was an optimal lead candidate. IC-PrAg + LF exhibited a clear therapeutic window for use in C57BL6/J mice and was highly effective at treating B16-BL6 melanoma syngrafts; at a dose 6-fold below its no observed adverse effect level (NOAEL) a 58% reduction in tumor burden was achieved.

IC-PrAg + LF was then further evaluated for preclinical anti-HNSCC activity using four separate xenografted human HNSCC cell lines. In all cases dramatic reduction in tumor volume was observed. The greatest antitumor response was seen in HN12 xenografts, where 40% of treated mice (6 of 15) had complete tumor regression.

Building upon this finding, IC-PrAg + LF has now been translated to a clinical setting. A Phase 0 veterinary clinical trial has been initiated in cats with spontaneously occurring oral cancer. While this trial is still in progress, initial findings are highly encouraging. The first patient had a measurable, 31%, reduction in tumor volume following receipt of three intratumoral microdose treatments.

Collectively, this dissertation research demonstrates that an engineered variant of anthrax lethal toxin requiring co-localized activation by MMPs and uPA, IC-PrAg + LF, is a promising candidate for further development as an anti-HNSCC agent for both human and veterinary patient populations.

ACKNOWLEDGEMENTS

I am extremely grateful to have had a strong support system guiding me through even the most difficult aspects of graduate school. I am so fortunate to have had Dr. Thomas Bugge as my advisor and mentor. His constant support and encouragement has instilled in me a sense of confidence and independence as a researcher that I truly value.

For their substantial guidance and involvement in my research, I am also very thankful to Dr. Stephen H. Leppla, Dr. Alfredo Molinolo, Dr. Shihui Liu and Dr. Elizabeth McNiel.

I would like to acknowledge my present, and past, committee members, Dr. Philip Hinds, Dr. David Greenblatt, Dr. Martin Beinborn, Dr. Alexei Degterev and Dr. Michael Court, for their inspiring discussions, insightful ideas and ultimately for enabling me to successfully pursue my dissertation research at the National Institutes of Health.

I would like to pay special thanks to my husband, Brian. His understanding and support has made this dissertation possible, and his expert knowledge of Microsoft Word has saved me countless angst while writing. He has stuck by my side through moves, crises and celebrations and I can't imagine this experience without him.

I would like to thank my aunt, Dr. Kristin Coffman-Haddad, for being an inspiration and a role model. She procured my first laboratory position for me, and with her to look up to I have always known what I can accomplish with hard work and curiosity.

Finally, I would like to thank my extracurricular support system, including Lauren, my sister and partner in crime, and Danielle, Natasha, Stine, Morgan, Clint and Michael, great friends who also happen to be great researchers.

TABLE OF CONTENTS

LIST OF TABLES

LIST OF FIGURES

LIST OF ABBREVIATIONS

ALP	alkaline phosphatase
ALT	alanine aminotransferase
AMY	amylase
ANTXR1	anthrax toxin receptor 1, also known as tumor endothelial marker 8, TEM8
ANTXR2	anthrax toxin receptor 2, also known as capillary morphogenesis gene 2, CMG2
AST	aspartate aminotransferase
cAMP	cyclic adenosine monophosphate
CBC	complete blood count
CK	creatine kinase
CT	x-ray computed tomography
DMEM	Dulbecco's Modified Eagle Medium
ED50	effective dose 50
EDTA	ethylenediaminetetraacetic acid
EdTx	anthrax edema toxin; PrAg + EF
EF	anthrax edema factor
EF2	elongation factor 2
FBS	fetal bovine serum
FDA	Food and Drug Administration
FHSA	Foster Hospital for Small Animals at the Tufts University Cummings School of Veterinary Medicine
FP59	a fusion protein composed of the N-terminal binding domain of anthrax lethal factor coupled to the enzymatic domain of *Pseudomonas* exotoxin A
GI	gastrointestinal
GMP	good manufacturing practice
H&E	hematoxylin and eosin
Hct	hematocrit
Hmg	hemoglobin
HNSCC	head and neck squamous cell carcinoma

I.D.	intradermal
I.P.	intraperitoneal
I.T.	intratumoral
I.V.	intravenous
IC50	inhibitory concentration 50
IC-PrAg	dual MMP/uPA activated anthrax protective antigen
IHC	immunohistochemistry
LD	lactate dehydrogenase
LeTx	anthrax lethal toxin; PrAg + LF
LF	anthrax lethal factor
LF-E687A	enzymatically-inactive anthrax lethal factor
LF-HMAGG	a variant of anthrax lethal factor containing two non-native amino acids at its N-terminus (HM)
MAPKK	mitogen activated protein kinase kinase
MCV	mean corpuscular volume
MMPs	matrix metalloproteinases
MTD	maximum tolerated dose
MTD3	maximum tolerated dose, 3 administrations
MTD6	maximum tolerated dose, 6 administrations
MTT	3-(4,5-dimethylthiazol-2-yl)-2,5-diphenyltetrazolium bromide
NIH	National Institutes of Health
NOAEL	no observed adverse effect level
OSCC	oral squamous cell carcinoma
PAI-1	plasminogen activator inhibitor 1
PBS	phosphate buffered saline
PrAg	anthrax protective antigen
PrAg-L1	MMP-activated anthrax protective antigen
PrAg-U2	uPA-activated anthrax protective antigen
PrAg-U7	protease-resistant anthrax protective antigen

pXO1	*B. anthracis* virulence plasmid encoding anthrax toxin proteins
pXO2	*B. anthracis* virulence plasmid encoding capsule proteins
RBC	red blood cell
S.C.	subcutaneous
s.d.	standard deviation
s.e.m.	standard error of the mean
uPA	urokinase plasminogen activator
uPAR	urokinase plasminogen activator receptor
WBC	white blood cell count
WHO	World Health Organization
WT	wildtype

LIST OF ORIGINAL MANUSCRIPTS

This dissertation is based on the following manuscripts:

1. **Peters D.E.**, Hoover B., Grey Cloud L., Liu S., Molinolo A.A., Leppla S.H., and Bugge T.H. Comparative toxicity and efficacy of engineered anthrax lethal toxin variants with broad anti-tumor activities. *In submission*

2. Schafer J.M.*, **Peters D.E.***, Morley T.*, Liu S., Molinolo A.A., Leppla S.H., and Bugge, T.H. (2011). Efficient targeting of head and neck squamous cell carcinoma by systemic administration of a dual uPA and MMP-activated engineered anthrax toxin. *PLoS ONE*, **6**, e20532. **Authors contributed equally*

3. **Peters D.E.,** Vitale Cross L., Liu S., Molinolo A.A., Leppla S.H., Bugge T.H., and McNiel E. Effects of a dual MMP/uPA-activated anthrax toxin in feline oral squamous cell carcinoma *Experiments in progress*

Articles written during, but not directly related to, this dissertation:

1. Szabo R., **Peters D.E.**, Kosa P., Camerer E. and Bugge T.H. Regulation of the feto-maternal barrier by matriptase- and PAR-2-mediated signaling is required for placental morphogenesis and mouse embryonic survival. *In submission*

2. **Peters D.E.**, Szabo R., Friis S., Shylo N.A., Uzzun Sales K., Holmbeck K., and Bugge T.H. The Membrane-Anchored Serine Protease Prostasin (CAP1/PRSS8) Supports Epidermal Development and Postnatal Homeostasis Independent of its Enzymatic Activity. *J Biol Chem*, In Press.

3. Heard K.R., Wu W., Li Y., Zhao P., Woznica I., Lai J.H., Beinborn M., Sanford D.G., Dimare M.T., Chiluwal A.K., **Peters D.E.**, Whicher D, Sudmeier JL, Bachovchin WW. (2013). A general method for making peptide therapeutics resistant to serine protease degradation: application to dipeptidyl peptidase IV substrates. *J Med Chem*, 56(21):8339-51.

4. Madsen D.H., Leonard D., Masedunskas A. Moyer A., Jürgensen H.J., **Peters D.E**, Amornphimoltham P., Selvaraj A., Yamada S.S., Brenner D.A., Burgdorf S., Engelholm L.H., Behrendt N., Holmbeck K., Weigert R., Bugge T.H. (2013). M2-like macrophages are responsible for collagen degradation through a mannose receptor-mediated pathway. *J Cell Biol*, 202(6):951-66.

5. Friis S., Uzzun Sales K., Godiksen S., **Peters D.E.**, Lin C.Y., Vogel L.K., Bugge, T.H. (2013). A matriptase-prostasin reciprocal zymogen activation complex with unique features: prostasin as a non-enzymatic co-factor for matriptase activation. *J Biol Chem*, 288(26):19028-39.

6. **Peters D.E.**, Zhang Y., Molinolo A.A., Miller-Randolph S., Szabo R., Bugge, T.H., Leppla S.H., and Liu S. (2012). Capillary morphogenesis protein-2 is required for mouse parturition by maintaining uterine collagen homeostasis. *BBRC*, 422(3):393-7

NOVEL THERAPEUTIC AGENTS FOR THE TREATMENT OF HEAD AND NECK SQUAMOUS CELL CARCINOMA:

PRECLINICAL FEASIBILITY AND VETERINARY CLINICAL APPLICATION

Chapter 1:
Introduction and Background

1.1 Head and Neck Squamous Cell Carcinoma

Head and neck squamous cell carcinoma (HNSCC) ranks among the top ten cancers worldwide by both incidence and mortality, with over 630,000 new cases diagnosed annually and an estimated 350,000 deaths occurring each year (1, 2). In the United States alone, an estimated 42,440 cases of HNSCC will be diagnosed in 2014, accounting for 2.5% of all cancer diagnoses (3).

HNSCCs arise from the mucosal epithelium lining the upper aerodigestive tract. They occur most commonly in the oral cavity, larynx and pharynx, as depicted in Figure 1.1, where they account for the majority of malignant neoplasias arising in these anatomical locations (4, 5).

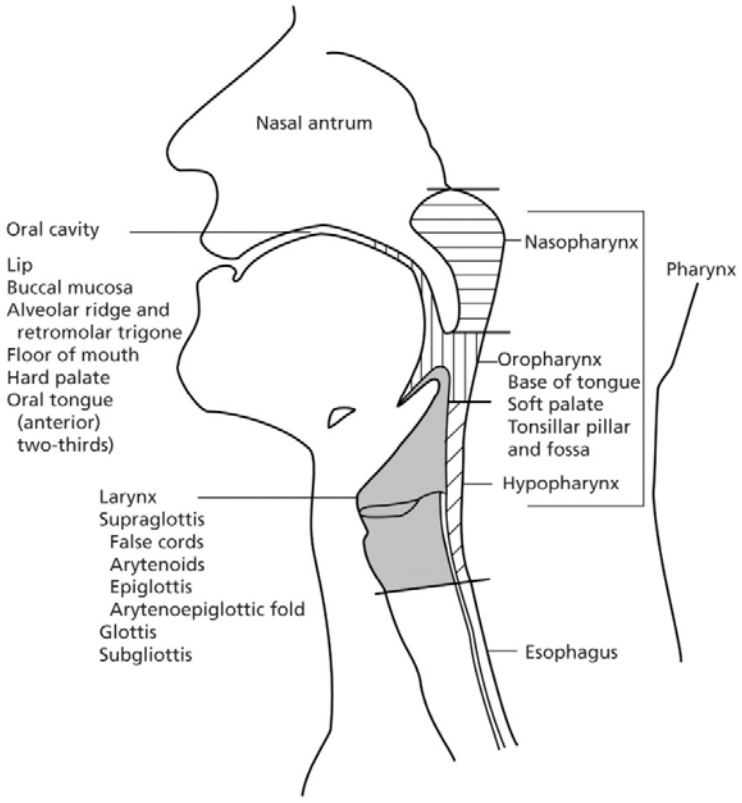

Figure 1.1: Anatomic sites and subsites of head and neck squamous cell carcinoma. The approximate distribution of head and neck cancer is: oral cavity, 44%; larynx, 31%; and pharynx, 25% (5). (Reprinted with permission from CMP Healthcare Media. Source: Cancer Management: A Multidisciplinary Approach. 9th Edition. Copyright 2005.)

Despite significant advances in understanding the molecular mechanisms underlying HNSCC development, the five year survival rate for newly diagnosed patients has improved only marginally in the past 3 decades, increasing from 54% in 1976 to 65% in 2009 (6, 7).

Treatment recommendations for HNSCC are complex and vary based upon the stage at which the disease is first diagnosed as well as the subsite localization of the primary tumor (8, 9). In the United States, 30-40% of all HNSCC diagnoses are made at an early disease-stage where cure, defined as 5-year recurrence-free survival, is highly probable (7-9). The remaining 2/3 of cases, however, are diagnosed at more advanced stages where prognosis remains poor (5-year survival rate < 50%) (10).

Early-stage HNSCCs are routinely, and successfully, treated with single modality therapy consisting of either surgical resection or radiation (8, 9). While cure rates for these two approaches are similar (9), the treatment-associated morbidities differ and often guide treatment selection. Tumors within the oral cavity are most frequently surgically excised, while radiation is often the treatment of choice for laryngeal and pharyngeal tumors due to its organ sparing benefits and the hypothesis that structural organ preservation leads to improved functional outcomes (9, 10). It is important to note, however, that while surgery and radiation can both effectively treat early-stage HNSCCs, treatment-associated morbidities can have a profound negative impact on patient quality of life post-treatment (11, 12). Surgical resection can impair basic physiological processes such as chewing, swallowing and speech, and can also cause substantial disfigurement. Radiotherapy is also associated with serious long-term side effects, consequent to damage of bystander tissues, such as the salivary glands (13), taste buds (14) and/or thyroid gland (15).

Xerostomia, a debilitating dry mouth condition resulting from impaired saliva production, is a particularly frequent complication of radiotherapy, which may be permanent in greater than 30% of patients, and which affects swallowing, nutritional balance, general oral health and overall quality of life (16-18).

For the 60% of patients who are diagnosed at an advanced disease stage, cure is unlikely. Nevertheless, aggressive multi-modal therapies involving surgery, radiation and/or chemotherapy are often utilized palliatively to reduce tumor burden, since locoregional tumor growth is the primary cause of death in these patients (19, 20). Concurrent administration of chemotherapeutic agents, most often high dose cisplatin, in combination with radiation has become standard of care for treatment of inoperable locoregionally advanced HNSCCs (21, 22). A recent meta-analysis comparing 93 trials (17,346 total patients) found that chemoradiotherapy increased 5-year survival by 6.5% relative to radiotherapy alone; an absolute increase from 27.2% to 33.7% 5-year survival (23). While significant, the benefit associated with chemoradiotherapy is tempered by the fact that it is associated with far greater toxicity than either of its component monotherapies (22, 24).

Another pharmacologic intervention that has been highly studied in recent years for the treatment of locoregionally advanced HNSCC is cetuximab: a monoclonal antibody targeting the epidermal growth factor receptor (EGFR) (25). Researchers were optimistic that this targeted therapy would be effective in managing HNSCC for multiple reasons. First, elevated EGFR expression is present in greater than 90% of HNSCC biopsies (26), and this overexpression is correlated with inferior survival, resistance to radiotherapy and locoregional control failure (26-30). Furthermore, there was strong preclinical evidence

demonstrating that cetuximab could both produce an antitumor effect when administered alone, as well as increase the efficacy of both ionizing radiation and cisplatin when used in combination in murine models of human HNSCC (31, 32). Initial clinical results for cetuximab were encouraging, demonstrating that addition of cetuximab to radiotherapy protocols could improve median patient survival from 14.9 to 24.4 months (29, 33). However, recent prospective trials directly comparing cetuximab-based bioradiotherapy versus the standard of care, cisplatin chemoradiotherapy, have indentified that the cisplatin-based regimens are significantly better in terms of locoregional control and progression-free survival (34, 35). Overall survival is similar between the two treatments at 1.5-2 year follow-up timepoints, although there is a trend towards cisplatin superiority (34, 35). Surprisingly, although cetuximab was anticipated to have an enhanced toxicity profile due to its targeted mechanism of action, the incidence of severe toxicities was the same in the two treatment groups (34, 35). This parallels the findings of multiple retrospective analyses, where cetuximab-based bioradiotherapy has been reported to be more toxic than case-controlled cisplatin-chemoradiotherapy (36-38). Thus, despite initial promise, cetuximab shows no benefit relative to current standard-of-care in terms of efficacy or toxicity.

The need to develop novel therapeutic agents for the treatment of HNSCC is evident. Ideally, these agents would not only exhibit efficacy in late-stage disease where current treatment strategies are toxic and ineffective, but they would also exhibit efficacy in early stage disease, where cure may be achieved with fewer treatment-associated morbidities. To this end, we are particularly interested in assessing the suitability of using engineered, tumor-targeted, versions of anthrax lethal toxin to address this unmet clinical need.

1.2 *Bacillus anthracis*

Bacillus anthracis, the causative agent of anthrax, is a gram-positive, spore-forming bacterium. *B. anthracis* spores are a common contaminant of soil, where they can persist for decades exhibiting high resistance to environmental insults, including pH and temperature extremes or desiccation, as well as to man-made decontamination techniques, including chemical disinfection (39-41). Due to the prevalence of *B. anthracis* spores in soil, naturally-occurring anthrax infections are most commonly seen in ruminants and other herbivores, who ingest spores while grazing (42). Once ingested, the spores germinate and the bacteria reenter a vegetative state; they then proliferate and secrete virulence factors ultimately killing their host, leading to further dissemination of spores as depicted in Figure 1.2 (42, 43).

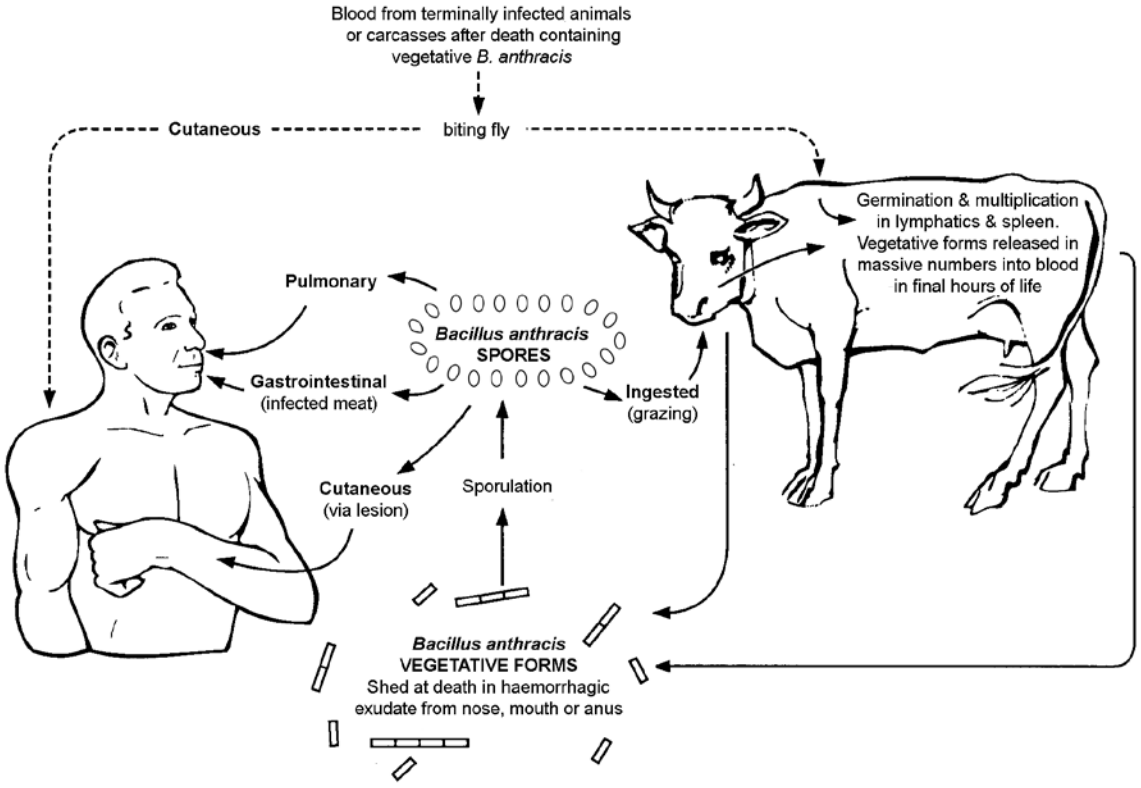

Figure 1.2 Natural life-cycle of *Bacillus anthracis.* Adapted with permission from the publisher. Source: WHO Guidelines for the Surveillance and Control of Anthrax in Humans and Animals Copyright 1998 (43).)

1.2.1 Anthrax Infection in Humans

Cutaneous anthrax infection is the most common disease manifestation in humans (42, 44). It occurs most commonly in persons working with animals or animal products, where it is caused by incidental inoculation of an open wound with spores found on contaminated animal hides, wool, hair etc (42). Isolated cases of cutaneous transmission through insect bites have also been reported (45, 46). Cutaneous anthrax is readily treated with a single course of oral antibiotics, and either doxycycline or ciprofloxacin are recommended as first line agents (47). With treatment, survival exceeds 99%; however, even without treatment cutaneous anthrax is often self-limiting with survival greater than 80% (47).

Humans can also acquire anthrax infection through gastrointestinal exposure, a route which is most often associated with ingestion of contaminated meat (48). In the US, this is an exceedingly rare occurrence, due to strict livestock vaccination and importation protocols, paired with a vigilant meat inspection process (49). In fact, only three documented cases exist in US history. These occurred in Massachusetts in 1942 (a worker in a brush factory was infected after handling contaminated, imported, animal hair (50)), Minnesota in 2000 (a family ingested contaminated cattle meat originating from their own personal farm (49)), and New Hampshire in 2009 (a drumming circle participant was infected following drumming on contaminated animal hide drums nearby a food preparation area (51)). With systemic antibiotic treatment, survival rates for gastrointestinal anthrax infection exceed 60% (48).

The most deadly form of anthrax infection is inhalation anthrax. This disease is $\geq$ 50% lethal when managed optimally (early diagnosis, combinatorial antibiotic regimens, and

aggressive management of disease-associated morbidities) and is > 90% lethal when untreated (47, 48, 52). Inhalation anthrax can occur naturally in persons working in high risk areas, such as wool mills, slaughterhouses or tanneries, leading to a colloquial name "Woolsorter's Disease" (53). General concern regarding inhalation anthrax stems from the potential weaponization of anthrax spores (54). Following the notorious anthrax letters of 2001, which led to 11 cases of inhalation anthrax and 5 deaths, public awareness of this threat of anthrax bioterrorism has heightened (54).

In recent years, a novel route of acquiring anthrax has emerged: injectional anthrax. Injectional anthrax occurs secondarily to intravenous drug use, and is specifically associated with contaminated heroin (55, 56). The first case was reported Norway in the year 2000 (57), and since this time fatal disease outbreaks have been confirmed in multiple northern European countries including Scotland (58), Wales (59), England (59), Denmark (60), Germany (61, 62) and France (56). The largest number of cases have been documented in Scotland, where between December 2009 and December 2010, 47 cases were confirmed, which led to 19 deaths (55, 58). The source of the contaminated heroin was traced to either Pakistan or Afghanistan, both countries in which anthrax is endemic (58, 63), and it has been further proposed that contaminated goat hides used during trafficking, led to contamination of the heroin with the anthrax spores (58).

1.2.2 Anthrax Virulence Factors

The pathogenicity of *Bacillus anthracis* is a consequence of its intrinsic virulence factors, which enable the bacterium to evade immune detection, disseminate, and to intoxicate host cells (64). These virulence factors are encoded by two distinct plasmids, pXO1 and

pXO2, and absence of either plasmid can attenuate the lethality observed in murine models of anthrax (65, 66).

pXO2 encodes the genes required for synthesis of a poly-D-glutamic acid capsule; this capsule protects the bacterium from phagocytosis by host neutrophils and macrophages (67).

pXO1 encodes three separate anthrax toxin proteins: protective antigen (PrAg), lethal factor (LF) and edema factor (EF) (68). These proteins interact to form two distinct AB-type exotoxins, which is described in greater detail in Section 1.2.3. The combination of PrAg + LF is commonly referred to as anthrax lethal toxin (LeTx), while PrAg + EF is known as anthrax edema toxin (EdTx). LeTx and EdTx contribute to bacterial dissemination during infection, and cause many of the pathologies associated with systemic and local anthrax disease (64, 69).

1.2.3 Anthrax Toxin: Mechanism of Action

As illustrated in Figure 1.3, in order to intoxicate host cells, protective antigen (PrAg) first binds to one of two ubiquitously expressed cell-surface receptors: ANTXR1 (also known as tumor endothelial marker 8, TEM8) (70) or ANTXR2 (or capillary morphogenesis gene 2, CMG2) (71). [ANTXR2 has recently been identified as the primary receptor contributing to anthrax toxin-induced lethality *in vivo*, as genetic deletion of *Antxr2* protects mice from challenge with lethal doses of both purified LeTx and anthrax spores, while *Antxr1* null mice remained sensitive to toxicity (72).]

Following receptor binding, PrAg (83 kDa) is cleaved by cell-surface furin, or furin-like pro-protein convertases, releasing a 20 kDa fragment, and generating an activated PrAg

monomer (63 kDa) that remains receptor-bound (73). The activated PrAg monomers self-assemble forming heptamer (74), or octamer (75), complexes.

LF and EF competitively bind to the PrAg complexes though a common N-terminal binding domain (76, 77). Each PrAg heptamer can bind up to 3 LF/EF molecules (78, 79), while each octamer can bind up to 4 molecules (75). The toxin complexes are then internalized via clathrin-dependent endocytosis (80). Acidification of the endosome triggers a conformational rearrangement causing the PrAg oligomer to insert into the membrane forming a pore (81-83). LF and/or EF are then translocated to the cytoplasm where they exert their biologic effects (84, 85).

LF is a zinc-containing metalloprotease that cleaves the amino-terminal residues of mitogen activated protein kinase kinases (MAPKK), interfering with the MAPK signaling pathway, resulting in direct cytotoxicity to cells that are reliant upon this pathway for survival (86-89). EF is a calcium- and calmodulin-dependent adenylate cyclase that catalyzes excess cAMP production by host cells (90). EF is associated with reduced macrophage phagocytosis of anthrax spores *in vitro*, and it is hypothesized that this may be one role of EdTx *in vivo* (91).

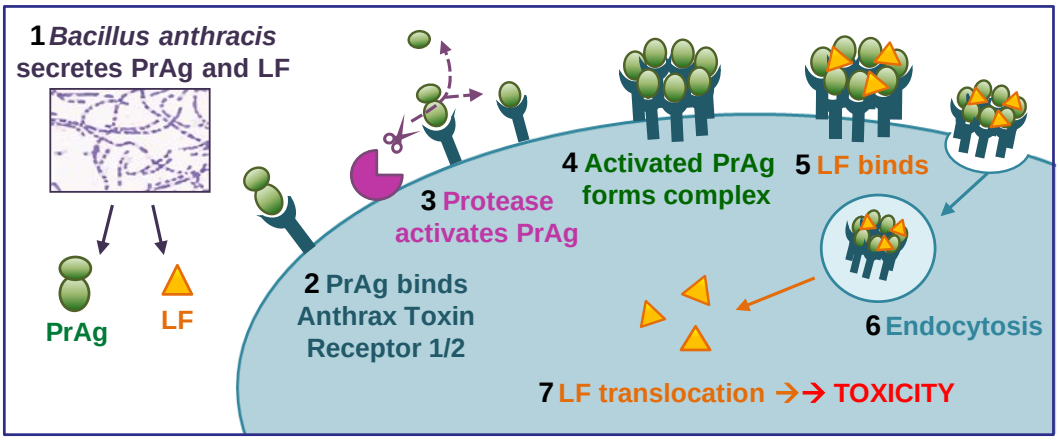

Figure 1.3 Mechanism of anthrax lethal toxin cellular internalization.

1.3 Tumor-Targeted Anthrax Toxins

As outlined above, before cellular intoxication can occur, anthrax PrAg must first be proteolytically activated at the cell surface. This affords the unique ability to re-direct the toxicity of this system by altering the enzymatic specificity of this activation step (92). This approach has been employed to generate engineered versions of PrAg that require activation by tumor-overexpressed proteases, and this process is elaborated upon in Sections 1.5, 1.6 and 1.7.

1.4 Summary of Cytotoxins

The tumor-targeted PrAg variants are non-toxic entities that serve as receptors for cytotoxin transport. As such, they are always co-administered with a cytotoxin. In this dissertation research three unique cytotoxins are utilized:

LF: wildtype anthrax lethal factor (86-89).

LF-HMAGG: a variant of anthrax lethal factor containing two additional non-native amino acids, HM, at its N-terminus (93). These residues were inadvertently added during cloning manipulation in the recombinant shuttle vector pSJ115 (93). This expression system is used by a commercial vendor, and therefore LF-HMAGG has likely been used in place of LF in many published studies (93). LF-HMAGG is 3-fold less potent than LF *in vitro* (93) and exhibits less toxicity *in vivo* (unpublished observations).

FP59: a fusion protein containing the N-terminal PrAg-binding domain of LF, coupled to the catalytic domain of *Pseudomonas aeruginosa* exotoxin A (77, 94). Similar to diphtheria toxin, *Pseudomonas aeruginosa* exotoxin A ADP-ribosylates a diphthamide residue on elongation factor-2 (EF2), leading to inhibition of protein synthesis and cell

death (95). This is an exquisitely potent cytotoxin, and it is estimated that a single molecule entering the cytoplasm is sufficient to cause cell death (96, 97).

1.5 MMP-activated Anthrax Protective Antigen: PrAg-L1

In 2000, Liu et al. generated an engineered version of anthrax PrAg which required activation by matrix-metalloproteinases (MMPs), rather than by furin (98). MMPs are a family of multi-domain, zinc-containing, endopeptidases which function to cleave extracellular matrix proteins, contributing to tissue remodeling and repair in normal physiologic settings, and promoting invasion and metastasis in cancerous tissues (99, 100). Accordingly, MMPs are ubiquitously overexpressed in the tumor microenvironment, where their level of expression is generally correlated with the stage of tumor progression (99).

The engineered MMP-activated protective antigen, PrAg-L1, was made by replacing the furin cleavage sequence of wildtype PrAg, RKKR, with an MMP-preferred sequence, GPLGMLSQ (98). This replacement sequence was selected from previously published screens, in which a library containing 60 synthetic oligopeptides, patterned after naturally-occurring collagenase cleavage sites, was used to assess the cleavage preferences of various MMPs (101, 102). GPLGMLSQ is a sequence optimized for cleavage by MMP-2 and MMP-9, two MMPs that are frequently associated with increased cancer invasiveness (99, 100). This sequence is also cleaved by other MMPs, including the tumor-surface associated MMP, MMP-14 (MT1-MMP) (103).

1.5.1 PrAg-L1: Verification of Selective Activation

To assess activation selectivity, PrAg-L1 was first incubated with purified, soluble furin or active forms of MMP-2 or MMP-9, followed by Western blot analysis to detect full-

length and cleaved forms. PrAg-L1 was rapidly cleaved by both MMP-2 and MMP-9, while no furin cleavage was observed, even with extended incubation (98).

Following demonstration that PrAg-L1 could be selectively cleaved by purified MMP-2 or MMP-9, cell-based cytotoxicity assays were performed to assess the specificity of PrAg-L1 activation in a more complex system. Tumor cell lines expressing various MMPs, as indicated, as well as a normal cell line with limited MMP expression, were incubated with PrAg-L1 + FP59 (98). A2058 melanoma (+MMP-2), HT1080 fibrosarcoma (+MMP-2,+MMP-9) and MDA-MB-231 breast cancer (+MMP-9) cells were found to be sensitive to PrAg-L1 + FP59 toxicity, while the non-tumor primate kidney cell line, Vero (-MMP) was resistant, confirming MMP-dependent activation of PrAg-L1 (98).

Interestingly, when MMP-expressing and non-expressing cells were co-cultured and exposed to PrAg-L1 + FP59, cytotoxicity was only observed in the MMP-expressing cells (98). This indicated that PrAg-L1 was not cleaved by secreted MMPs, and instead was cleaved at the cell-surface following receptor binding. If this specificity were to persist *in vivo* selective cytotoxicity to cells exhibiting cell-surface MMP-activity would be expected (98).

The *in vitro* selectivity of PrAg-L1 activation was further confirmed through the use of cytotoxicity assays performed in the presence of multiple MMP inhibitors, including the small molecule inhibitors, BB-94 (Batimastat), BB-2516 (Marimastat) and GM6001 (Galardin), as well as TIMP2, a physiologic MMP inhibitor. In all cases, MMP-inhibition dramatically reduced PrAg-L1 + FP59 toxicity (98).

The MMP-specific activation of PrAg-L1 has also been independently verified by another group. In 2008, Alfano et al. tested 25 melanoma cell lines for their sensitivity to PrAg-L1 + LF in cell culture, and reported that levels of cell-surface associated MMP-2 and MMP-9, as measured by gelatin zymography, were significantly correlated with cell sensitivity to PrAg-L1 + LF toxicity (104).

1.5.2 PrAg-L1: *in vivo* Toxicity

PrAg-L1 was found to be much better tolerated than wildtype PrAg when 6 intraperitoneal (I.P.) doses were administered to C57BL/6J mice, in combination with LF-HMAGG (105). To illustrate this, a dose of 15 µg PrAg-WT + 5 µg LF-HMAGG was found to be 100% lethal, while mice receiving a protein equivalent dose of the MMP-activated toxin (15 µg PrAg-L1 + 5 µg LF-HMAGG) exhibited normal survival (105).

The highest concentration of toxin tested was 45 µg PrAg-L1 + 15 µg LF-HMAGG, and complete necropsies performed following the 6^{th} administration, which included gross and histopathological analyses, did not identify any abnormalities (105).

While all C57BL/6J and BALB/c mice treated with 6 I.P. doses of 45 µg PrAg-L1 + 15 µg LF-HMAGG survived, 30% of nude mice treated at this same concentration died, indicating that there may be strain-dependent differences in toxin sensitivity (105) .

1.5.3 PrAg-L1: *in vivo* Efficacy

C32 melanoma, HT144 melanoma, A549 lung carcinoma, and Colo205 colon carcinoma xenografts all exhibited significant reduction in tumor volume when treated with 6 I.P. doses of PrAg-L1 + LF-HMAGG (105), while LL3 Lewis lung carcinoma and B16-BL6 melanoma syngrafts were efficiently treated with 5 I.P. doses (105).

Immunohistochemistry was performed on toxin-treated A549 lung carcinoma tumors, in comparison to PBS-treated controls, and PrAg-L1 + LF-HMAGG's antitumor effect was attributed to increased necrosis, reduced proliferation and reduced tumor vessel density (105). The anti-vasculature effect was of particular interest, and was further studied using a directed *in vivo* angiogenesis assay in which nude mice were implanted with "angioreactors" and blood vessel infiltration was measured (105, 106). Treatment with 6 I.P. doses of PrAg-L1 + LF-HMAGG significantly decreased *in vivo* angiogenesis in this assay, suggesting that this toxin may exert direct toxicity towards proliferating vascular endothelial cells (105).

In 2010, Alfano et al. further tested the antitumor efficacy of PrAg-L1 + LF-HMAGG using orthotopic models of human anaplastic thyroid carcinoma, generated from DRO and BHT-101 cell lines (107). 6 I.P. injections of PrAg-L1 + LF-HMAGG led to significant increases in survival in tumor-bearing mice treated at an early disease-stage, and was associated with dramatic reduction in tumor burden in specimens collected 7-days after the final administration, with 50-fold reduction in tumor mass observed in DRO-tumors and 77-fold reduction in BHT-101 tumors (107). Established, late-stage tumors also responded to PrAg-L1 + LF-HMAGG treatment. Established tumors were treated with 1, 2 or 4 I.P. doses of toxin. 18-hours after a single dose approximately half of the tumor area was necrotic for both DRO and BHT-101 tumors, and this increased to 100% necrosis with either 2 or 4 administrations (107).

1.6 uPA-activated Anthrax Protective Antigen: PrAg-U2

Shortly after generating the MMP-activated PrAg-L1, Liu et al. designed and characterized another version of anthrax protective antigen, which required activation by

the tumor-over expressed protease, urokinase plasminogen activator (uPA). This uPA-activated version was designated PrAg-U2 (108).

uPA is a serine protease, with enzymatic activity that is restricted to the cell surface. It is initially secreted as an inactive zymogen (pro-uPA) which binds to the urokinase plasminogen activator receptor (uPAR), where it is then cleaved enabling its proteolytic activity (109, 110). uPA's native substrate is plasminogen, and the proteolytic conversion of plasminogen to plasmin contributes to multiple biologic processes including fibrinolysis, thrombolysis, extracellular matrix degradation and tissue remodeling (109, 110). In physiologic settings, the activity of uPA is tightly regulated by its cognate inhibitor, plasminogen activator inhibitor-1, PAI-1 (109, 110). Elevated expression of uPA is a characteristic feature of many diverse cancers including carcinomas, sarcomas, melanomas, and leukemias (109-111). Often the level of uPA expression is correlated to the degree of malignancy, and it is believed that aberrant cleavage of plasminogen results in tissue degradation that may facilitate tumor invasion and metastasis (109, 110).

To require selective activation by uPA, the native furin-cleavage sequence of wildtype PrAg, RKKR, was replaced with the uPA-preferred sequence PGSGRSA (108). This cleavage sequence was selected from a previously published study in which a substrate phage display library was used to identify sequences cleaved with high efficiency and selectivity by either uPA, or the closely related protease, tissue plasminogen activator (tPA) (112, 113). SGRSA was identified as a minimum optimized substrate for uPA. This sequence was efficiently cleaved by uPA; with a K_{cat}/K_m that was 1363-fold higher than that for its physiologic target sequence (113). Additionally, this sequence was preferentially cleaved by uPA, with a uPA:tPA selectivity ratio of 20 (113).

1.6.1 PrAg-U2: Verification of Selective Activation

PrAg-U2 was incubated with soluble furin, uPA or tPA followed by Western blot analysis at multiple time points to assess cleavage rate. PrAg-U2 was rapidly cleaved by uPA, minimally cleaved by tPA, and no furin cleavage was observed (108).

Next cell lines expressing or lacking the urokinase plasminogen receptor (uPAR), as indicated, were incubated with PrAg-U2 + FP59 in the presence of exogenous pro-uPA. HeLa cervical adenocarcinoma (+uPAR) and A2058 melanoma (+uPAR) cells were able to bind and process PrAg-U2, which was demonstrated both directly, via Western blot analysis, as well as indirectly, through cytotoxicity assays (108). The non-tumor, embryonic kidney HEK293 (-uPAR) cell line was resistant to PrAg-U2 + FP59 (108). These results demonstrated that uPAR was required for PrAg-U2 activation in a cell culture setting.

The stringency of PrAg-U2 activation in cell culture was further explored using the toxin-sensitive HeLa cells. It was determined that HeLa cell-sensitivity to PrAg-U2 + FP59 was dependent upon the concentration of pro-uPA added, and that it could be completely blocked by addition of the physiologic uPA inhibitor, PAI-1 (108). PrAg-U2 + FP59 cytotoxicity could also be inhibited in a dose-dependent manner through addition of uPAR blocking inhibitors including: ATF (the amino-terminal receptor binding fragment of uPA) or R3 (a monoclonal antibody that specifically blocks uPA/uPAR interaction) (108).

Further *in vitro* evidence of uPA/uPAR-dependent activation of PrAg-U2 was provided by Abi-Habib and colleagues in 2006 (114). They assessed the sensitivity of 39 different cancer cell lines, and 5 normal cell lines, to PrAg-U2 + FP59 in culture, and

demonstrated that levels of uPAR and uPA were directly correlated to toxin sensitivity (114). They further identified minimum thresholds for toxin sensitivity, reporting that greater than 200 uPAR receptors/cell were required, and that the concentration of uPA in the supernatant must exceed 1 ng/mL (114).

Strong evidence for uPA-selective activation of PrAg-U2 *in vivo* was provided through the use of genetic models (115, 116). When $uPA^{-/-}$ and $uPAR^{-/-}$ mice were challenged with a dose of PrAg-U2 + FP59 that was 5X the LD100 for wildtype mice all of the transgenic mice survived, demonstrating that PrAg-U2 was not activated in these mice (115, 116). Conversely, PAI-$1^{-/-}$ mice, which lack the primary inhibitor of uPA, exhibited increased sensitivity to the toxin (115, 116).

1.6.2 PrAg-U2: *in vivo* Toxicity

PrAg-U2 was much better tolerated than PrAg-WT when administered systemically to mice in combination with FP59. Specifically, the MTD for a single intraperitoneal (I.P.) administration of PrAg-U2 + FP59 was found to be 15-fold higher than that of PrAg-WT + FP59 (115). Furthermore, at this MTD no gross or histological signs of toxicity were present (115). With increasing concentrations, single dose PrAg-U2 + FP59 treatment caused toxicity in the bone marrow, osteoblasts, adrenal cortex and T-cell regions of the spleen and lymph nodes (115). Additionally, in PAI-$1^{-/-}$ mice, along with the aforementioned toxicities, edema of the small intestines with or without hemorrhage was also observed (115).

Severe dose-limiting toxicities, and extreme mortality, have been documented with multiple I.P. administrations of PrAg-U2 + FP59 (117, 118).

Su et al., reported that 2 I.P. doses of 7.2 µg PrAg-U2 + 1.2 µg FP59 killed greater than 80% of treated mice, and caused moribundity in all surviving animals (117). Necropsies performed on both dead and terminally-ill mice, demonstrated presence of severe damage to the lung, kidney, liver and heart, although this histological analysis must be interpreted cautiously as it does not discriminate between ante- and post-mortem changes (117). Co-administration of the anti-inflammatory glucocorticoid, dexamethasone, was found to be protective, permitting 100% survival even with 8 I.P. administrations of 7.2 µg PrAg-U2 + 1.2 µg FP59 (117).

Similarly, Rønø et al. found the combination of PrAg-U2 + FP59 to be highly toxic in mice with multiple I.P. administrations, reporting significant mortality at all doses tested (118). Gross inspection of mice treated with the highest doses, identified reduction in body weight, ulcerations of the anal region and pronounced dilation of the small intestine (118). Histological examination uncovered inflammation and necrosis of small intestinal villi; however, contrary to the aforementioned studies, no pathologies were identified in the lung, kidney, liver, heart or spleen (118). Co-administration of dexamethasone was found to attenuate the GI toxicity and to improve survival, and it was in fact required in order to administer effective doses of the toxin without substantial lethality (118).

1.6.3 PrAg-U2: *in vivo* Efficacy

Either one or two local administrations of PrAg-U2 + FP59 resulted in significant antitumor effects in T241 fibrosarcoma, B16-BL6 melanoma and LL3 Lewis lung carcinoma syngrafts (115). A single toxin dose resulted in 92%, 85% and 65% tumor volume reduction, respectively, at the study endpoint, and this was further enhanced by administration of a second dose, which resulted in 98%, 92% and 86% reduction (115).

This local treatment was associated with significant peritumoral edema and leukocyte infiltration (115). The authors speculate that this may have been a consequence of rapid, and extensive, necrotic tumor cell death, as intradermal toxin injections in non-tumor bearing mice had minimal adverse effect (115).

Systemic administration of PrAg-U2 + FP59 required the co-administration of dexamethasone to achieve efficacy without significant mortality (117, 118); however, this combination was reported to be highly efficacious.

Four I.P. administrations of PrAg-U2 + FP59 + dexamethasone were used to treat H1299 non-squamous lung carcinoma xenografts (117). These tumors were very sensitive to toxin treatment, and 30% of all treated mice had complete remission confirmed by both gross and histological examination (117). Furthermore, mice bearing established, end-stage, H1299 xenografts were treated with two I.P. administrations of PrAg-U2 + FP59 + dexamethasone (117). These large tumors also responded dramatically to treatment, with 56% tumor reduction after the first dose, and 78% reduction following the second dose (117). This antitumor effect was characterized by massive necrosis, reduced cellular proliferation and increased apoptosis; no changes in vessel density were observed (117).

Three I.P. administrations of PrAg-U2 + FP59 or PrAg-U2 + FP59 + dexamethasone were used to treat B16-BL6 melanoma syngrafts (118). Similar antitumor efficacy was observed in these two cohorts with ~80% tumor reduction at the trial endpoint. However, mortality was dramatically different: 5 of 8 (63%) PrAg-U2 + FP59 treated mice died during the trial, while only 1 of 9 (11%) PrAg-U2 + FP59 + dexamethasone treated mice died (117). Antitumor efficacy was also demonstrated with PrAg-U2 + FP59 in LL3 lung

carcinoma and T241 fibrosarcomas, with reported lethalities of 33% and 50%, respectively (117).

1.7 Dual MMP/uPA-activated Anthrax Protective Antigen: IC-PrAg

While both MMP-activated PrAg-L1 and uPA-activated PrAg-U2 exhibit substantially reduced toxicity relative to wildtype PrAg when administered *in vivo* (105, 115), it was further hypothesized that conferring the additional requirement for co-localized activation by both MMPs and uPA, might further reduce toxicity and add additional tumor-selectivity to this system.

In order to require dual-proteolytic activation, another mechanistic feature of the anthrax toxin cellular internalization pathway was considered and modified; specifically the formation of functional lethal factor (LF) and edema factor (EF) binding sites. As described in Section 1.2.3, following proteolytic-cleavage, PrAg monomers form oligomeric complexes containing binding sites for LF and EF (119, 120). LF, or EF, binding requires interaction with three distinct binding subsites that span adjacent PrAg monomers as illustrated in Figure 1.4A (119-121). A single binding site involves subsite I (Arg178) and subsite III (Ile207, Ile210 and Lys214) of one PrAg monomer, and subsite II (Lys197 and Arg200) of a neighboring PrAg monomer (119, 120).

Bearing this in mind, engineered versions of PrAg were generated that not only required activation by tumor-overexpressed proteases, but that also included point mutations in their LF-binding subsites. Specifically, PrAg-L1-I210A required activation by MMPs, and also contained a mutation in LF-binding subsite III (I210A), while PrAg-U2-R200A required cleavage by uPA and harbored a mutation in LF-binding subsite II (R200A) (121).

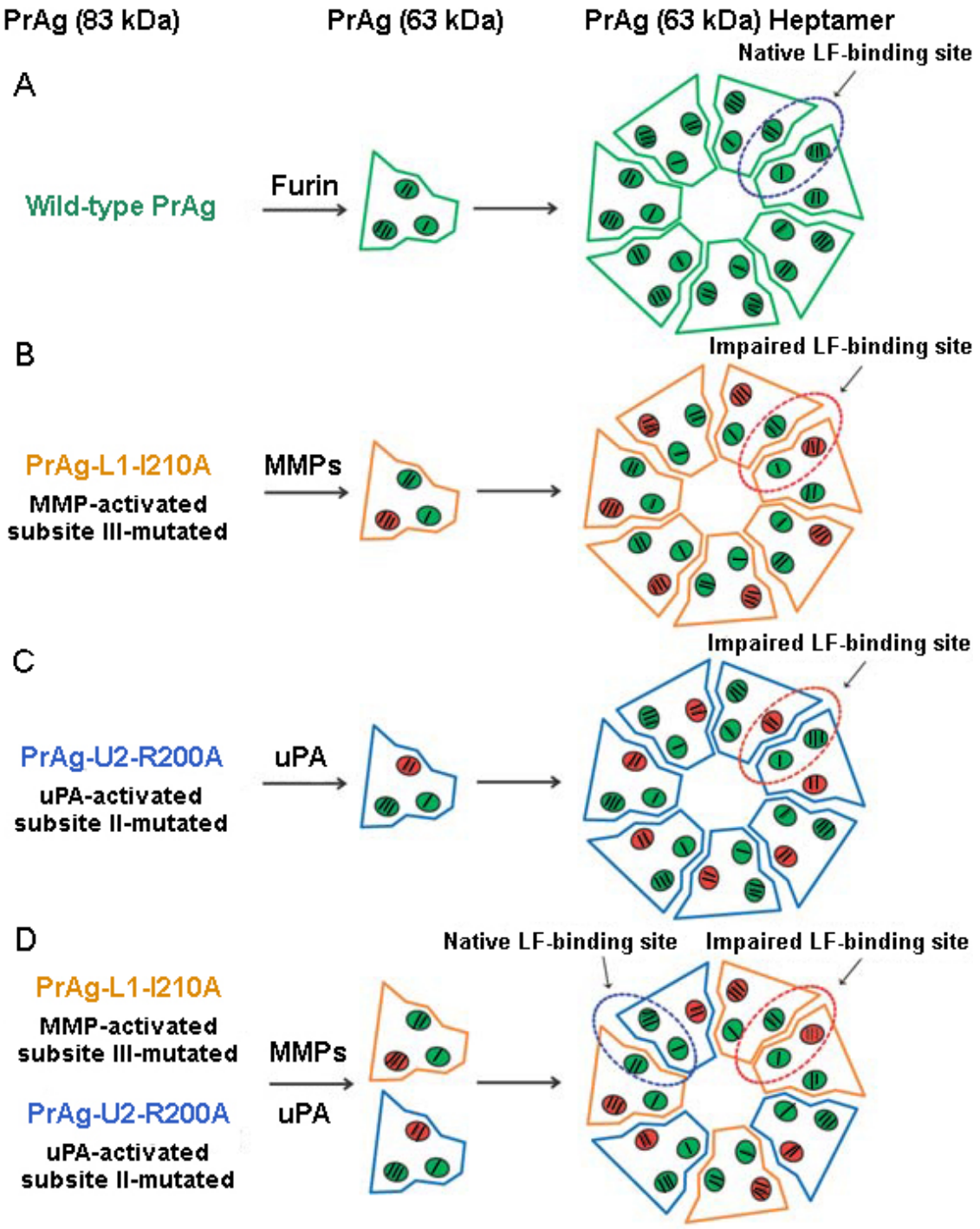

Figure 1.4: Schematic representation of intermolecular complementation by mutated PrAg proteins. LF-binding subsites I, II and III are represented in green as I, II and III respectively. Note that a single LF binding site, spans two adjacent PrAg (63 kDa) monomers (A). Mutations in any of these subsites (shown in red) result in impaired LF-binding (B, C); however, with intermolecular complementation as many as three active LF-binding sites can be regained (D). (Adapted with permission from Macmillan Publishers Ltd: Liu et al., *Nature Biotechnology* (121), Copyright 2005.)

In the scenario where only MMPs or uPA are present, only one of the engineered PrAg variants will be activated at the cell surface (Figure 1.4B-C), forming heptamers where all putative LF binding sites contain the same subsite point mutation, dramatically reducing LF binding (121).

Alternatively, when both MMPs and uPA are present, there is colocalized cell-surface activation of PrAg-L1-I210A and PrAg-U2-R200A and mixed heptamers form in which some of the native LF-binding sites are restored (Figure 1.4D). This process is called intermolecular complementation, and we refer to the combination of PrAg-L1-I210A + PrAg-U2-R200A as IC-PrAg (121).

1.7.1 IC-PrAg: Verification of Selective Activation

Theoretically, IC-PrAg requires both dual protease-activation and intermolecular complementation for maximal cytotoxin binding and internalization. This was validated experimentally using *in* vitro cytotoxicity assays performed in the presence or absence of known MMP and uPA inhibitors. Maximal cell killing was achieved only when PrAg-L1-I210A and PrAg-U2-R200A were administered together, demonstrating the occurrence of intermolecular complementation in this *in vitro* system (121). Furthermore, inhibition of MMP-activity with the physiologic inhibitor, TIMP1, or inhibition of uPA with its cognate inhibitor, PAI-1, led to reduced cytotoxicity, further demonstrating that cytotoxin internalization was dependent upon both MMP and uPA proteolytic activities (121). While dramatically attenuated, it is relevant to note that some cytotoxicity was observed with PrAg-L1-I210A-alone and PrAg-U2-R200A-alone, indicating that some cytotoxin binding does occur on these homogenous heptamers (121).

1.7.2 IC-PrAg: *in vivo* Toxicity

IC-PrAg was found to be much better tolerated than PrAg-U2, PrAg-L1 or PrAg-WT when co-administered with FP59, as summarized in Table 1.1 (121).

Table 1.1: Summary of the maximum tolerated doses for three intraperitoneal administrations of various PrAgs in combination with FP59. Data from Liu et al. 2005, *Nature Biotechnology* (121).

	PrAg-WT (Furin)	PrAg-L1 (MMPs)	PrAg-U2 (uPA)	PrAg-L1-I210A + PrAg-U2-R200A (MMPs/uPA)	PrAg-L1-I210A (MMPs)	PrAg-U2-R200A (uPA)
MTD3 (μg) [Coadministered with 3 μg FP59†]	0.25	4	10	30 + 15	50	> 100

† FP59 is a fusion protein containing the PrAg binding domain of LF fused to the catalytic domain of *Pseudomonas* exotoxin A

At the MTD3, mice treated with IC-PrAg + FP59 had no evidence of gross abnormalities; however, histological examination uncovered necrosis of the bone and bone marrow (121).

1.7.3 IC-PrAg: *in vivo* Efficacy

Three local administrations of IC-PrAg + FP59 resulted in dramatic antitumor effects in B16-BL6 melanoma, T241 fibrosarcoma and LL3 Lewis lung carcinoma syngrafts, with 94%, 92% and 70% tumor regression reported at the study endpoints (121).

Control cohorts treated locally with either PrAg-L1-I210A + FP59 or PrAg-U2-R200A + FP59, had minimal to no antitumor response, providing *in vivo* evidence that intermolecular complementation was required for tumoricidal activity (121).

An additional cohort of B16-BL6-bearing mice was treated with three intraperitoneal administrations of IC-PrAg + FP59. Significant antitumor efficacy was observed with this systemic treatment; however, a modest reduction in body weight was noted (Dose administered was 2/3MTD3) (121).

1.8 PrAg-L1, PrAg-U2 and IC-PrAg *in vivo*: A Post-Hoc Analysis

MMP-activated PrAg-L1, uPA-activated PrAg-U2 and dual MMP/uPA-activated IC-PrAg, have all been tested extensively *in vivo*, and each has documented efficacy in multiple models of cancer highlighting the potential broad-spectrum therapeutic utility of these agents (105, 107, 115, 117, 118, 121-123). However, retrospectively comparing the engineered PrAgs from data reported in these early studies has been complicated by the fact that differences existed in multiple aspects of experimental design, including the identity of the co-administered cytotoxins, indications treated, dose routes, number of doses and/or PrAg:cytotoxin ratios (Table 1.2).

Table 1.2: Literature summary of *in vivo* tumor models where significant antitumor efficacy was reported when PrAg-L1, PrAg-U2 or IC-PrAg were administered in combination with various cytotoxins

Engineered PrAg	Cytotoxin	Tumor	Dose Route	Dose #	PrAg:Cytotoxin Ratio	(Ref.)
MMP-activated PrAg, PrAg-L1	LF-HMAGG*	LL3	I.P.	5	3:1	(105)
		B16-BL6	I.P.	5	3:1	(105)
		C32	I.P.	6	3:1	(105)
		HT144	I.P.	6	3:1	(105)
		A549	I.P.	6	3:1	(105)
		Colo205	I.P.	6	3:1	(105)
		DRO	I.P.	1, 2, 4 or 6	3:1	(107)
		BHT-101	I.P.	1, 2, 4 or 6	3:1	(107)
uPA-activated PrAg, PrAg-U2	FP59†	LL3	I.D.	2	3:1	(115)
			I.P.	3	3:1, 10:1, 25:1	(118)
		T241	I.D.	2	3:1	(115)
			I.P.	3	25:1, 50:1	(118)
		B16-BL6	I.D.	2	3:1	(115)
			I.D.	3	12:1 or 4:1	(121)
			I.P.	3	13:1, 25:1, 38:1, 50:1	(118)
		HT1299	I.P.	4	6:1, 10:1	(117)
dual MMP/uPA-activated PrAg, IC-PrAg (PrAg-L1-I210A + PrAg-U2-R200A)	FP59†	LL3	I.D.	3	6:6:1	(121)
		T241	I.D.	3	6:6:1	(121)
		B16-BL6	I.D.	3	6:6:1 or 2:2:1	(121)
			I.P.	3	3:7:1	(121)

* LF-HMAGG is a version of anthrax lethal factor, LF, having the non-native N-terminal sequence: HMAGG
† FP59 is a fusion protein containing the PrAg binding domain of LF fused to the catalytic domain of *Pseudomonas* exotoxin A
Dose Route: I.D. = intradermal, I.P. = intraperitoneal

Alongside reports of significant antitumor efficacy, toxicities of varying severity have also been reported when the engineered anthrax toxins were administered intraperitoneally in mice (115, 117, 118, 121). These are briefly summarized in Table 1.3.

Table 1.3: Literature summary of toxicities associated with intraperitoneal administration of PrAg-L1, PrAg-U2 or IC-PrAg in combination with various cytotoxins

Engineered PrAg	Cytotoxin	Dose #	PrAg + Cytotoxin	Toxicity	(Ref.)
MMP-activated PrAg, PrAg-L1	LF-HMAGG*	6	45 µg + 15 µg	None (Full necropsies were performed.)	(105)
	FP59†	3	12 µg + 3 µg	MTD3	(121)
uPA-activated PrAg, PrAg-U2	FP59†	2	7.2 µg + 1.2 µg	Death (> 80% Lethality). Profound histologic damage in kidney, liver, heart and lung. (Necropsies performed on both dead and terminally ill animals. This analysis does not distinguish ante-/post-mortem changes)	(117)
		6	25 µg + 1 µg	Death (67% Lethality)	(117)
		6	40 µg + 1 µg	Death (40% Lethality) Small intestinal edema, villi inflammation and necrosis. Ulceration of the anal region.	(118)
		6	4 µg + 1.36 µg	Death (11% Lethality)	(118)
		1	200 µg + 10 µg	Death (100% Lethality) Ante-mortem histology identified cytotoxicity in the bone marrow, adrenal cortex, osteoblasts and T-cell areas of the spleen and lymph nodes.	(115)
		1	40 µg + 10 µg	MTD	(115)
		3	30 µg + 3 µg	MTD3	(121)
dual MMP/uPA-activated PrAg, IC-PrAg (PrAg-L1-I210A + PrAg-U2-R200A)	FP59†	3	15 µg + 30 µg + 3 µg	MTD3 Bone and bone marrow necrosis.	(121)
		3	22.5 µg + 45 µg + 3 µg	Death Bone and bone marrow necrosis.	(121)

* LF-HMAGG is a version of anthrax lethal factor, LF, having the non-native N-terminal sequence: HMAGG

† FP59 is a fusion protein containing the PrAg binding domain of LF fused to the catalytic domain of *Pseudomonas* exotoxin A

The most extreme toxicities were observed with administration of PrAg-U2 + FP59 where in order to administer effective doses without significant lethality, co-administration of the anti-inflammatory glucocorticoid, dexamethasone, was required (117, 118). Taken at a glance, this data could be interpreted to mean that uPA-activated PrAg-U2 is an unsuitable candidate for further development. However, when viewed in a broader context, this conclusion becomes less black-and-white. When the maximum tolerated doses for three I.P. administrations of PrAg-U2 and PrAg-L1 were determined in parallel, in combination with FP59, it was demonstrated that PrAg-U2 was actually 2.5-fold better tolerated than PrAg-L1 (121). This finding, paired with the knowledge that high doses of PrAg-L1 can be administered systemically with no reported toxicity [albeit with a different cytotoxin LF-HMAGG (107, 124)] implicates that the identity of the cytotoxin employed in these early *in vivo* studies had a profound impact on observed toxicity. Therefore, in order to accurately compare the suitability of PrAg-L1, PrAg-U2 and IC-PrAg for further development, at a minimum it was necessary to re-evaluate their toxicities, and efficacies, using a common cytotoxin. Due to the apparent exacerbated toxicity observed with co-administration of FP59, we elected to perform this comparison using wild type anthrax lethal factor, LF. All experiments reported in Chapters 2, 4 and 5 were performed in combination with LF, containing a native N-terminal sequence; however, experiments in Chapter 3 were performed in combination with LF-HMAGG.

We anticipated that a thorough evaluation of the unique toxicological profiles associated with each engineered PrAg variant, performed in a direct head-to-head manner, might cause one to emerge as an optimal candidate for further assessment, and characterization, for use as an anti-HNSCC agent.

1.9 Synopsis of the Dissertation

The goal of this dissertation research was to assess the feasibility of utilizing tumor-targeted versions of anthrax toxin to treat head and neck squamous cell carcinoma. This first chapter summarizes the clinical need for developing novel anti-HNSCC agents, and details the initial development and characterization of three distinct protease-activated anthrax protective antigens (PrAgs): PrAg-L1 (MMP-activated), PrAg-U2 (uPA-activated) and IC-PrAg (dual MMP/uPA-activated).

In Chapter 2, we asked the question: Which of these three engineered PrAg variants is the optimal candidate for further development? Detailed toxicological profiling and head-to-head efficacy studies are described in response to this inquiry. Ultimately, we emerged with one candidate that had an enhanced toxicity profile relative to the other two versions, while it maintained similar antitumor efficacy in the aggressive B16-BL6 melanoma model of cancer.

Building upon the findings from Chapter 2, in Chapter 3 we explored the anti-HNSCC activity of this lead candidate. A combination of *in vitro* cytotoxicity assays, *in vivo* xenograft trials and immunohistochemical analyses were performed to evaluate the antitumor activity of this specific engineered anthrax toxin in murine models of human HNSCC. We observed that 4 separate xenografted human HNSCC cell lines were sensitive to systemic toxin treatment.

In Chapter 4, results from the preclinical studies detailed in Chapters 2 and 3, were translated to a clinical setting. A Phase 0 veterinary clinical trial was initiated in feline oral squamous cell carcinoma patients, and data from the first completed patient is presented in the form of a case report. This trial is still in progress; however, initial

findings are highly encouraging as our first patient demonstrated a measurable reduction in primary tumor size, despite low-dose treatment.

Key findings and future directions are expanded upon in Chapter 5.

Overall, this dissertation research was driven by the desire to further characterize a novel agent with potential to address an unmet clinical need. This work spans from early preclinical toxicology (Chapter 2), to preclinical syngraft and xenograft models of efficacy (Chapters 2 and 3), and ultimately to first-in-patient veterinary clinical testing (Chapter 4). This work has led to significant advances in our understanding of the mechanisms of action and toxicity of these engineered anthrax toxins, and provides a solid framework for future preclinical and/or clinical development.

Chapter 2:

Comparative Toxicity and Efficacy of Engineered Anthrax Lethal Toxin Variants with Broad Antitumor Activities

This chapter contains content and figures taken from an article that is currently in submission, in which the dissertation author was a primary contributing author:

Peters DE, Hoover B, Grey Cloud L, Liu S, Molinolo AA, Leppla SH, Bugge TH. Comparative toxicity and efficacy of engineered anthrax lethal toxin variants with broad antitumor activities. *In submission*

Specific Experimental Contributions:

All data was analyzed by, and all figures were prepared by, D.E.P

Comparative toxicity trials were performed by D.E.P. (Data in Tables 2.2, 2.3 and Figure 2.1)

Comparative efficacy trials were performed by D.E.P., B.H. and L.G.C. (Data in Table 2.4 Figure 2.2)

Terminal blood draws and blood work analysis was performed by D.E.P. (Data in Table 2.5 and Figures 2.3, 2.4, 2.5, 2.6, 2.7, 2.8, 2.9, 2.10, 2.11 and 2.12)

Immunohistochemistry and quantification were performed by D.E.P. and L.G.C. (Data in Figures 2.13 and 2.14)

Proteins were expressed and purified by Rasem Fattah.

D.E.P., S.L., S.H.L, A.A.M. and T.H.B. contributed to experimental design.

A.A.M. reviewed necropsy histology.

2.1 Abstract

We have previously designed and characterized versions of anthrax lethal toxin that are selectively cytotoxic in the tumor microenvironment and which display broad and potent antitumor activities *in vivo*. Here, we have performed the first direct comparison of the safety and efficacy of three engineered anthrax lethal toxin variants requiring activation by either matrix-metalloproteinases (MMPs), urokinase plasminogen activator (uPA) or co-localized MMP/uPA activities. C57BL/6J mice were challenged with six doses of engineered anthrax lethal toxins via intraperitoneal (I.P.) or intravenous (I.V.) dose routes to determine the maximum tolerated dose for six administrations (MTD6) and dose-limiting toxicities. Efficacy was evaluated using the B16-BL6 syngraft model of melanoma. Tumor-bearing mice were treated with six I.P. doses of engineered toxins, and tumor measurements and immunohistochemistry, paired with terminal blood work, were used to elaborate upon the antitumor mechanism and relative efficacy of each toxin. We found that MMP-, uPA- and dual MMP/uPA- activated anthrax lethal toxins exhibited the same dose-limiting toxicity; dose-dependent GI toxicity. In terms of efficacy, all three toxins significantly reduced primary B16-BL6 tumor burden, ranging from 32%-87% reduction, and they also delayed disease progression, as evidenced by dose-dependent normalization of blood work values. While target organ toxicity and effective doses were similar amongst the toxin variants, the dual MMP/uPA-activated anthrax lethal toxin exhibited the highest I.P. MTD6 and was 1.5-3-fold better tolerated than the single MMP-activated and uPA-activated toxins. This dual-activated toxin exhibited a clear therapeutic window in C57BL/6J mice, and at a dose 9-fold below the maximum tolerated dose a 58% reduction in B16-BL6 melanoma tumor burden was achieved.

Overall, we demonstrate that a dual MMP/uPA-activated anthrax lethal toxin can be administered safely, is highly effective, and is a promising candidate for clinical development.

2.2 Introduction

Development of anti-cancer agents that are specifically activated in the tumor microenvironment is an appealing strategy due to the potential for reduced off-target toxicity. One means to achieve tumor-specific activation is to exploit the fact that many tumors overexpress proteases that are present at low levels in normal tissues (reviewed in (110, 125-128)). Two classic examples of tumor-over-expressed proteases are matrix metalloproteinases (MMPs) and urokinase plasminogen activator (uPA). We have previously generated and characterized versions of anthrax toxin requiring proteolytic activation by either, or both, of these enzymes (98, 108, 121).

Targeting of anthrax toxin to the tumor microenvironment was achieved by altering the cleavage sequence required for anthrax protective antigen (PrAg) activation; replacing the native furin-preferred cleavage sequence with sequences preferred by alternative proteases. Ultimately, this change in PrAg cleavage sequence led to redirection of internalization of anthrax lethal factor (LF), and/or related cytotoxins, from cells expressing cell-surface furin-like activity to those with a different specified proteolytic activity. As aforementioned, employing this principle we have previously generated versions of PrAg requiring activation by MMPs (PrAg-L1) (98), uPA (PrAg-U2) (108), or co-localized MMP/uPA activities (IC-PrAg, consisting of two separate proteins, PrAg-L1-I210A and PrAg-U2-R200A) (121). Multiple studies have been performed, summarized in Table 1, demonstrating that when these engineered PrAgs are co-administered with various cytotoxins, that significant antitumor activity can be achieved in a variety of syngraft, xenograft and orthotopic models, highlighting the potential broad-spectrum therapeutic utility of these agents (105, 107, 115, 117, 118, 121-123).

However, while these highly similar toxin combinations all exhibit potent antitumor efficacies, simultaneously toxicities of varying severity have been reported with their use. A particularly striking toxicity was evident with systemic administration of PrAg-U2 + FP59, where in order to administer effective doses of PrAg-U2 + FP59, without significant mortality, co-administration of the anti-inflammatory glucocorticoid, dexamethasone, was required (117, 118) (FP59 is a potent protein synthesis inhibitor composed of the N-terminal PrAg-binding domain of LF coupled to the enzymatic domain of *Pseudomonas aeruginosa* exotoxin A).

Table 2.1: Literature summary of *in vivo* tumor models where significant antitumor efficacy was reported when engineered PrAgs were administered in combination with various cytotoxins

Engineered PrAg	Cytotoxin	*In vivo* Tumor Model (Ref.)
MMP-activated PrAg, PrAg-L1	LF-HMAGG*	LL3, Lewis lung carcinoma syngraft (105) B16-BL6, melanoma syngraft (105) C32, melanoma xenograft (105) HT144, melanoma xenograft (105) A549, lung carcinoma xenograft (105) Colo205, colon carcinoma xenograft (105) DRO, anaplastic thyroid carcinoma orthotopic implant (107) BHT-101, anaplastic thyroid carcinoma orthotopic implant (107)
uPA-activated PrAg, PrAg-U2	FP59†	LL3, Lewis lung carcinoma syngraft (115,118) T241, fibrosarcoma syngraft (115,118) B16-BL6, melanoma syngraft (115,118,121) HT1299, non-squamous cell lung carcinoma xenograft (117)
	LF‡	B16-BL6, melanoma syngraft (123)
dual MMP/uPA-activated PrAg, IC-PrAg (PrAg-L1-I210A + PrAg-U2-R200A)	FP59†	LL3, Lewis lung carcinoma syngraft (121) T241, fibrosarcoma syngraft (121) B16-BL6, melanoma syngraft (121)
	LF-HMAGG*	HN12, head and neck squamous cell carcinoma xenograft (122) HN6, head and neck squamous cell carcinoma (122) Hep2, head and neck squamous cell carcinoma (122) Cal27, head and neck squamous cell carcinoma (122)

‡ LF is wild-type anthrax lethal factor having the native N-terminal sequence: AGG

* LF-HMAGG is a version of LF having the non-native N-terminal sequence: HMAGG

† FP59 is a fusion protein containing the PrAg binding domain of LF fused to the catalytic domain of *Pseudomonas* exotoxin A

The present study was initiated to provide a detailed preclinical evaluation of the dose-limiting toxicities, efficacy, and antitumor mechanisms associated with multiple systemic doses of PrAg-L1, PrAg-U2 and IC-PrAg, when co-administered with LF. Herein we identify that IC-PrAg + LF is, in fact, the best tolerated version. We describe in detail the dose-limiting toxicity associated with IC-PrAg + LF administration, dose-dependent GI toxicity, and further show that effective doses of this toxin can be administered far below where this dose-limiting toxicity is first encountered. This study demonstrates that IC-PrAg + LF is well-tolerated, highly effective, and is a promising candidate for further development as an anti-cancer agent.

2.3 Materials and Methods

2.3.1 Ethics Statement

All animal work was performed in accordance with protocols approved by the National Institute of Dental and Craniofacial Research Animal Care and Use Committee (Animal Study Proposal Numbers: 10-585 and 13-712).

2.3.2 Protein Purification

Recombinant anthrax protective antigens (PrAg) including: PrAg-WT (wildtype, furin-activated), PrAg-U2 (uPA-activated), PrAg-L1 (MMP-activated), IC-PrAg (dual MMP/uPA-activated, consisting of two individual proteins: PrAg-L1-I210A and PrAg-U2-R200A), PrAg-U7 (protease resistant), and recombinant anthrax lethal factors including: LF (wildtype) and LF-E687A (enzymatically-inactive, similar to previously used LF-E687C (89)) were generated and purified as previously described (98, 108, 115, 121, 129). The LF used herein has the native N-terminal sequence: AGG. Protein expression and purification was performed by Rasem Fattah.

2.3.3 Animals

Female C57BL/6J mice (Jackson Laboratory, Bar Harbor, ME) between 6 and 8 weeks of age, and weighing between 16-18 grams, were used for all experiments. Animals were housed in a pathogen-free environment certified by the Association for Assessment and Accreditation of Laboratory Animal Care International.

2.3.4 Comparative Evaluation of Toxicity

Mice received 6 injections of PBS or engineered anthrax lethal toxins via intraperitoneal (I.P.) or intravenous (I.V.) dose routes over the course of two weeks on a MWFx2 schedule. On study day 14, all surviving mice were euthanized and complete gross

necropsies were performed. All organs where toxicity has been previously reported for similar toxin combinations were included in our analysis [gastrointestinal (GI) tract (18, 19), spleen (18), adrenal gland (18), kidney (20), lung (20), liver (20), heart (20) and femur (7, 18)]. In addition, skin, mammary gland, salivary gland, thyroid gland, abdominal wall, quadriceps femoris muscle, pancreas, gall bladder, bladder, ovaries, uterus, sternum and spinal cord were analyzed. Following harvesting, tissues were fixed in 4% paraformaldehyde for 24 hours, embedded in paraffin and sectioned. Tissues containing bone were decalcified with EDTA. All slide images were captured using an Aperio T3 Scanscope and were analyzed by an investigator blinded as to treatment group (Aperio Technologies, Vista, CA).

In this study, MTD6 was defined as the highest toxin concentration administered where no lethality was observed in a treated cohort of a minimum size of 10 mice. Comparison of survival data was performed using the Log-Rank test with GraphPad Prism software**.**

2.3.5 Comparative Evaluation of Efficacy

B16-BL6 melanoma cells (5×10^5 per mouse) were injected in the mid-scapular subcutis. When tumors reached a volume of 50–100 mm^3, the mice were divided into cohorts with equivalent mean tumor sizes. Each group contained a minimum of 10 mice. Mice received a total of 6 I.P. injections of either 400 µl PBS, or of engineered anthrax lethal toxin in 400 µl PBS. Eleven different engineered anthrax lethal toxin treatments were tested as listed in Table 2.4

At the time of dosing, a blinded investigator weighed the mice and measured the longest and shortest tumor diameters with digital calipers (FV Fowler Company, Newton, MA). Tumor volume was estimated using: V = [length (mm) * width $(mm)^2$]/2 (130). Statistical

significances of differences in tumor sizes were determined using the two-tailed Student's t-test.

Terminal blood collection was performed on all surviving mice on study day 14. Blood was collected via cardiac puncture, and was processed and submitted to the NIH Clinical Center Department of Laboratory Medicine (Bethesda, MD) for complete blood count and a limited blood chemistry panel. A sham-treated, tumor-free, cohort of ten mice was analyzed in parallel to obtain disease-free blood work values.

2.3.6 Comparative Evaluation of Antitumor Mechanism

Tumors were harvested, fixed in 4% paraformaldehyde for 24 hours, embedded in paraffin and sectioned. All slide images were captured using an Aperio T3 Scanscope and quantification was performed by a blinded investigator using Aperio Imagescope Software (Aperio Technologies, Vista, CA).

Percent necrosis was determined from hematoxylin and eosin (H&E) stained sections. Unstained sections were stained with a monoclonal rabbit anti-mouse CD31 (Santa Cruz Biotechnology, Inc., Santa Cruz, CA) and a polyclonal rabbit anti-human Ki67 (Novocastra Laboratories, Ltd., Newcastle, UK), to quantify, respectively, differences in blood vessel density and alterations in cellular proliferation. TUNEL staining was performed using a TdT In Situ Apoptosis Detection Kit – TACS Blue Label (Trevigen Inc., Gaithersburg, MD) per manufacturer’s instructions. Statistical significances of differences were calculated using the Student's t-test, two-tailed.

2.4 Results

2.4.1 Comparative Toxicity: Determination of MTD6

We first determined the maximum tolerated dose for six intraperitoneal (I.P.) administrations of the MMP-, uPA- and dual MMP/uPA-activated anthrax lethal toxins (Summarized in Table 2.2).

As expected, we found that each of the engineered PrAgs was non-toxic when administered I.P. without cytotoxin (100 µg PrAg-XX) or when they were co-administered with an enzymatically-inactive cytotoxin, LF-E687A (100 µg PrAg-XX + 33 µg LF-E687A). We verified that proteolytic cleavage of the engineered PrAgs was required for subsequent LF-mediated toxicity *in vivo*, as an uncleavable, protease-resistant, variant of PrAg (PrAg-U7) (115) was found to be non-toxic when administered at high doses with LF (100 µg PrAg-U7 + 33 µg LF) (Table 2.2).

The dual MMP/uPA-activated anthrax lethal toxin, IC-PrAg + LF, was identified as the best tolerated version, exhibiting the highest I.P. MTD6 (45 µg IC-PrAg + 15 µg LF). This was 3-fold improved from the I.P. MTD6 of the MMP-activated version (I.P. MTD6: 15 µg PrAg-L1 + 5 µg LF) and 1.5-fold improved from the uPA-activated version (I.P. MTD6: 30 µg PrAg-U2 + 10 µg LF). All three engineered anthrax lethal toxins were far better tolerated than wildtype anthrax lethal toxin, which resulted in 100% lethality following only 3 I.P. doses at a concentration of 15 µg PrAg-WT + 5 µg LF (Table 2.2).

Table 2.2: Mortality associated with intraperitoneal administration of engineered anthrax lethal toxins: Determining I.P. MTD6

	Description of Agent		Dose (μg)	# Mice	% Survival at Day 14	Log-Rank* (P)
Control Groups	vehicle control	PBS	---	10	100	---
	wild-type anthrax lethal toxin	PrAg-WT + LF	15/5	10	0	< 0.01
	uncleavable anthrax lethal toxin	PrAg-U7 + LF	100/33.3	5	100	n.s.
	MMP-activated PrAg alone	PrAg-L1	100	5	100	n.s.
	uPA-activated PrAg alone	PrAg-U2	100	5	100	n.s.
	dual MMP/uPA-activated PrAg alone	IC-PrAg (PrAg-L1-I210A + PrAg-U2-R200A)	100	5	100	n.s.
	MMP-activated PrAg + enzymatically-inactive LF	PrAg-L1 + LF-E687A	100/33.3	5	100	n.s.
	uPA-activated PrAg + enzymatically-inactive LF	PrAg-U2 + LF-E687A	100/33.3	5	100	n.s.
	dual MMP/uPA-activated PrAg + enzymatically-inactive LF	IC-PrAg (PrAg-L1-I210A + PrAg-U2-R200A) + LF-E687A	50/50/33.3	5	100	n.s.
Experimental Groups [I.P. MTD6 Determination]	MMP-activated anthrax lethal toxin	PrAg-L1 + LF	30/10	5	60	0.03
			22.5/7.5	5	60	0.03
			18.75/6.25	5	80	n.s.
			15/5[x]	10	100	n.s.
	uPA-activated anthrax lethal toxin	PrAg-U2 + LF	45/15	10	80	n.s.
			37.5/12.5	10	90	n.s.
			30/10[x]	10	100	n.s.
	dual MMP/uPA-activated anthrax lethal toxin	IC-PrAg (PrAg-L1-I210A + PrAg-U2-R200A) + LF	30/30/20	10	60	0.03
			52.5/17.5	5	80	n.s.
			22.5/22.5/15[x]	10	100	n.s.
			15/15/10	5	100	n.s.

*Log-Rank tests are in comprison to the Kaplan-Meier survival curve of the vehicle control (PBS) cohort
Abbreviations: n.s., not significant
[x] I.P. MTD6

While I.P. administration is routinely utilized for systemic dosing in mice, intravenous (I.V.) administration is a far more common route used for larger mammalian species, therefore, we next determined I.V. MTD6s for each of the engineered toxins (Summarized in Table 2.3).

Table 2.3: Mortality associated with intravenous administration of engineered anthrax lethal toxins: Determining I.V. MTD6

	Description of Agent		Dose (µg)	# Mice	% Survival at Day 14	Log-Rank* (P)
Control Groups	vehicle control	PBS	---	10	100	---
	wild-type anthrax lethal toxin	PrAg-WT + LF	6/2	5	0	<0.01
	MMP-activated PrAg + enzymatically-inactive LF	PrAg-L1 + LF-E687A	50/16.7	6	50	0.01
	MMP-activated PrAg alone	PrAg-L1	50	5	60	0.03
	uPA-activated PrAg alone	PrAg-U2	50	4	75	n.s.
	dual MMP/uPA-activated PrAg alone	IC-PrAg (PrAg-L1-I210A + PrAg-U2-R200A)	25/25	5	80	n.s.
Experimental Groups [I.V. MTD6 Determination]	MMP-activated anthrax lethal toxin	PrAg-L1 + LF	15/5	4	0	<0.01
			12/4	10	66	0.02
			9/3	10	70	n.s.
			6/2[x]	10	100	n.s.
			3/1	6	100	n.s.
	uPA-activated anthrax lethal toxin	PrAg-U2 + LF	15/5	8	75	n.s.
			12/4[x]	13	100	n.s.
			9/3	11	100	n.s.
	Dual MMP/uPA-activated anthrax lethal toxin	IC-PrAg (PrAg-L1-I210A + PrAg-U2-R200A) + LF	15/5	5	80	n.s.
			12/4[x]	12	100	n.s.
			9/3	11	100	n.s.

*Log-Rank tests are in comprison to the Kaplan-Meier survival curve of the vehicle control (PBS) cohort
Abbreviations: n.s., not significant
[x] I.V. MTD6

Similar to I.P. administration, we found that when administered I.V., PrAg-L1 + LF was the least tolerated version (I.V. MTD6: 6 µg PrAg-L1 + 2 µg LF), while both PrAg-U2 + LF and IC-PrAg + LF exhibited a 2-fold increase in tolerance (I.V. MTD6s: 12 µg PrAg-U2 + 4 µg LF and 12 µg IC-PrAg + 4 µg LF). Again, all engineered toxins were far better tolerated than wildtype anthrax lethal toxin, which yielded 100% lethality when administered at a dose of 6 µg PrAg-WT + 2 µg LF (Table 2.3).

Unexpectedly, mortality was observed when high I.V. doses of the engineered PrAgs were administered without LF. Specifically, six I.V. doses of 50 µg PrAg-L1, PrAg-U2 or IC-PrAg alone, resulted in 40%, 25% and 20% lethality respectively (Table 2.3). While unanticipated, this phenomenon of PrAg-alone toxicity is unlikely to be therapeutically relevant as the doses where PrAg alone toxicity occurred far exceed the MTD6s identified for I.V. administration of PrAg in conjunction with LF. However, determining the threshold at which the engineered PrAg can be safely administered alone may be an appropriate first stage in toxicity testing as this therapeutic modality is translated to other species.

2.4.2 Comparative Toxicity: Identification of Target Organs

Since the engineered PrAgs are activated by proteases with differing tissue expression levels, we anticipated that differences might also exist in their off-target toxicities. Bearing this in mind, we performed complete gross and histopathological necropsies on toxin-treated mice. We found that independent of the activating protease, the GI tract was the first organ system affected by I.P administered toxins and that in all cases the GI pathology was dose-dependent (Figure 2.1).

The first identifiable abnormality was a mild dilation of the small intestine visible on gross examination. Further histopathological examination of affected GI tracts confirmed the small intestinal dilation, and identified occasional pockets of focal inflammation with no alterations in villus structure. Mice with this level of GI abnormality exhibited normal behavior during the trial, maintained body weight throughout treatment, and had no identifiable pathology in other tissues examined.

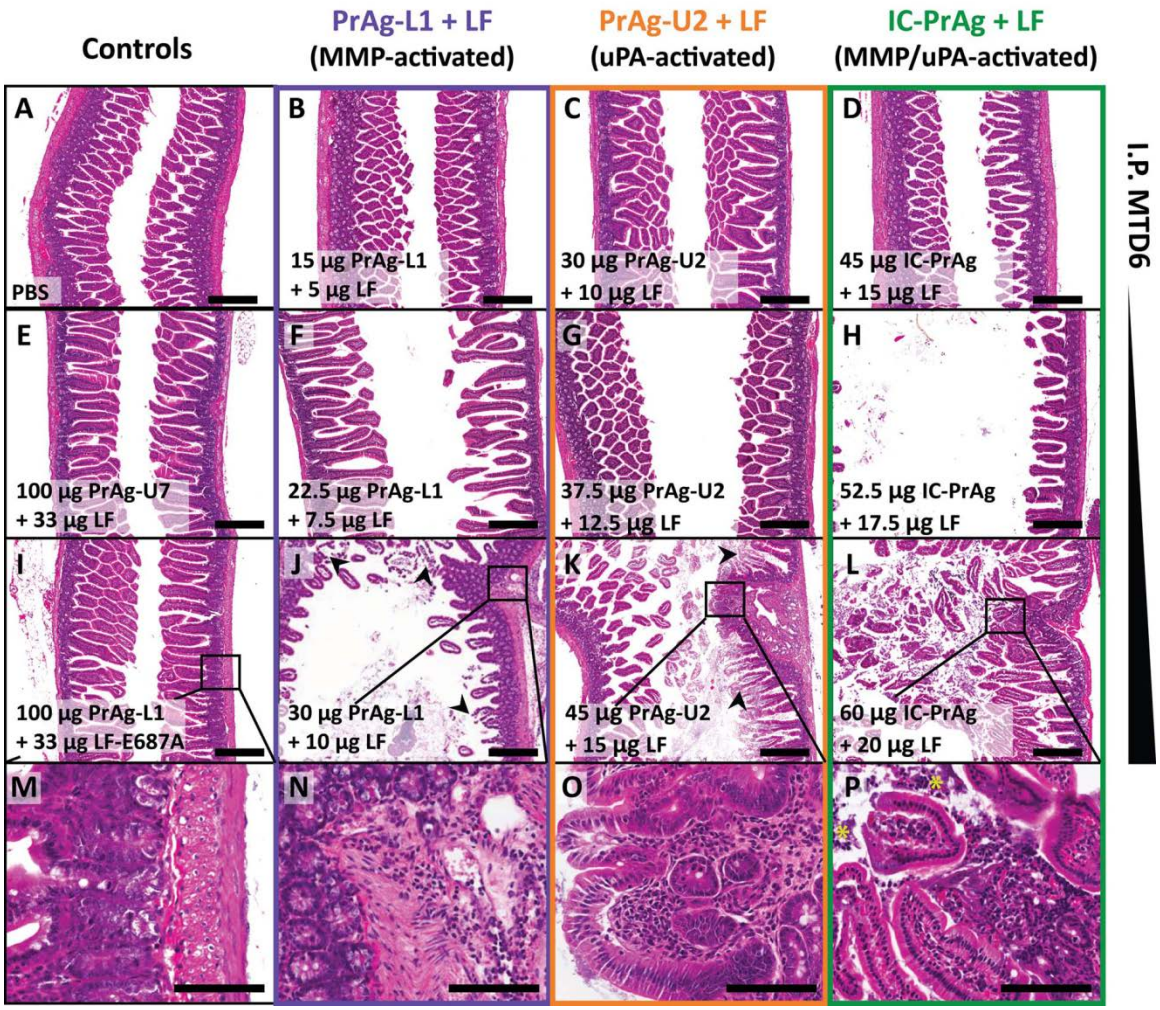

Figure 2.1: GI toxicity is dose-limiting for systemic administration of MMP-, uPA- and dual MMP/uPA-activated anthrax lethal toxins. Representative H&E sections of small intestine depicting the dose-dependent progression of GI toxicity observed when six doses of PrAg-L1 + LF (B,F,J,N) PrAg-U2 + LF (C,G,K,O) or IC-PrAg + LF (D,H,L,P) are administered intraperitoneally in C57BL/6J mice. At the MTD6 for each toxin, no GI pathology was present at the gross or microscopic level in 29/30 experimental mice (B-D). At this dose, note the similarity in appearance to control-treated mice receiving 6 I.P. doses of either PBS (A), uncleavable anthrax PrAg paired with LF, 100 µg PrAg-U7 + 33 µg LF (E), or MMP-activated PrAg paired with enzymatically-inactive cytotoxin, 100 µg PrAg-L1 + 33 µg LF-E687A (I). As doses were increased above the MTD6, GI toxicity initially presented as mild small intestinal dilation (F-H) which progressed in severity to involve GI inflammation, regions of villous necrosis, denuded and ulcerated GI epithelium and/or grossly visible GI hemorrhage (J-L, arrowheads depict necrotic villi). (M-P) Higher magnification images showing inflammation in the lamina propria of toxin-treated mice, but not controls. (P) * indicates inflammatory cells that have invaded into the lumen of the small intestine. Scale bars are 300 µm A-L; 100 µm M-P.

Mild GI pathology as described above, and depicted in Figure 2.1 F-H, was first observed at doses of: 18.75 µg PrAg-L1 + 6.25 µg LF, 37.5 µg PrAg-U2 + 12.5 µg LF and 45 µg IC-PrAg + 15 µg LF, affecting 3/4, 4/9 and 1/10 mice respectively. As the doses of each toxin were increased, focal regions of villi with necrotic tips could be identified and inflammation was more diffuse. At the highest doses, pronounced GI changes were apparent, including regions of denuded and/or ulcerated epithelium and gross hemorrhage, which was segmental in nature and selectively affected the small intestine and cecum.

There was no evidence of direct toxicity to other organ systems; however, at doses above those which caused mild GI toxicity, the I.P. toxin injections were consistently associated with dose-dependent peritonitis. In the most severe cases fibrinous peritonitis was observed, and it was not uncommon to identify comorbid conditions such as: necrotizing pancreatitis, liver congestion, venous thrombosis, hypocellular bone marrow and/or thymic depletion. As no evidence of pancreas, liver, heart, bone or thymus pathology was present at lower doses, we speculate that these high dose pathologies occur secondarily to the observed GI lesions and associated inflammation, stress and/or functional deficits.

To determine if the toxin-related GI pathology was an inadvertent consequence of the I.P. route of administration, we also performed necropsies on mice receiving I.V. injections. We found that small intestinal dilation was also the earliest toxicity observed when the toxins were administered I.V. and that at the I.V. MTD6s no abnormalities were identified in other organ systems.

2.4.3 Comparative Efficacy: B16-BL6 Syngraft Model

We compared the antitumor efficacies of the engineered toxin variants using the B16-BL6 model of murine melanoma as it allowed us to perform efficacy testing in the same strain of mice utilized for toxicity characterization. Mice bearing B16-BL6 syngrafts were treated with six doses of PBS or toxin over the course of two weeks, using the same treatment schedule as in the toxicity trials.

We found that PrAg-L1 + LF, PrAg-U2 + LF and IC-PrAg + LF were equally efficient at reducing primary tumor burden when administered at protein equivalent doses (Table 2.4 and Figure 2.2A-C). The greatest antitumor effect was achieved using the dual MMP/uPA activated toxin, IC-PrAg + LF, which had a maximal antitumor effect of 87% following four doses, and 79% at the conclusion of the trial when administered at its I.P. MTD6 (45 µg IC-PrAg + 15 µg LF) (Table 2.4).

Table 2.4: Summary of antitumor and survival effects associated with I.P. administration of engineered anthrax lethal toxins

Description of Agent		Dose (µg)	Dose / MTD6	n	Maximum % Tumor Reduction		% Tumor Reduction at Day 14		% Survival at Day 14	
vehicle control	PBS	---	---	31	---	---	---	---	45	---
MMP-activated anthrax lethal toxin	PrAg-L1 + LF	15/5	1.00	10	66	[d.11]	61	**	70	n.s.
		5/1.7	0.33	10	57	[d.9]	32	*	90	*
		1/0.3	0.07	10	0	---	0	n.s.	10	n.s.
uPA-activated anthrax lethal toxin	PrAg-U2 + LF	24.3/8.1	0.80	10	75	[d.9]	63	**	100	**
		15/5	0.50	17	78	[d.9]	66	**	94	**
		5/1.7	0.17	10	59	[d.11]	50	*	70	n.s.
		1/0.3	0.03	17	0	---	0	n.s.	24	n.s.
dual MMP/uPA-activated anthrax lethal toxin	IC-PrAg [PrAg-L1-I210A + PrAg-U2-R200A] + LF	22.5/22.5/15	1.00	10	87	[d.9]	79	**	70	n.s.
		7.5/7.5/5	0.33	17	63	[d.11]	62	**	82	**
		2.5/2.5/1.7	0.11	10	60	[d.11]	59	*	70	n.s.
		0.5/0.5/0.3	0.02	10	0	---	0	n.s.	30	n.s.

Abbrieviations: [d.X], date on which maximum % tumor reduction was observed relative to PBS-treated mice.
% Tumor Reduction at Day 14: ** $P < 0.01$, * $P < 0.05$, Student's t-test, two-tailed. Determined relative to vehicle control.
% Survival at Day 14: ** $P < 0.01$, Log-Rank test. Determined relative to Kaplan-Meier survival curve of vehicle control.

Additionally, treatment with each of the three toxins was observed to improve survival in a dose-dependent manner (Figure 2.2D-F).

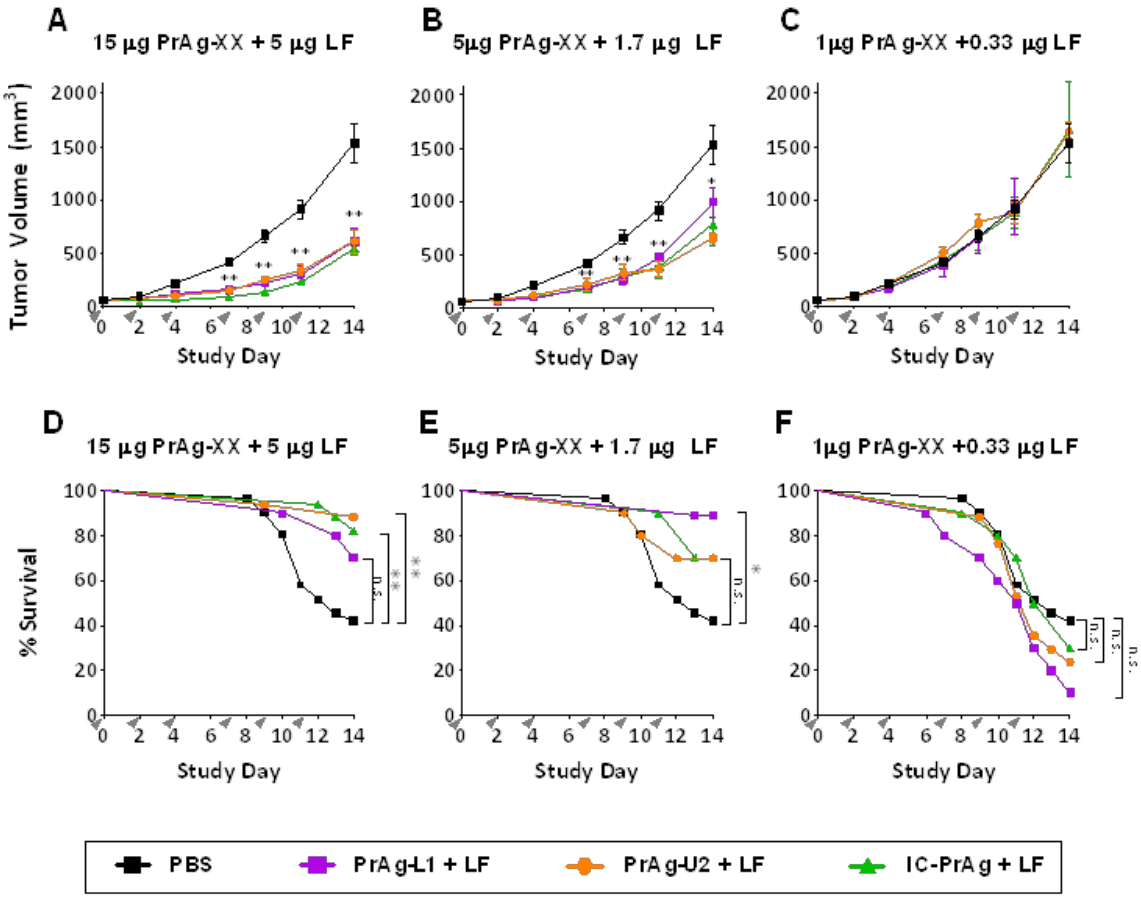

Figure 2.2: Engineered anthrax lethal toxins reduce B16-BL6 tumor burden and improve survival in a dose-dependent manner. (A-C) Tumor growth and (D-F) survival of C57BL/6J mice bearing B16-BL6 melanoma syngrafts that were treated with six I.P. doses of PBS (black lines) or engineered anthrax lethal toxins, MMP-activated PrAg-L1 + LF (purple), uPA-activated PrAg-U2 + LF (orange) or dual MMP/uPA-activated IC-PrAg + LF (green), at time points indicated by grey arrowheads. All cohorts were treated in parallel and the PBS control groups depicted in panels A-C and D-F are the same. Note that the antitumor effect was independent of the proteolytic-activation site; PrAg-L1 + LF, PrAg-U2 + LF and IC-PrAg + LF exhibited indistinguishable antitumor effects when administered at protein equivalent doses. (A-C) Tumor volume data are expressed as mean ± s.e.m.; *, $P < 0.05$, **, $P < 0.01$, Student's t-test, two-tailed. (D-F) Kaplan-Meier survival curves were compared via Log-Rank test; *, $P < 0.05$, **, $P < 0.01$.

2.4.4 Comparative Efficacy: CBC and Blood Chemistry

Terminal blood work was performed on all B16-BL6 melanoma bearing-mice, in order to assess which blood parameters were elevated due to progression of the disease versus which might be elevated as a direct consequence of toxin administration. To determine baseline values, blood was collected from tumor-free mice that had received sham treatments directly mimicking those of the B16-BL6 bearing cohorts.

As expected, presence of B16-BL6 melanoma caused significant changes in blood work relative to the tumor-free baseline mice (Table 2.5).

Table 2.5: B16-BL6 melanoma-induced changes in blood work values

			Treatment Group		
			Tumor-Free PBS (n=9)	B16-BL6 Tumor PBS (n=7)	
Bloodwork Parameter			Median	Median	P
Complete Blood Count	Absolute White Blood Cell Count [WBC]	K/µL	6.2	11.4	n.s.
	Absolute Neutrophil Count	K/µL	0.4	1.7	**
	Absolute Lymphocyte Count	K/µL	5.6	7.8	n.s.
	Absolute Monocyte Count	K/µL	0.16	0.37	*
	Absolute Eosinophil Count	K/µL	0.08	0.05	n.s.
	Absolute Basophil Count	K/µL	0.33	0.27	n.s.
	Absolute Red Blood Cell Count [RBC]	M/µL	9.6	3.75	**
	Hemoglobin [Hmg]	g/dL	14.6	7.2	**
	Hematocrit [Hct]	%	43.3	20.7	**
	Mean Corpuscular Volume [MCV]	K/µL	45.1	47.5	*
	Absolute Platelet Count	K/µL	835	792	n.s.
Chemistry	Alkaline Phosphatase [ALP]	U/L	175	52	***
	Alanine Aminotransferase [ALT]	U/L	43	142	***
	Aspartate Aminotransferase [AST]	U/L	103	735	***
	Amylase [AMY]	U/L	2872	2712	n.s.
	Creatine Kinase [CK]	U/L	167	643	*
	Lactate Dehydrogenase [LD]	U/L	329	2218	***

Student's t-test, two-tailed;*, P < 0.05;**, P < 0.01;***, P < 0.001.

2.4.4.1 B16-BL6-induced Changes in CBC

Mice bearing B16-BL6 melanoma syngrafts had a mild, non-significant, increase in white blood cell count, which could be accounted for by significant increases in both neutrophil and monocyte populations.

Red blood cell parameters were impacted greatly in the B16-BL6 disease state, and presence of untreated melanoma syngrafts led to development of anemia in tumor-bearing mice, which was characterized by significant reductions in total red blood cell count, hemoglobin and hematocrit, paired with a significant increase in mean corpuscular volume. In this study, further cytological and functional assays to describe the specific nature of the anemia were not performed; however we speculate that this acquired anemia may either have been a sequela to blood loss resultant from tumor ulceration, or a consequence of terminal disease.

Anemia is frequently observed in human cancer patients where prevalence exceeds 30%, even in the absence of concomitant chemotherapy (131, 132). The pathogenesis of cancer-induced anemia is complex and multi-factorial. Malignancies can directly contribute to the acquisition of anemia through processes such as tumor-related acute or chronic exogenous blood loss, intratumoral bleeding, and/or impairment of bone marrow function (and subsequent erythropoietin production) via tumor encroachment, bone metastasis, myelofibrosis, or tumor-induced bone marrow necrosis (133-136). Simultaneously, cancer-related co-morbidities, such as autoimmune hemolysis, renal insufficiency and/or nutrient deficiency, can independently cause, or worsen, an anemic state (133-136).

B16-BL6 melanoma is an aggressive cancer and in this study only 45% of PBS-treated tumor-bearing mice (14/31) survived the length of the trial (Figure 2.2 and Table 2.4). It is therefore plausible that multiple factors associated with end-stage disease contributed to acquisition of anemia in the PBS-treated, tumor-bearing cohort.

2.4.4.2 B16-BL6-induced Changes in Blood Chemistry

A limited blood enzyme panel was also performed and significant alterations in blood chemistry values were identified in the PBS-treated B16-BL6 tumor-bearing cohort (Table 2.5).

2.4.4.2.1 Alkaline Phosphatase

Alkaline phosphatase (ALP) levels were significantly reduced in PBS-treated B16-BL6 tumor-bearing mice. ALP is an enzyme that hydrolyzes phosphate esters, and that, under normal conditions, is predominantly secreted by the liver and bone with lesser amounts produced by the intestines and kidney. Cancer is frequently associated with elevations in ALP, caused by either direct tumor secretion of distinct ALP isozymes (137-140) or as a consequence of metastasis and invasion into the liver and/or bones (141-143). Reduction in ALP is a less common clinical finding, which, when present, has been associated with anemia (144-146). Therefore, it is possible that the reduction in ALP observed here is related to the B16-BL6 induced anemia described in section 2.4.4.1.

2.4.4.2.2 Lactate Dehydrogenase

Lactate dehydrogenase (LDH) catalyzes the conversion of pyruvate to lactate, and vice versa. Unlike most normal cells, cancer cells utilize lactate as an energy source during both aerobic and anaerobic conditions, and LDH serves as a key-player in tumor cell metabolism (147). In subcutaneous xenograft models, LDH levels have been

demonstrated to parallel tumor-size during both growth and treatment periods (148). This same pattern was observed here with B16-BL6-tumor bearing mice having markedly increased LD levels relative to tumor-free controls.

2.4.4.2.3 Creatine Kinase

Presence of B16-BL6 melanoma resulted in significant increases in creatine kinase (CK), an enzyme predominantly expressed in the brain and skeletal muscle. Elevation of CK is often an indicator of muscle damage.

At the time of euthanasia, surviving PBS-treated, B16-BL6-bearing mice were in an advanced disease-state and exhibited a significant, 17%, reduction in body weight relative to PBS-treated tumor-free controls ($P = 0.001$, Student's t-test, two-tailed). The body weight loss in the PBS-treated B16-BL6 cohort, along with the elevation in CK, implicates the presence of muscle wasting in these mice.

2.4.4.2.4 Alanine Aminotransferase

Alanine aminotransferase (ALT) levels were significantly increased in B16-BL6 tumor-bearing mice. ALT is a liver transaminase that is commonly monitored when evaluating hepatocellular injury; however, ALT is also expressed at lower levels in extra-hepatic tissues and it can be elevated in certain non-liver injury conditions, including muscle wasting (149). Given the short duration of this study, 19 days from tumor-cell injection to euthanasia, liver metastasis would not be expected and we anticipate that the observed elevation in ALT, paired with the marked increase in CK and reduction in body weight, is suggestive of disease-induced cachexia.

2.4.4.2.5 Aspartate Aminotransferase

Aspartate aminotransferase (AST) levels were also significantly increased in the B16-BL6 melanoma diseased-state. Similar to ALT, AST is also a transaminase expressed within the liver. AST has a broader expression pattern than ALT, and it is also found in cardiac muscle, skeletal muscle, kidneys, brain, and red blood cells. We hypothesize that the elevated AST here is another consequence of muscle breakdown.

2.4.4.3 Dose-dependent Normalization of Blood Work Abnormalities

Surprisingly, treatment with any version of the engineered anthrax lethal toxin trended towards normalizing the B16-BL6-induced blood work changes in a dose-dependent manner. For example, alkaline phosphatase levels were reduced in PBS-treated B16-BL6-tumor bearing mice relative to tumor free controls; however, treatment with six I.P. doses of either MMP-activated, uPA-activated or dual MMP/uPA toxins trended towards restoring ALP levels to the disease-free level in a dose-dependent fashion (Figure 2.3).

A trend towards dose-dependent normalization was also observed for: absolute red blood cell count (Figure 2.4), hemoglobin (Figure 2.5), hematocrit (Figure 2.6), mean corpuscular volume (Figure 2.7), alanine aminotransferase (Figure 2.8), aspartate aminotransferase (Figure 2.9), creatine kinase (Figure 2.10) and lactate dehydrogenase (Figure 2.11). These data demonstrate that treatment with PrAg-L1 + LF, PrAg-U2 + LF or IC-PrAg + LF not only reduces primary B16-BL6 tumor burden, but also delays progression of tumor-associated morbidities.

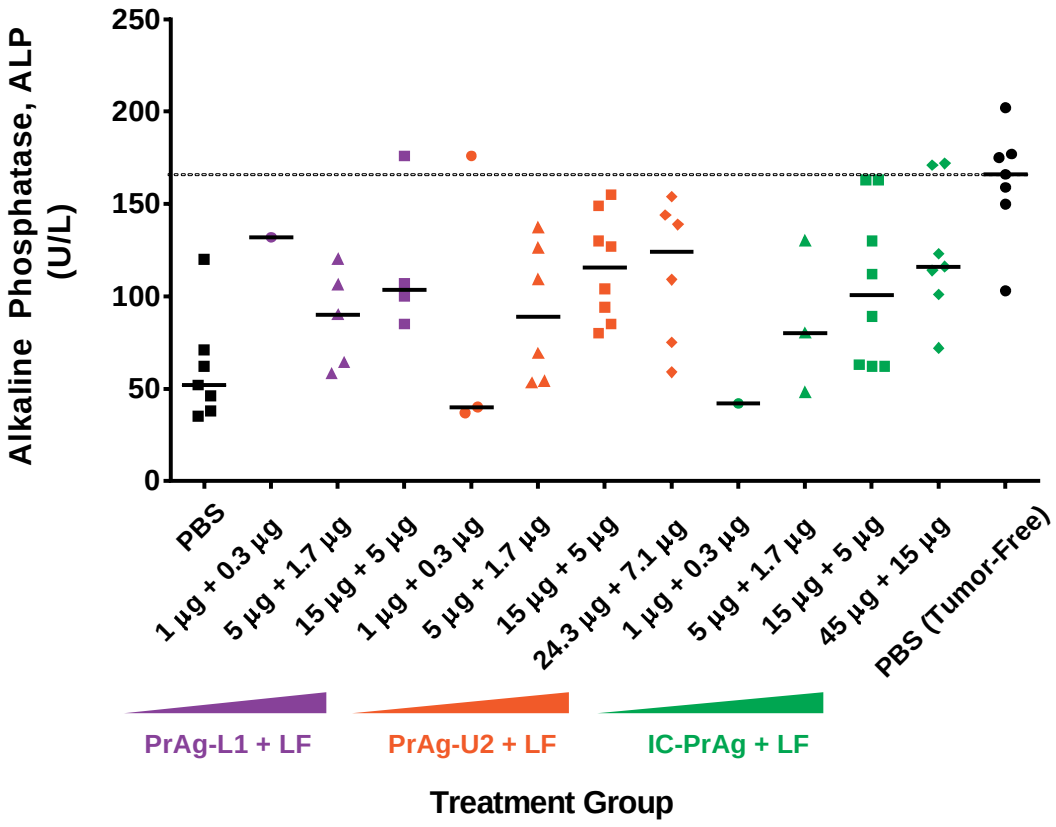

Figure 2.3: Dose-dependent normalization of alkaline phosphatase. Presence of B16-BL6 melanoma caused a significant reduction in alkaline phosphatase levels, which can be seen by comparing values for PBS-treated tumor-bearing mice [black squares, left] with PBS-treated tumor-free mice [black circles, right]. These alterations were normalized with increasing doses of MMP-activated PrAg-L1 + LF (purple), uPA-activated PrAg-U2 + LF (orange) or dual MMP/uPA-activated IC-PrAg + LF (green). Bars indicate medians, dashed line indicates disease-free median determined in parallel in a cohort of tumor-free, sham-treated, control mice.

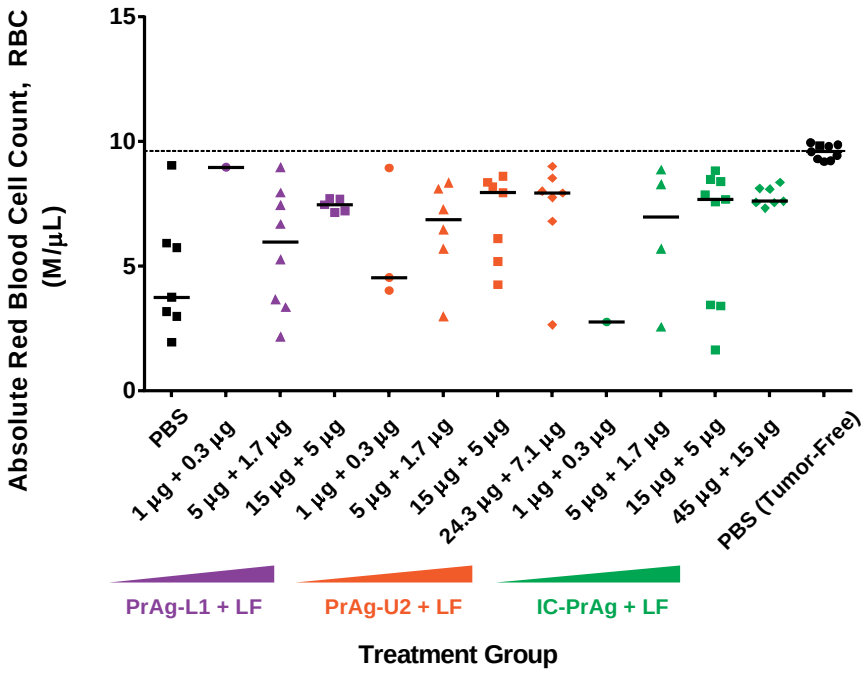

Figure 2.4: Dose-dependent normalization of absolute red blood cell count. Bars indicate medians, dashed line indicates disease-free median determined in parallel in a cohort of tumor-free, sham-treated, control mice.

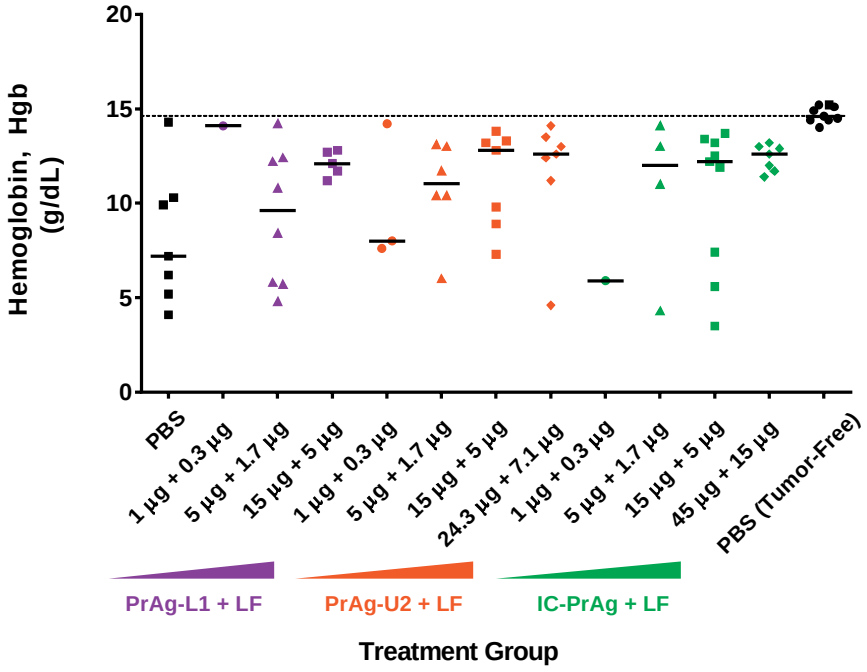

Figure 2.5: Dose-dependent normalization of hemoglobin. Bars indicate medians, dashed line indicates disease-free median determined in parallel in a cohort of tumor-free, sham-treated, control mice.

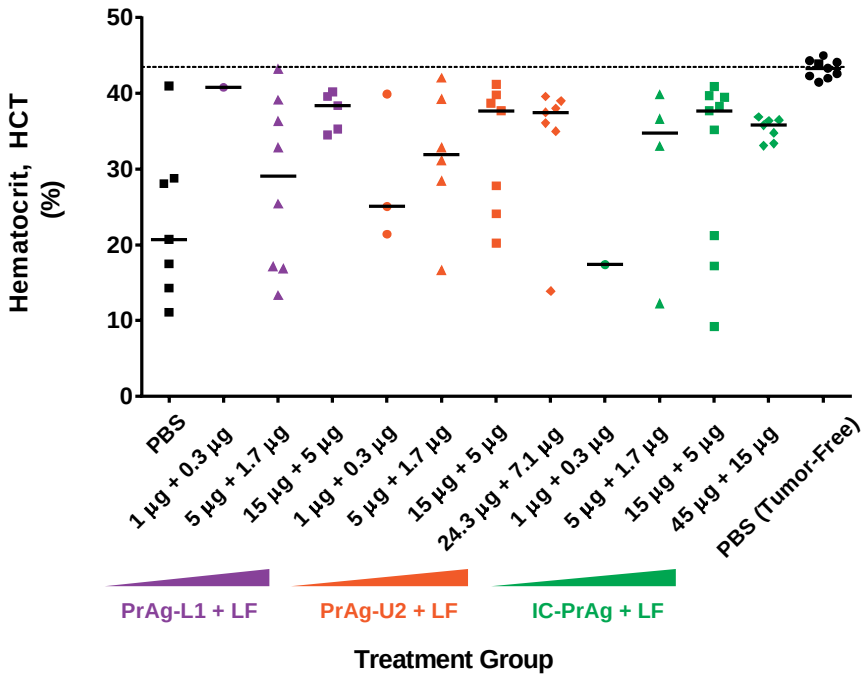

Figure 2.6: Dose-dependent normalization of hematocrit. Bars indicate medians, dashed line indicates disease-free median determined in parallel in a cohort of tumor-free, sham-treated, control mice.

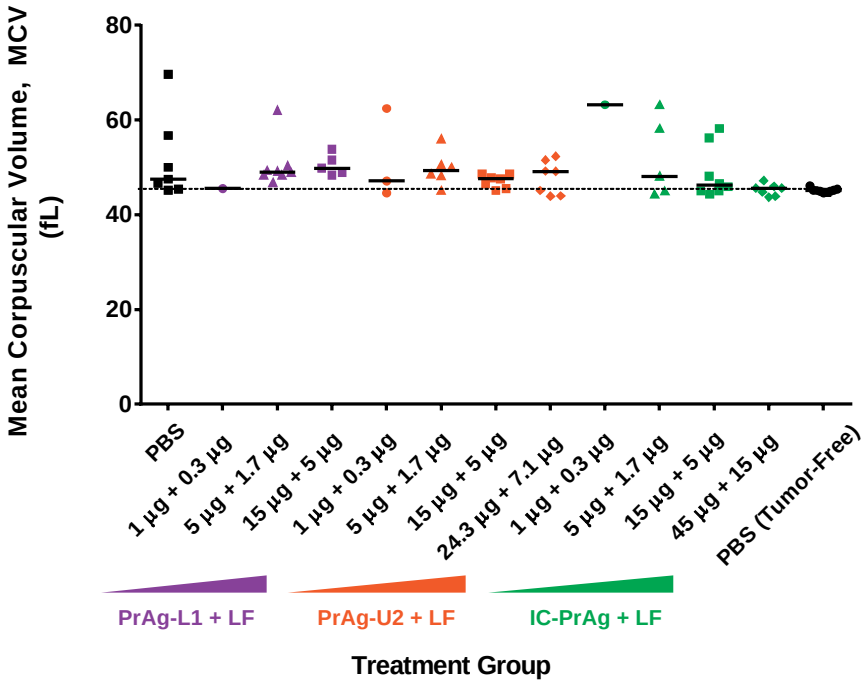

Figure 2.7: Dose-dependent normalization of mean corpuscular volume. Bars indicate medians, dashed line indicates disease-free median determined in parallel in a cohort of tumor-free, sham-treated, control mice.

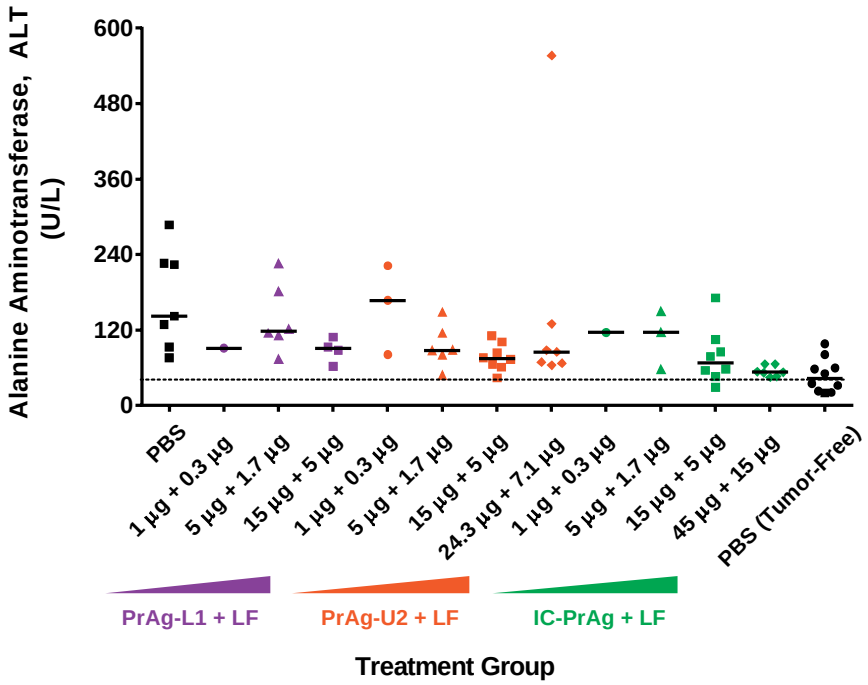

Figure 2.8: Dose-dependent normalization of alanine aminotransferase. Bars indicate medians, dashed line indicates disease-free median determined in parallel in a cohort of tumor-free, sham-treated, control mice.

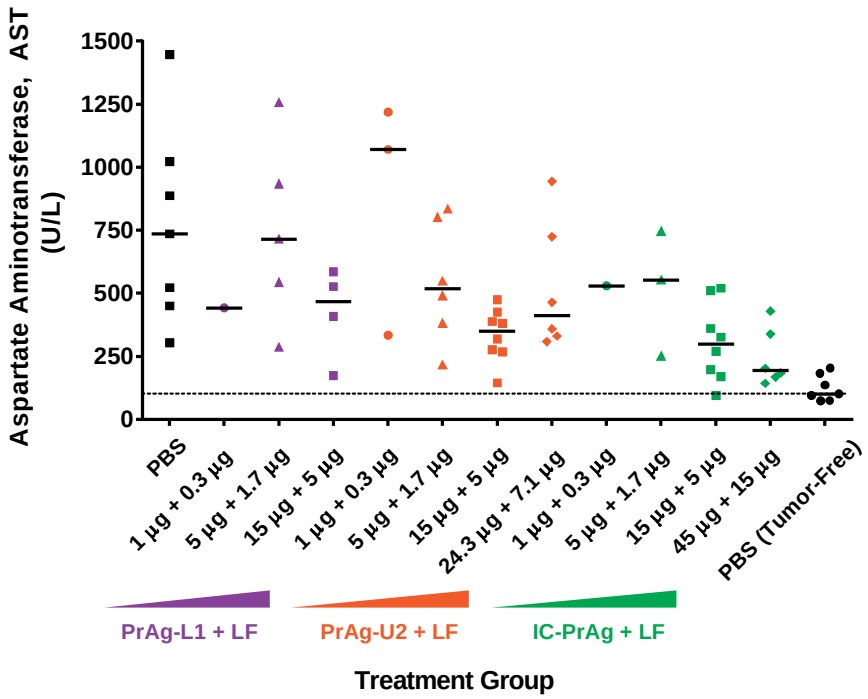

Figure 2.9: Dose-dependent normalization of aspartate aminotransferase. Bars indicate medians, dashed line indicates disease-free median determined in parallel in a cohort of tumor-free, sham-treated, control mice.

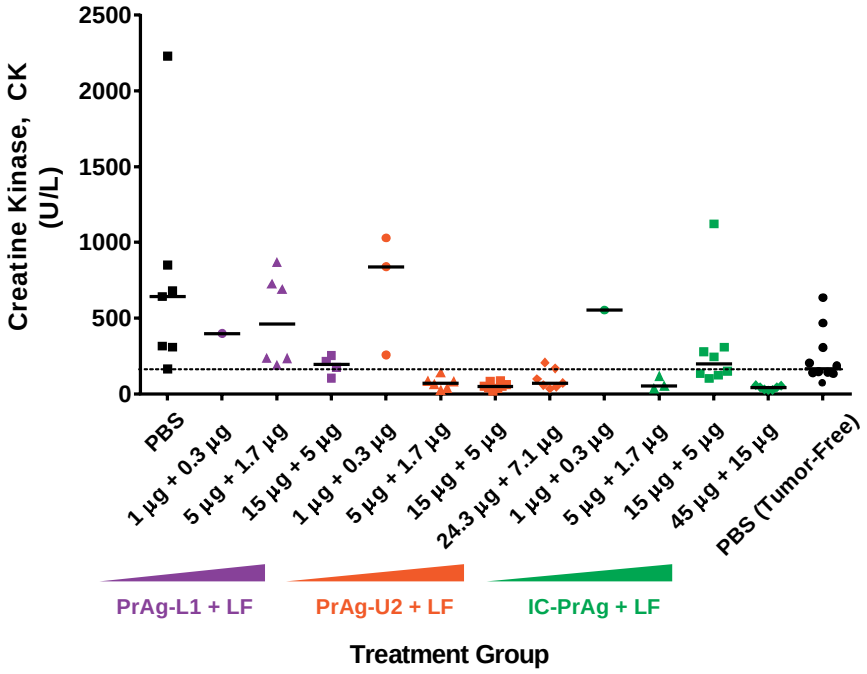

Figure 2.10: Dose-dependent normalization of creatine kinase. Bars indicate medians, dashed line indicates disease-free median determined in parallel in a cohort of tumor-free, sham-treated, control mice.

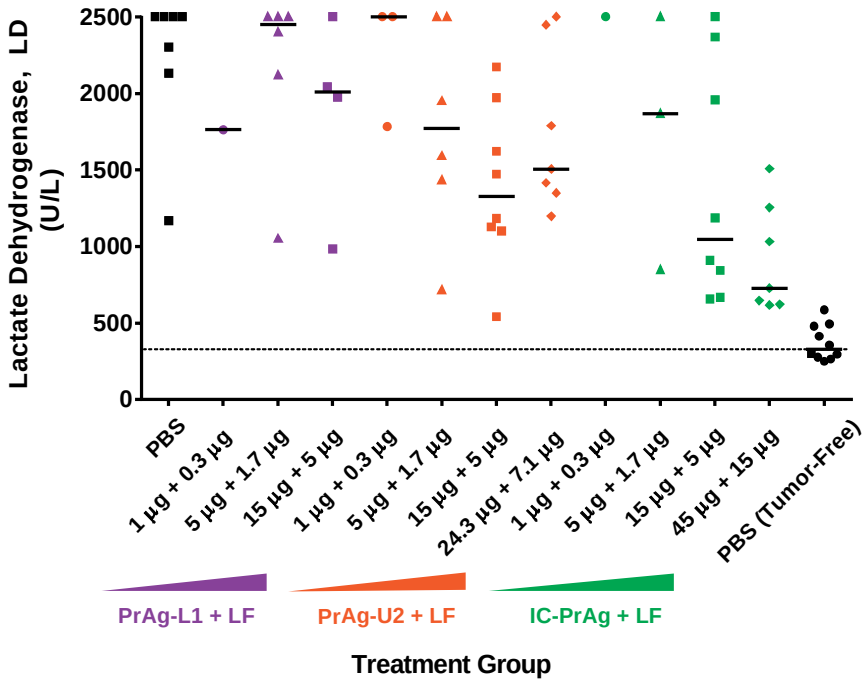

Figure 2.11: Dose-dependent normalization of lactate dehydrogenase. Bars indicate medians, dashed line indicates disease-free median determined in parallel in a cohort of tumor-free, sham-treated, control mice.

2.4.4.4 Engineered PrAg Variants Cause Dose-Dependent Thrombocytosis

Importantly, one toxin-mediated blood work alteration was identified; absolute platelet count was observed to increase in a dose-dependent manner when the engineered toxins were administered (Figure 2.12).

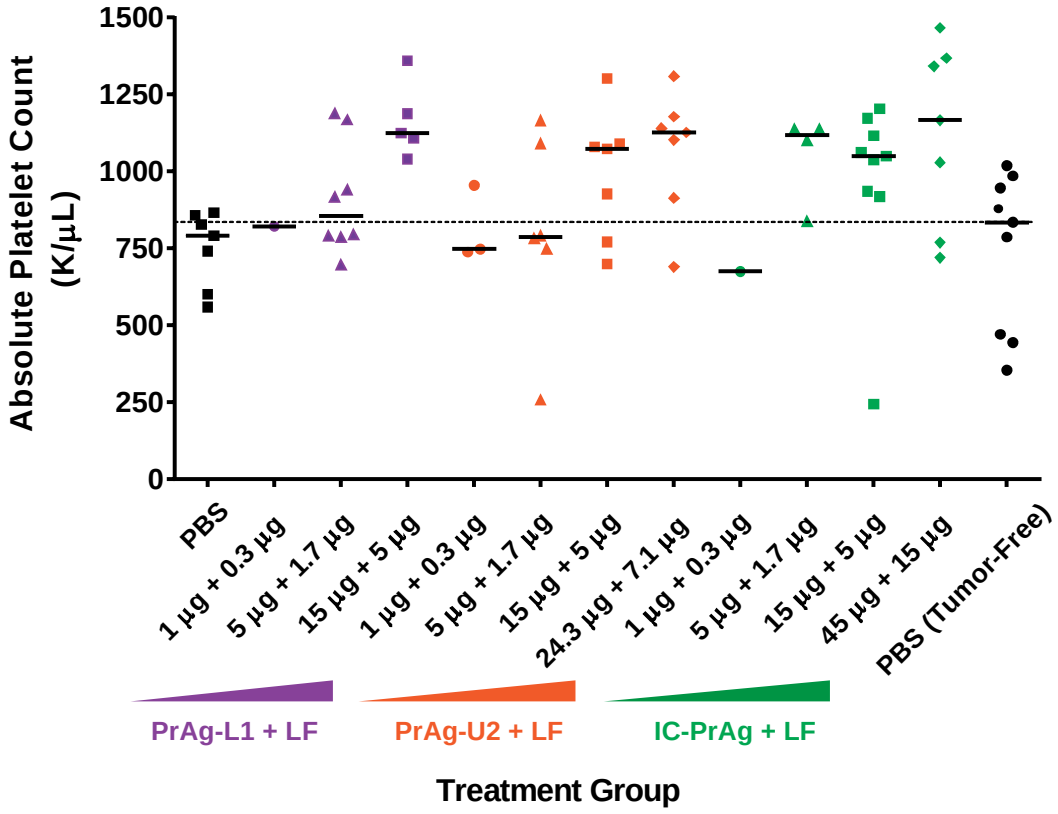

Figure 2.12: Engineered anthrax lethal toxins cause dose-dependent thrombocytosis. Mice treated with increasing doses of PrAg-L1 + LF (purple), PrAg-U2 + LF (orange) or IC-PrAg + LF (green) were found to have higher platelet counts than either tumor-bearing [black squares, left] or tumor-free [black circles, right] control cohorts. Bars indicate medians, dashed line indicates disease-free median determined in parallel in a cohort of tumor-free, sham-treated, control mice.

2.4.5 Comparative Mechanism

We next assessed if there were any mechanistic differences in the antitumor mode of action for the MMP-, uPA- or dual MMP/uPA-activated anthrax lethal toxins. B16-BL6 tumors treated with 15 µg PrAg-XX + 5 µg LF were evaluated for necrosis, apoptosis, vessel density and proliferation. It was observed that all three toxins exerted their antitumor effects predominantly through increasing apoptosis, which was found to be 55-, 12-, and 22-fold elevated following treatment with PrAg-L1 + LF, PrAg-U2 + LF and IC-PrAg + LF, respectively (Figure 2.13). No differences were observed in necrosis, vessel density and proliferation (Figure 2.14).

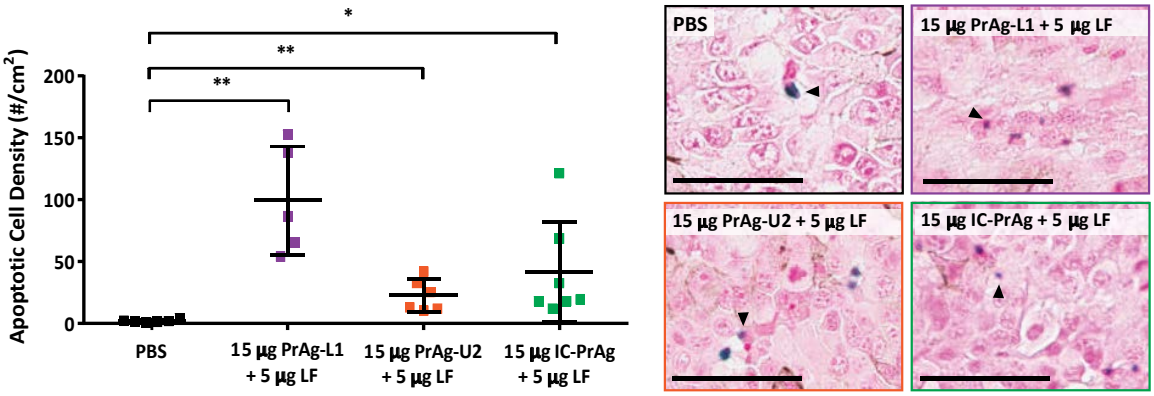

Figure 2.13: Mechanism of tumoricidal activity: apoptosis. Quantification of apoptosis in B16-BL6 tumors harvested from mice treated with 6 I.P. doses of engineered anthrax lethal toxins at a concentration of 15 µg engineered PrAg + 5 µg LF. In all panels: PBS (black), MMP-activated PrAg-L1 + LF (purple), uPA-activated PrAg-U2 + LF (orange) and dual MMP/uPA-activated IC-PrAg + LF (green). Student's two-tailed t-test; *, $p<0.05$; **, $P<0.01$. (Right) TUNEL stain. Arrowheads highlight examples of TdT positive apoptotic cells stained with TACS blue label, scale bars = 100 µm. Representative images are shown.

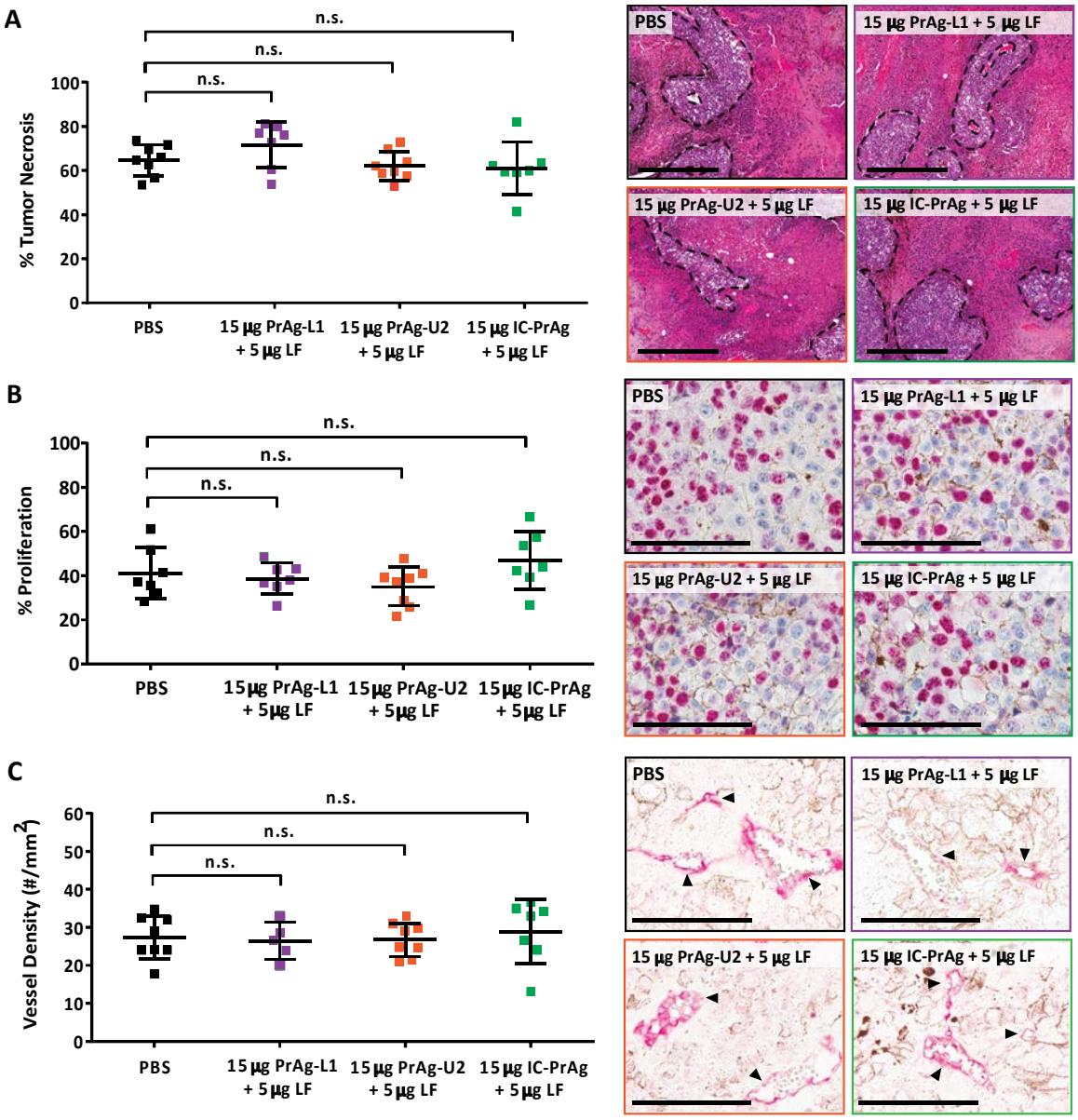

Figure 2.14: Mechanism of tumoricidal activity: necrosis, proliferation and vessel density. Quantification of necrosis (A), proliferation (B) and vessel density (C) in B16-BL6 tumors harvested from mice treated with 6 I.P. doses of engineered anthrax lethal toxins at a concentration of 15 µg engineered PrAg + 5 µg LF. In all panels: PBS (black), MMP-activated PrAg-L1 + LF (purple), uPA-activated PrAg-U2 + LF (orange) and dual MMP/uPA-activated IC-PrAg + LF (green). (A-C) Student's t-test, two-tailed; P = n.s. (A, right) H&E stain. Regions of viable cells are outlined with black dashed lines, scale bars = 500 µm. (B, right) Ki67 positive nuclei are stained pink with Vulcan FastRed, scale bars = 100 µm. (C, right) Arrowheads highlight CD31 positive blood vessels stained with Vulcan FastRed, scale bars = 100 µm. In all cases representative images are shown.

2.4.6 Calculation of Therapeutic Index

Therapeutic index was calculated using the following equation: MTD6/ED50, where ED50 was defined as the lowest dose administered where B16-BL6 tumor volume was reduced by a minimum of 50% on study day 14. MTD6 data is reported in Table 2.2, while ED50 data can be found in Table 2.4. IC-PrAg + LF was found to have the highest therapeutic index, 9, PrAg-U2 + LF had a therapeutic index of 6, and PrAg-L1 + LF had no separation between its maximum tolerated dose and ED50 with a therapeutic index of 1.

2.5 Discussion

We have previously established that engineered variants of anthrax PrAg can be utilized for the targeted intracellular delivery of cytotoxins. This unique system relies upon proteolytic activation by the tumor over-expressed proteases MMPs and uPA, and we and others have demonstrated that administration of these protease-activated PrAg derivatives, in conjunction with various cytotoxins, can be used to elicit significant *in vivo* antitumor responses in diverse cancer models including melanomas, carcinomas and sarcomas (105, 107, 115, 117, 118, 122).

Here we have performed the first in-depth toxicity characterization of MMP-, uPA- and dual MMP/uPA-activated PrAgs, when co-administered with wildtype anthrax LF. We found that, independent of the proteolytic-activation site, the GI tract is the primary target for toxicity. The observed GI toxicity is dose-dependent and is seen following both I.P. and I.V. administration of the engineered toxins. This is consistent with the mechanism of action of these agents, as while both MMPs and uPA are tightly regulated in normal homeostatic tissues, they are both expressed during tissue remodeling and repair (150). Therefore the presence of active MMPs and uPA in the GI tract, resulting in some off-target activation, is not unexpected.

Ongoing investigations in our laboratory focus on exploring the direct cellular target of the engineered toxins within the GI tract. Further understanding this toxicity is relevant not only to the continued characterization of our experimental agents, but also to the pathogenesis of wildtype toxin. While the primary toxicity associated with wildtype anthrax lethal toxin is hemodynamic shock and cardiovascular collapse (151-153) reports of gastrointestinal toxicity have occasionally been made in mice treated systemically with

purified wildtype toxin (154-158). In 2012, Sun et al. found that I.V. administration of sub-lethal doses of wildtype anthrax lethal toxin (~LD50) led to delayed onset GI toxicity within the surviving population that was strikingly similar in appearance to that reported herein, characterized by edema of the small intestine, villous necrosis, mucosal erosion and ulceration, and gross hemorrhage (158). While Sun et al., provide compelling evidence that their observed GI toxicity is a manifestation of direct epithelial damage, evidence also exists suggesting that this GI toxicity might instead be a consequence of GI smooth muscle injury, as Abi-Habib et al. reported that systemic administration of wildtype anthrax lethal toxin resulted in the development of fatal paralytic ileus without any alterations in intestinal histology (155). In our current study, mice treated with the highest doses of engineered toxin had evidence of reduced GI motility (full stomach/empty colon on gross necropsy) and epithelial damage (villous necrosis, denuded/ulcerated GI epithelia) and therefore, it will be interesting to determine the order in which these toxicities arise.

Following appearance of initial GI pathology, we have found that mice treated intraperitoneally with the engineered toxins consistently develop dose-dependent peritonitis. At this time, however, it remains unclear if this is a sequela to the GI toxicity, an unidentified direct toxicity, or a consequence of the I.P. route of administration. We now know that small intestinal dilation is the first observed pathology in mice treated with the engineered toxins. This GI dilation may increase the risk of needle perforation of the intestines during I.P. administration; intestinal perforation being a well-known risk factor for peritonitis. In this study, we did not see any evidence of chronic peritonitis in

mice treated with the engineered toxins I.V., but necropsies were not performed at high doses exceeding the I.V. MTD6s where this manifestation of toxicity might be expected.

During the course of our efficacy studies, we became aware of one additional toxin-dependent change: Tumor-bearing mice treated I.P. with the MMP-, uPA- or dual MMP/uPA-activated toxins displayed a dose-dependent increase in absolute platelet count. The clinical relevance of this mild reactive thrombocytosis is unclear, however this effect should certainly be kept in mind as further characterization is performed on these agents. Platelet count should likely be monitored with treatment, and it is possible that recipients would benefit from prophylactic administration of an anti-coagulant, such as aspirin, to reduce risk of thrombosis, the primary complication associated with thrombocytotic state.

With regard to efficacy, we found that each of the three toxin variants lead to significant reduction in primary B16-BL6 tumor burden and delayed progression of disease-related morbidities in a dose-dependent manner. Each toxin exhibited similar activity when administered at protein equivalent doses and in all cases the primary mechanism of tumoricidal activity was increased apoptosis. While target-organ toxicity and efficacy were similar amongst the variants, IC-PrAg + LF, an engineered anthrax lethal toxin requiring co-localized activation by both MMPs and uPA, emerged as the best candidate exhibiting the highest MTD6 and the highest threshold for target-organ toxicity, while maintaining significant antitumor efficacy.

While here we demonstrate that IC-PrAg + LF has significant antitumor activity towards B16-BL6 melanoma, it is relevant to note that a highly similar toxin combination, IC-PrAg + LF-HMAGG (a version of wildtype anthrax LF containing two non-native

amino acids, HM, at its N-terminus), has been recently shown to exhibit potent *in vivo* activity towards HN12, HN6, Hep2 and Cal27 head and neck squamous cell carcinomas, which is described in detail in Chapter 3 of this dissertation (122). Given the strong similarities between these two toxin combinations, it is highly likely that IC-PrAg + LF will also exhibit broad antitumor efficacy, and this expectation, paired with our current demonstration that effective doses can be administered that are far below the threshold for toxicity, supports the assertion that IC-PrAg + LF is a promising candidate for further development as an anti-cancer agent. Indeed, veterinary clinical trials are currently in progress evaluating IC-PrAg + LF as a treatment for naturally-occurring feline oral squamous cell carcinoma, presented in Chapter 4 of this dissertation.

Chapter 3:

Efficient Treatment of Human Head and Neck Squamous Cell Carcinoma Xenografts by Systemic Administration of a Dual MMP/uPA-activated Anthrax Lethal Toxin

This chapter contains content and figures taken from a previously published article in which the dissertation author was a primary contributing author:

Schafer JM*, Peters DE*, Morley T*, Liu S, Molinolo AA, Leppla SH, Bugge TH. Efficient targeting of head and neck squamous cell carcinoma by systemic administration of a dual uPA and MMP-activated engineered anthrax toxin. (2011) *PLoS One* 6(5):e20532. **Authors contributed equally.*

Specific Experimental Contributions:

All data was analyzed by, and all figures were prepared by, D.E.P

In vitro cytotoxicity assays were performed by T.M. and S.L. (Data in Figures 3.1, 3.2, 3.3)

In vivo xenograft trials were performed by J.M.S., T.M. and S.L. (Data in Figures 3.4, 3.5)

In vivo xenograft trials, immunohistochemistry and quantification were performed by D.E.P. and A.A.M. (Data in Figures 3.6, 3.7)

Proteins were expressed and purified by Rasem Fattah.

S.L., S.H.L and T.H.B contributed to experimental design.

3.1 Abstract

Head and neck squamous cell carcinoma (HNSCC) is the sixth most common cancer occurring worldwide by incidence. Although considerable progress has been made toward elucidating the etiology of this disease, the prognosis for individuals diagnosed with HNSCC remains poor underscoring the need for development of additional treatment modalities. HNSCC is characterized by the upregulation of a large number of proteolytic enzymes, including urokinase plasminogen activator (uPA) and an assortment of matrix metalloproteinases (MMPs) that may be expressed by tumor cells, by tumor-supporting stromal cells, or by both. Here we have explored the use of an engineered anthrax lethal toxin requiring activation by the combined cell-surface activities of uPA and MMPs for the treatment of HNSCC. We have found that this dual MMP/uPA-activated anthrax lethal toxin displays strong systemic antitumor activity towards four xenografted human HNSCC cell lines. Interestingly, the HNSCC cell lines were insensitive to the dual MMP/uPA-activated toxin when cultured *in vitro*, suggesting that either the toxin targets the tumor-supporting stromal cell compartment or that tumor cell reliance on ERK/MAPK signaling differs under *in vivo* and *in vitro* conditions. Ultimately, we demonstrate that a dual MMP/uPA-activated anthrax lethal toxin exhibits strong antitumor activity in multiple xenograft models of human HNSCC and is a promising candidate for further development as an anti-HNSCC agent.

3.2 Introduction

With more than 500,000 new cases diagnosed each year, head and neck squamous cell carcinoma (HNSCC) represents the sixth most common cancer occurring worldwide (159). Although the risk factors and molecular pathways that underlie HNSCC development are now well-known, with conventional multimodal treatment the five-year survival rate following diagnosis has remained unchanged for many decades highlighting the relevance of developing novel therapeutics (22, 160-163).

The overexpression, prognostic significance, and causal involvement of extracellular/pericellular proteases in the progression of HNSCC have been extensively studied (reviewed in (125, 164-166)). Multiple proteases are known to be expressed at very high levels by HNSCC tumor cells, stromal cells, or both, including: urokinase plasminogen activator (uPA), tissue plasminogen activator, matrix metalloproteinases (MMP)-1, -2, -3, -7, -9, -10, -11, -13, and -14, cathepsins B, D, H, and L, kallikreins 5, 7, 8, and 10, and matriptase (167-188).

Strategies to therapeutically exploit the signature overexpression of proteolytic enzymes in cancer have mostly focused on inhibiting their enzymatic activity in order to blunt invasive and metastatic processes (150, 189, 190). More recently, however, strategies have been devised to generate tumor cytotoxic pro-drugs that are activated by specific tumor-expressed proteases (191-193). In this regard, we previously generated an engineered version of anthrax toxin that is activated by the combined cell-surface activities of uPA and MMPs, and we have shown that this toxin has greatly diminished off-target toxicity when compared to native anthrax toxin (121). This dual MMP/uPA-activated toxin consists of two separate proteins: PrAg-L1-I210A, an engineered anthrax

protective antigen (PrAg) activated by MMPs, and PrAg-U2-R200A, an engineered PrAg that is activated by uPA. PrAg-L1-I210A and PrAg-U2-R200A also each harbor additional, but different, mutations in the anthrax lethal factor (LF) binding site that make heptamers composed of PrAg-L1-I210A alone or of PrAg-U2-R200A alone unable to bind LF. However, heptamers that are composed of a mixture of PrAg-L1-I210A and PrAg-U2-R200A can form functional LF binding sites through intermolecular complementation; we therefore refer to the combination of PrAg-L1-I210A and PrAg-U2-R200A as intercomplementing PrAg (IC-PrAg).

Because MMPs and uPA are consistently overexpressed in human HNSCC, here we explored the potential use of IC-PrAg, in combination with LF, as a novel targeted treatment for this disease. Indeed, we found that systemic administration of this dual MMP/uPA-activated anthrax lethal toxin led to regression of several xenografted human HNSCC cell lines. Interestingly, the *in vivo* efficacy of the toxin was independent of the sensitivity of the cultured tumor cells to the toxin, suggesting that this toxin may inhibit tumor growth by targeting both the tumor cell compartment and the stromal cell compartment.

3.3 Materials and Methods

3.3.1 Ethics Statement

All animal work was performed in accordance with protocols approved by the National Institute of Dental and Craniofacial Research Animal Care and Use Committee (Animal Study Proposal Numbers: 09-523 and 10-585).

3.3.2 Protein Purification

Recombinant PrAgs (PrAg-WT, PrAg-L1-I210A and PrAg-U2-R200A) and cytotoxins (LF and FP59) were generated and purified as previously described (98, 121, 194). The LF used here has the non-native N-terminal sequence of HMAGG (93).

3.3.3 Cell Culture

Five human HNSCC cell lines were utilized in this study: Cal27, Hep2, HN6, HN12, and HN30 (195-197). All cell lines were cultured in a humidified 5% CO_2 environment at 37^{o}C. Cells were maintained in Dulbecco's Modified Eagle Medium (DMEM) supplemented with 10% fetal bovine serum and 1% penicillin/streptomycin (Invitrogen, Carlsbad, CA).

3.3.4 *In vitro* Cytotoxicity Assays

Cytotoxicity was assessed using a colorimetric 3-(4,5-dimethylthiazol-2-yl)-2,5-diphenyltetrazolium bromide (MTT) assay in 96-well plates (198). Cells exhibiting ~40% confluence were incubated with serial dilutions of PrAg-WT (0-10 nM) or PrAg-L1-I210A + PrAg-U2-R200A (0-10 nM) in the presence of either FP59 (1.9 nM) or LF (5.5 nM) to a final volume of 200 μl per well. Cell viability was determined after 48 h for the FP59 assays, and 4 h for the LF assays. All assays were performed in triplicate and representative data are shown.

3.3.5 Animals

Female Hsd:Athymic Nude-Foxn1nu mice (Harlan Laboratories Inc., Indianapolis, IN) between 4 and 6 weeks of age were used in this study. Animals were housed in a pathogen-free environment certified by the Association for Assessment and Accreditation of Laboratory Animal Care International.

3.3.6 *In vivo* Tumor Xenograft Model

Cells (9 x 10^5 per mouse) were injected in the mid-scapular subcutis. When tumors reached a volume of 50-100 mm^3, the mice were divided into groups of ten mice with equivalent mean tumor sizes. Treatment was initiated on day 0. Mice received intraperitoneal (I.P.) injections of 500 µl PBS or PrAg-L1-I210A + PrAg-U2-R200A + LF in 500 µl PBS, respectively. Specific doses included: 25 µg PrAg-L1-I210A + 25 µg PrAg-U2-R200A + 17 µg LF (HN12 xenograft-bearing mice) or 20 µg PrAg-L1-I210A + 20 µg PrAg-U2-R200A + 13 µg LF (Cal27, HN6 and Hep2 xenograft-bearing mice). Mice received five total injections on a Monday, Wednesday, Friday dosing schedule. At the time of treatment, an investigator unaware of the treatment group measured the longest and shortest tumor diameters with digital calipers (FV Fowler Company, Inc., Newton, MA). Tumor volume was estimated using the equation: V = (length in mm * (width in $mm)^2$)/2 (130). The statistical significance of differences in tumor sizes and mouse weight were determined using the two-tailed Student's t-test.

3.3.7 Histopathological Analysis

HN12 (n=5) and Hep2 (n=4) tumor-bearing mice were treated I.P. with 500 µL PBS or with 15 µg PrAg-U2-R200A + 15 µg PrAg-L1-I210A + 10 µg LF in 500 µL PBS on study days 0, 2 and 4. The mice were euthanized by CO_2 inhalation 24 h after the last

injection. Tumors were excised, fixed in 4% paraformaldehyde for 24 hours, embedded in paraffin, sectioned, and stained with hematoxylin and eosin (H&E). Sections with identifiable carcinoma cells on H&E were also stained with a monoclonal rabbit anti-mouse CD31 (Santa Cruz Biotechnology, Inc., Santa Cruz, CA) and a polyclonal rabbit anti-human Ki67 (Novocastra Laboratories, Ltd., Newcastle, UK). TUNEL staining was performed by Histoserv, Inc. (Germantown, MD). Images were captured using an Aperio T3 Scanscope (Aperio Technologies, Vista, CA) and were quantified using Aperio Imagescope Software (Aperio Technologies, Vista, CA) by a blinded investigator. Statistical significance of differences for necrosis, apoptosis, cellular proliferation and tumor vascularization were determined using the Student's t-test, two-tailed, using GraphPad Prism software.

3.4 Results

3.4.1 Expression of Anthrax Toxin Receptors by Human HNSCC Cells

We first explored whether HNSCC cells express functional anthrax toxin receptors by exposing five human HNSCC cell lines, Cal27, Hep2, HN6, HN12, and HN30, to increasing concentrations of wildtype PrAg (PrAg-WT) in combination with 1.9 nM FP59 (Figure 3.1). FP59 is a fusion protein consisting of the N-terminal PrAg binding domain of LF coupled to the ADP-ribosylation domain of *Pseudomonas aeruginosa* exotoxin A. When translocated into the cytoplasm via PrAg, FP59 efficiently kills all cells by ADP-ribosylating elongation factor 2, resulting in inhibition of protein synthesis (94). We observed that this combination of PrAg-WT + FP59 killed all of the HNSCC cell lines with LD50s ranging from less than 7 to 400 pM, demonstrating the presence of functional anthrax toxin receptors.

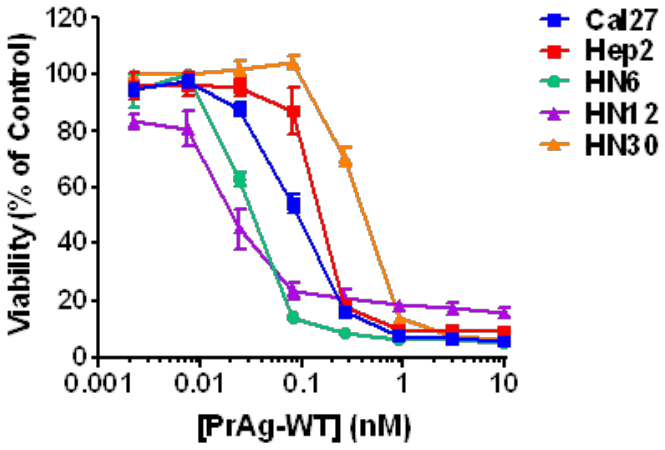

Figure 3.1: Human HNSCC cell lines express functional anthrax toxin receptors. Cal27 (blue), Hep2 (red), HN6 (green), HN12 (purple), and HN30 (orange) human HNSCC cell lines were incubated with varying concentrations of wildtype PrAg in combination with 1.9 nM FP59, an engineered cytotoxin. All cell lines tested exhibited dose-dependent lethality, demonstrating the presence of functional anthrax toxin receptors. Mean ± s.d. is plotted, n=4.

3.4.2 MMP and uPA Proteolytic Activity of Human HNSCC Cells

To assess if the human HNSCC cell lines possess uPA and MMP proteolytic activity, we next exposed the five cell lines to FP59 in combination with increasing concentrations of IC-PrAg (PrAg-L1-I210A + PrAg-U2-R200A) (Figure 3.2). Three of the HNSCC cell lines (Cal27, HN6, HN12) were toxin sensitive (LD50s, 0.5 nM to 8 nM) demonstrating functional uPA and MMP expression, while the two other cell lines, Hep2 and HN30, were toxin resistant indicating the absence of uPA activity, MMP activity, or both.

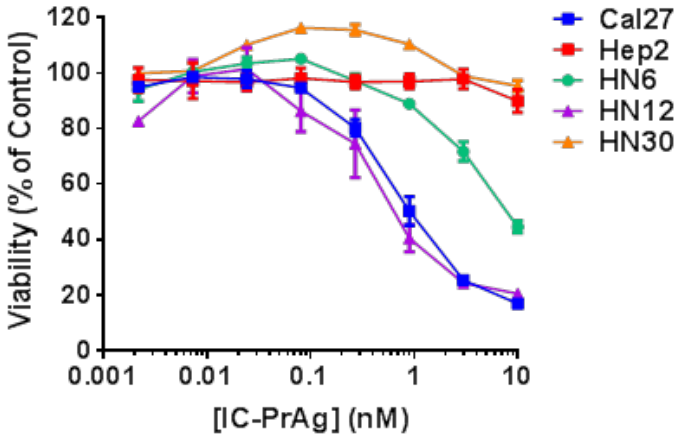

Figure 3.2: uPA and MMP proteolytic activity of human HNSCC cell lines. Cal27 (blue), Hep2 (red), HN6 (green), HN12 (purple), and HN30 (orange) human HNSCC cell lines were incubated with varying concentrations of IC-PrAg (PrAg-L1-I210A + PrAg-U2-R200A) in combination with 1.9 nM FP59. Cal27, HN6 and HN12 cell lines were toxin sensitive, while Hep2 and HN30 cells were resistant to toxin even at the highest concentrations. Mean ± s.d. is plotted, n=4.

3.4.3 *In vitro* Sensitivity of Human HNSCC Cells to Anthrax Lethal Toxin

We next determined if the five HNSCC cell lines were sensitive to wildtype anthrax lethal factor (LF) when grown in culture by incubating them with 5.5 nM LF in combination with increasing concentrations of either PrAg-WT (Figure 3.3A) or IC-PrAg (Figure 3.3B). LF is a zinc metalloproteinase that once internalized, via PrAg binding, cleaves and inactivates mitogen-activated protein kinase kinases (MEKs) disrupting the

extracellular signal-related kinase (ERK)/mitogen activated protein kinase (MAPK) pathway (86-88). All five HNSCC cell lines remained viable when treated with either PrAg-WT + LF (Figure 3.3A) or IC-PrAg + LF (Figure 3.3B), demonstrating that these cell lines are not reliant on MEK/MAPK signaling activity for survival in culture.

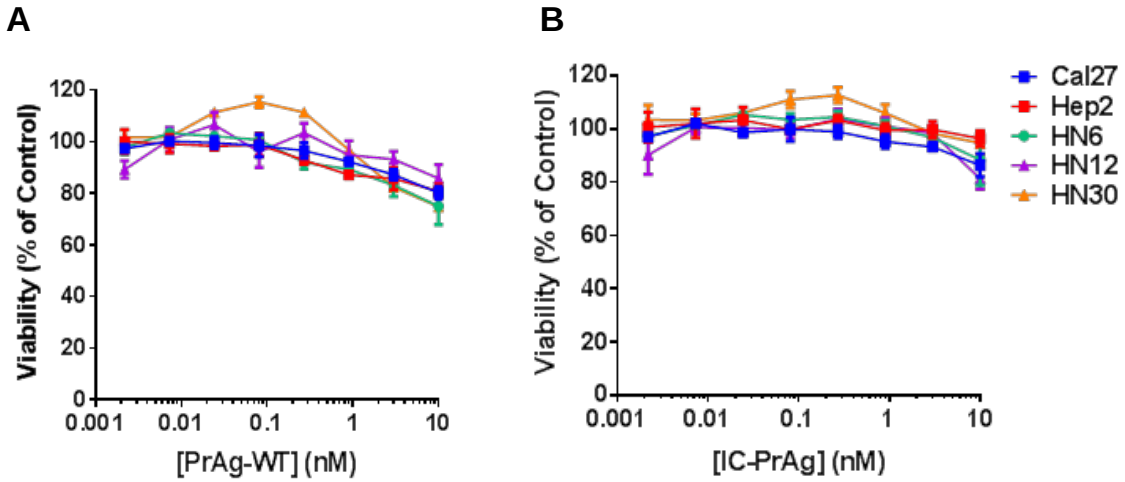

Figure 3.3: LF sensitivity of human HNSCC cell lines *in vitro*. Cal27 (blue), Hep2 (red), HN6 (green), HN12 (purple), and HN30 (orange) human HNSCC cell lines were incubated with varying concentrations of either wildtype PrAg (A) or IC-PrAg (B) in combination with 5.5 nM LF. All cell lines were resistant to LF cytotoxicity. Mean ± s.d. is plotted, n=4.

3.4.4 *In vivo* Antitumor Efficacy of IC-PrAg + LF

Cal27, Hep2, HN6, and HN12 HNSCC cell lines form solid tumors when xenografted to immunocompromised mice and were therefore suitable for assessing the *in vivo* efficacy of IC-PrAg in combination with LF. These four cell lines were transplanted subcutaneously in nude mice, solid tumors of 50-100 mm^3 were allowed to form, and then mice were then treated with five intraperitoneal injections of intercomplementing anthrax lethal toxin, or with PBS as a control (Figure 3.4).

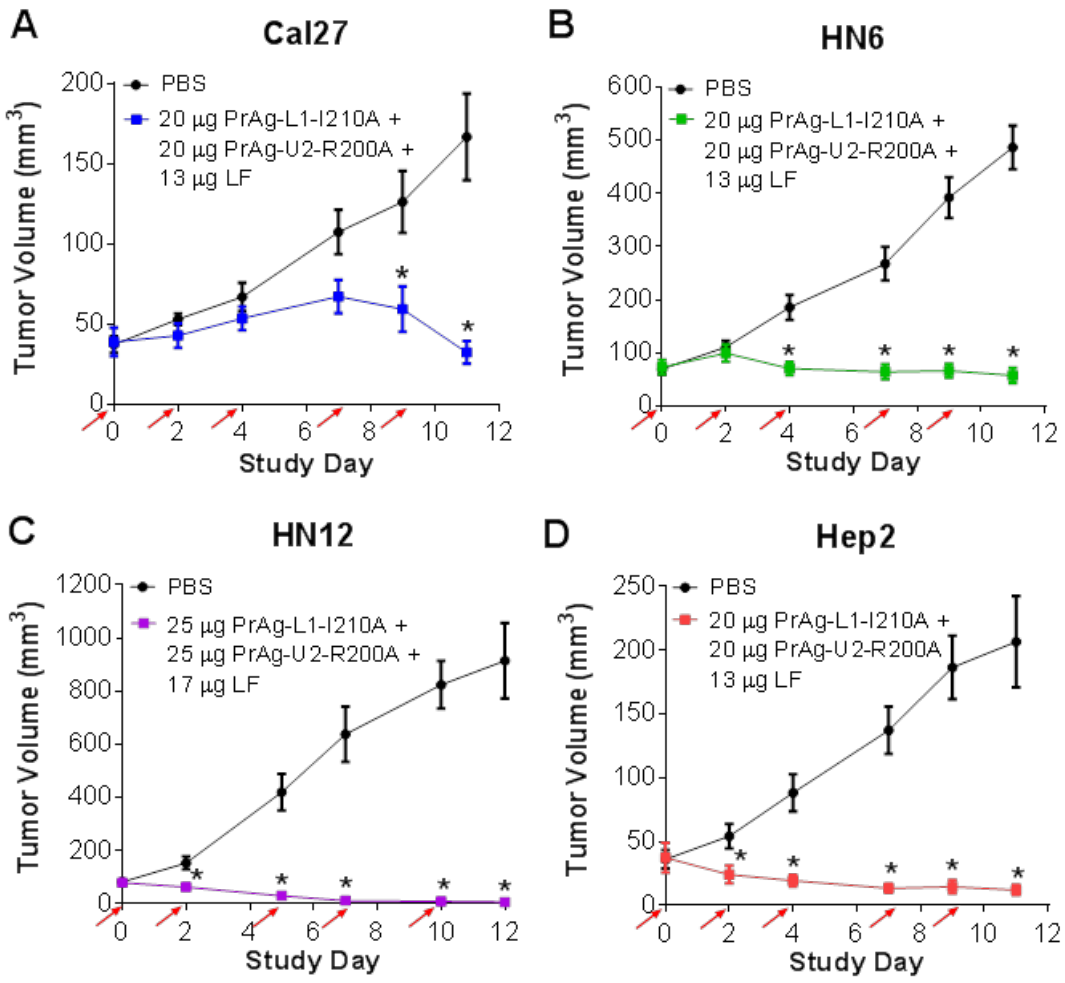

Figure 3.4: Treatment of HNSCC xenografts with systemic administration of intercomplementing anthrax lethal toxin. Nude mice bearing subcutaneous Cal27 (A), HN6 (B), HN12 (C), and Hep2 (D) HNSCC xenografts were treated with five intraperitoneal doses of PBS (black) or PrAg-L1-I210A + PrAg-U2-R200A + LF (color) at the time points indicated by red arrows. 10 mice were included in each treatment group. Data are expressed as mean ± s.e.m.; *, P <0.01, Student's t-test, two-tailed. n=10 per treatment group.

Cal27, HN6, and HN12 tumors were all efficiently treated with the toxin, consistent with the presence of both uPA and MMP activities in cell culture (Figure 3.4A-C). At treatment cessation, average tumor sizes in toxin-treated mice ranged from 0.6 to 26% of PBS-treated tumors. Interestingly, although Hep2 cells did not express uPA and/or MMP activity sufficient for toxin activation in culture, the Hep2 tumors were also treated efficiently *in vivo* with the average tumor size of toxin-treated mice being just 6% of the

average tumor size of PBS-treated mice at treatment cessation (Figure 3.4D). The greatest response to the dual MMP/uPA-activated anthrax lethal toxin was observed in HN12-bearing mice, with complete regression observed in 40% of treated mice; these mice remained tumor-free when observed for up to one year after treatment cessation.

The toxin was generally well tolerated. 2/40 of the toxin-treated mice died within the treatment period, whereas no death was observed in PBS-treated groups (P = n.s., chi-square test, two tailed). The largest weight loss in toxin-treated mice as compared to PBS-treated mice was observed at study day 11 in all trials (Figure 3.5). Excluding the mass attributed to tumor burden, the average body weight of all toxin treated mice was 8.3 percent lower than the average body weight for all mice in PBS-treatment groups on study day 11 ($P < 0.0004$, Student's t-test, two-tailed).

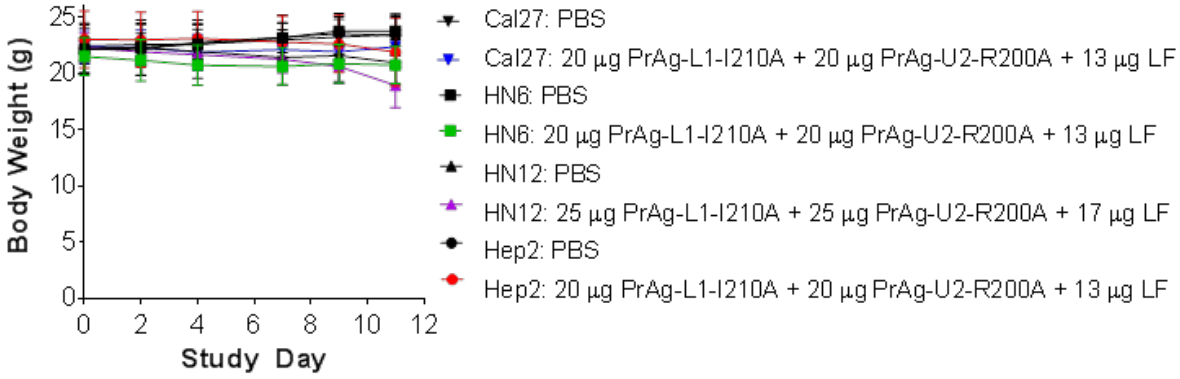

Figure 3.5: Body weights of HNSCC xenograft-bearing mice treated with PBS or with intercomplementing anthrax lethal toxin. Data are expressed as mean ± s.d. n=10 per treatment group.

3.4.5 Mechanism of Tumoricidal Activity

We next examined the mechanistic basis for the potent systemic anti-HNSCC activity of IC-PrAg + LF *in vivo*. For this purpose HN12 cells (sensitive to IC-PrAg + FP59 *in vitro*) and Hep2 cells (insensitive to IC-PrAg + FP59 *in vitro*) were transplanted in nude mice, and established tumors were treated with three intraperitoneal doses of toxin or PBS. The tumors were excised at study day 5 (as per Figure 3.4) and histological sections were subjected to an unbiased quantitative histomorphometric analysis.

3.4.5.1 HN12 Xenografts

No tumor cells were identified in histological sections from 2/5 toxin-treated HN12 tumors, demonstrating complete tumor regression in these samples. The three remaining toxin-treated HN12 tumors had a four-fold increase in necrosis when compared to PBS-treated tumors (Figure 3.6A). Cell proliferation in viable areas of toxin-treated tumors was reduced twelve-fold, as determined by staining of the cell proliferation marker, Ki67 (Figure 3.6B). In addition, vessel density was three-fold reduced (Figure 3.6C) and the apoptotic index was increased 13-fold (Figure 3.6D).

3.4.5.2 Hep2 Xenografts

Interestingly, unlike the case for the HN12 tumors examined above, IC-PrAg + LF exerted its antitumor effect in Hep2 tumors solely through increasing necrosis, which was found to be 13-fold increased (Figure 3.7A). Cell proliferation, vessel density, and apoptotic index were unaffected by toxin-treatment (Figure 3.7B-D).

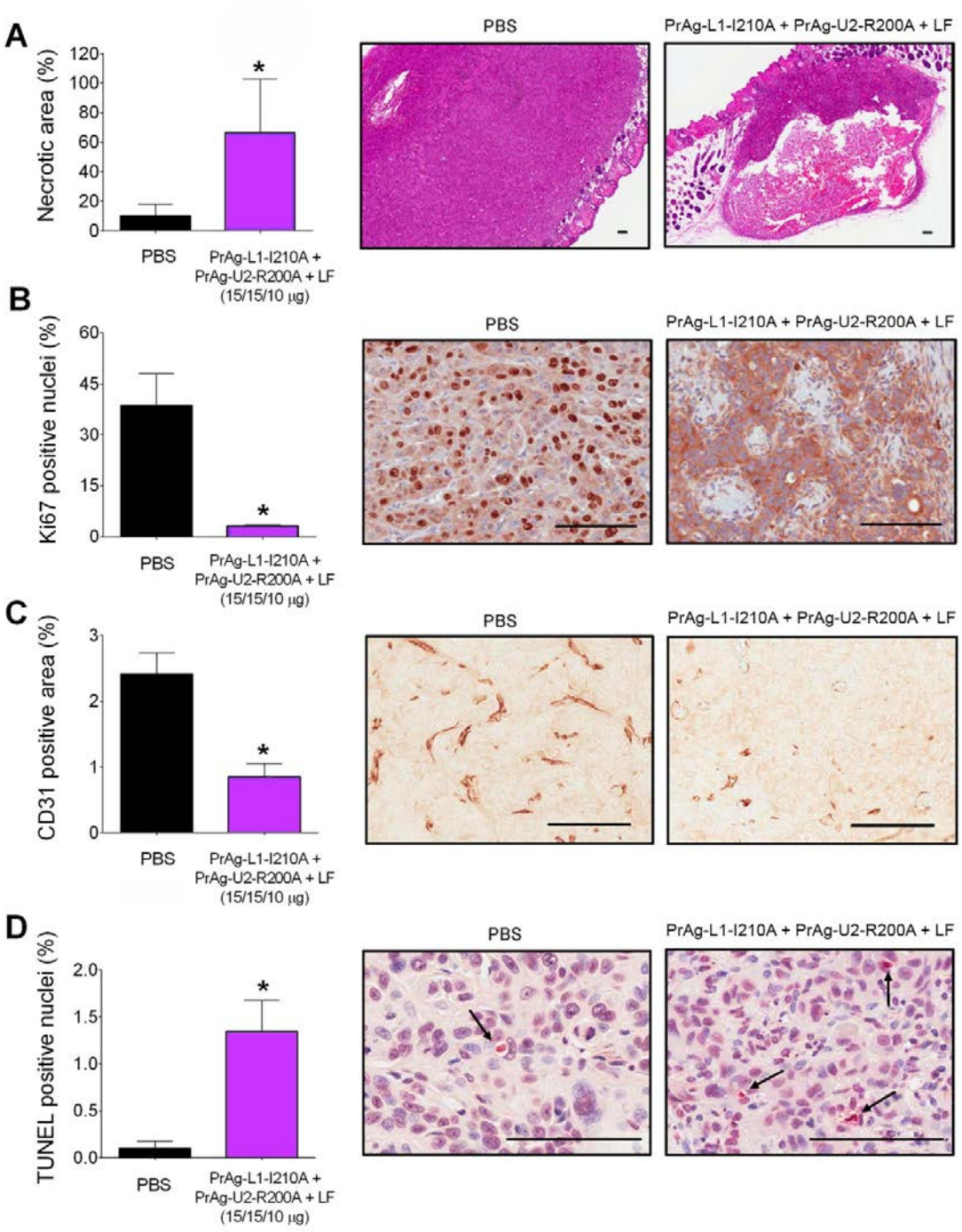

Figure 3.6: Mechanism of antitumor activity in HN12 xenografts. Increased necrosis (**A**), decreased proliferation (**B**), decreased tumor vascularization (**C**), and increased apoptosis (**D**) were observed in HN12 xenografts treated with 3 I.P. doses of intercomplementing anthrax lethal toxin (purple bars, right panels) relative to PBS treated controls (black bars, left panels). Columns, mean; bars, s.d., *, P <0.05, Student's t-test, two-tailed, n=5 per treatment group. In all cases, representative images are shown. Scale bars =100 μM. Arrows in panel D highlight examples of apoptotic nuclei.

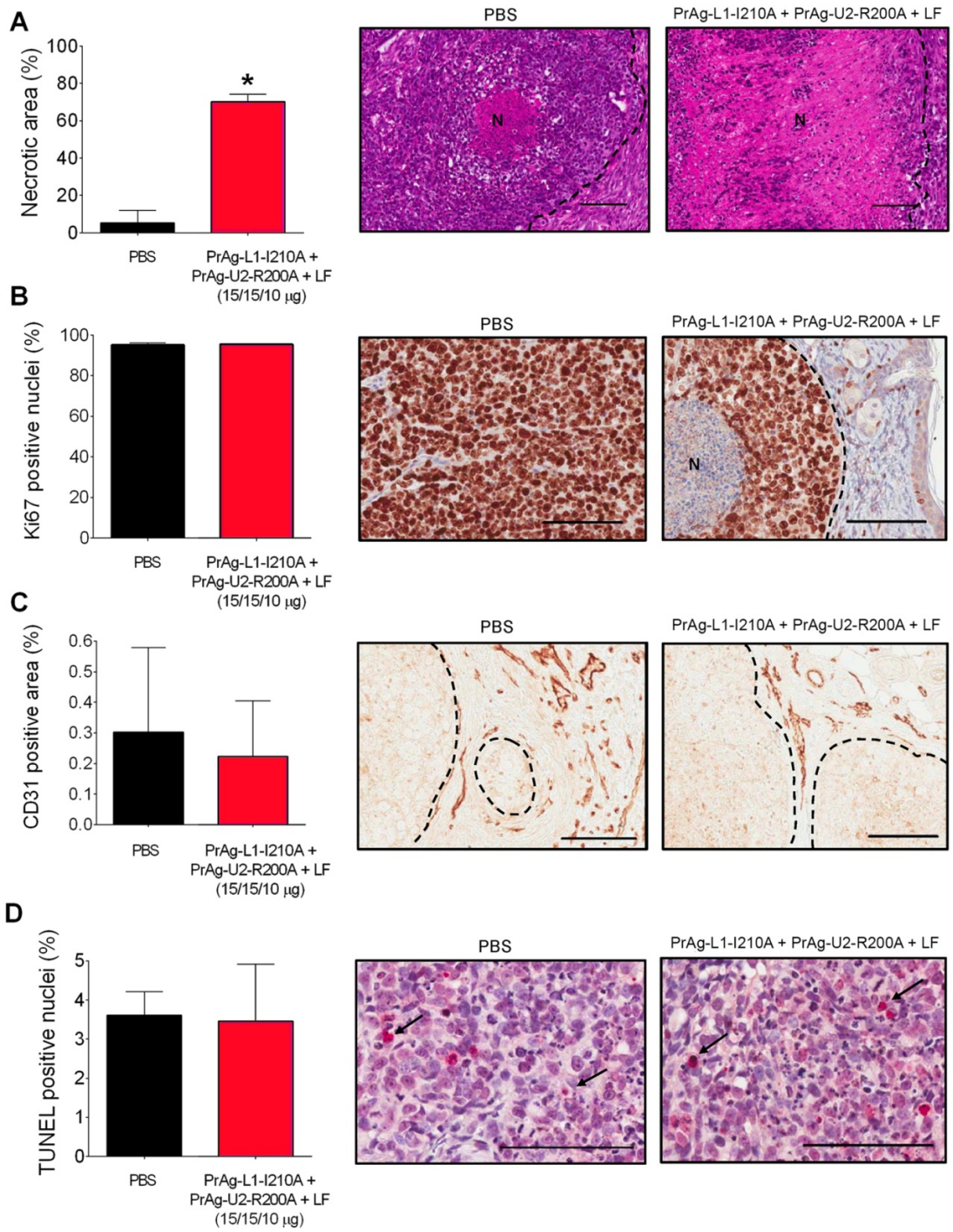

Figure 3.7: Mechanism of antitumor activity in Hep2 xenografts. Increased necrosis (A) was observed in Hep2 xenografts treated with 3 I.P. doses of intercomplementing anthrax lethal toxin (red bars, right panels) relative to controls (black bars, left panels). No differences in proliferation (B), tumor vascularization (C) or apoptosis (D) were observed. Columns, mean; bars, s.d., *, P <0.05, Student's t-test, two-tailed, n=5 per treatment group. In all cases, representative images are shown. Scale Bars; 100 μM. "N" in A and B indicates necrotic area. Tumor margins in A-C are indicated with dotted lines. Arrows in D highlight examples of TUNEL positive, apoptotic, nuclei.

3.5 Discussion

Research over the last decade has led to the generation of several modified anthrax toxin-based candidate compounds that exploit the signature overexpression of extracellular proteases by tumor cells and the cellular components of the tumor stroma to achieve tumor selectivity (98, 104, 105, 108, 114, 115, 117, 121, 124, 155, 199, 200). In the current study, we performed a comprehensive analysis of the suitability of one of these compounds: an intercomplementing anthrax lethal toxin, requiring dual MMP/uPA activation, for the treatment of HNSCC. A unique property of this toxin is its inclusion of no less than three specificity determinants: the requirement for cell surface uPA activity, co-localized MMP activity, and dependency upon the MEK/MAPK signaling pathway for survival (86, 121).

Xenograft studies revealed that this dual MMP/uPA-activated anthrax lethal toxin displayed excellent systemic antitumor activity toward four separate HNSCC cell lines. Using a treatment regimen consisting of five intraperitoneal toxin injections, we achieved effects ranging from tumor stasis to complete tumor eradication, as defined by the absence of relapse in mice that were followed for up to one year after treatment cessation.

A notable observation in the current study was that LF sensitivity in cell culture was not a predictor of the *in vivo* sensitivity of the tumor to the intercomplementing anthrax lethal toxin. Thus, although all four xenografts were efficiently treated with the combination of PrAg-L1-I210A + PrAg-U2-R200A + LF, none of these cell lines displayed sensitivity to this toxin combination in culture (Figure 3.3). This data suggests that cells grown in culture may be less reliant on the MEK/MAPK signaling pathway for survival than similar cells within the tumor microenvironment.

Additionally, presence of uPA and MMP proteolytic activity in HNSCC cell line cultures was also found to be a poor predictor of *in vivo* tumor sensitivity. Hep2 cells did not express sufficient cell surface uPA and/or MMP activity for functional IC-PrAg heptamer formation (Figure 3.2); however, Hep2 xenografts were treated efficiently by the toxin (Figure 3.4D). Two possible, and not mutually exclusive, explanations for this observation can be offered. First, the repertoire of cell surface proteases expressed by the tumor cells may differ in culture and *in vivo*. Secondly, the intercomplementing anthrax lethal toxin may exert its antitumor activity by targeting the cellular component of the HNSCC tumor stroma (tumor-associated inflammatory cells, fibroblasts, endothelial cells) (201). In direct support of the latter, we have previously shown that the sole MMP-activated PrAg, PrAg-L1, in combination with LF can efficiently impair the growth of a xenografted immortalized ovarian cell line that was made genetically deficient in anthrax toxin receptors (105).

The absence of correlation between *in vivo* efficacy and sensitivity of cultured HNSCC cell lines to the intercomplementing toxin raises interesting questions as to the potential for prescreening HNSCC patients for treatment. Based on our findings, assaying toxin-sensitivity of cultured primary tumor cell explants may be of limited value. However, determination of tumor cell and stromal cell uPA and MMP protein expression or enzymatic activity in resected tumors or needle biopsies may be a clinically useful predictor of treatment efficacy.

Histological analysis of HN12 and Hep2 xenografts revealed markedly different effects of systemic PrAg-L1-I210A + PrAg-U2-R200A + LF treatment on the two tumor types. While toxin-treated HN12 xenografts displayed decreased proliferation, and increases in

both apoptotic and necrotic cell death, neither proliferation nor apoptosis was affected by toxin treatment of Hep2 xenografts. Rather, for Hep2 xenografts, the potent antitumor activity of the dual MMP/uPA-activated toxin was caused exclusively through induction of tumor necrosis. In light of the inability of cultured Hep2 cells to express sufficient uPA and MMP activity for cellular intoxication, it is tempting to speculate that tumor necrosis in Hep2 xenografts is induced by a vascular collapse caused by direct targeting of the tumor vasculature or other essential cellular components of the tumor stroma.

The antitumor efficacy of PrAg-L1-I210A + PrAg-U2-R200A + LF, and tolerability at administered doses, highlight the therapeutic potential of this agent. Procedures for recombinant expression and purification of large quantities of anthrax toxins in avirulent strains of *Bacillus anthracis* and *Escherichia coli* are already established and will not represent an impediment to the therapeutic development of this toxin for treatment of HNSCC. Systematic animal toxicity studies further exploring the dose-limiting toxicities of this toxin combination have recently been performed demonstrating a clear therapeutic window for use in mice (discussed in Chapter 2 of this dissertation), and further veterinary clinical trials are currently in progress aimed to assess the feasibility of administering PrAg-L1-I210A + PrAg-U2-R200A + LF in naturally occurring feline oral squamous cell carcinoma (discussed in Chapter 4 of this dissertation).

In summary, we have shown that a dual MMP/uPA-activated anthrax lethal toxin specifically targeting ERK/MAPK-dependent cells with high cell surface uPA and MMP activity holds promise as a novel candidate drug for the treatment of HNSCC. Future research towards the clinical development of this toxin is warranted.

Chapter 4:

Activity of a Dual MMP/uPA-activated Anthrax Lethal Toxin in Naturally-occurring Feline Oral Squamous Cell Carcinoma: A Case Report

This chapter contains currently unpublished materials, in which the dissertation author is a primary contributor.

Peters D.E., Vitale Cross L., Liu S., Molinolo A.A., Leppla S.H., Bugge T.H. McNiel E. Effects of a dual MMP/uPA-activated anthrax toxin in feline oral squamous cell carcinoma *Experiments in progress*

Specific Experimental Contributions:

Clinical protocol was written by D.E.P and E.M.

Experimental design was developed by D.E.P., S.L., S.H.L, T.H.B. and E.M.

Proteins were expressed and purified by Rasem Fattah.

Doses were prepped and aliquoted by D.E.P.

Clinical trial was performed by E.M.

Patient samples were analyzed by D.E.P. and A.A.M.

Supporting preclinical trials are in progress, D.E.P. and L.C.V.

4.1 Abstract

IC-PrAg + LF is an engineered anthrax lethal toxin that requires co-localized activation by matrix-metalloproteinases (MMPs) and urokinase plasminogen activator (uPA). This toxin has been previously demonstrated to exhibit potent anti-tumor activity in xenograft models of human head and neck squamous cell carcinoma (HNSCC) (122). Here, we further explore the use of IC-PrAg + LF in a clinically relevant model of human HNSCC; naturally-occurring feline oral squamous cell carcinoma (OSCC). A Phase 0 veterinary clinical trial has been initiated, in which five cats with confirmed diagnoses of OSCC will be treated with 3 local, low-dose, administrations of IC-PrAg + LF. This trial is ongoing; however, initial findings are encouraging as the first patient had a measurable, 31%, reduction in tumor volume over the course of treatment with no evidence of toxin-mediated adverse events.

4.2 Introduction

Head and neck squamous cell carcinomas account for 5% of all cancer diagnoses worldwide (159), and the World Health Organization predicts that its incidence will continue to increase over the next several decades (202). While substantial advances have been made in understanding the risk factors and molecular pathways contributing to HNSCC development, the prognosis associated with this disease has improved only marginally since the 1970's, with a 5-year survival rate hovering around 55% (22, 160-163). As such, there is a clinical need for novel therapeutic agents that will both improve patient survival, as well as reduce treatment-associated morbidities.

To this end, we have developed and characterized an engineered version of anthrax lethal toxin that is selectively activated within the tumor microenvironment (121). This agent, IC-PrAg + LF, requires co-localized activation by MMPs and uPA prior to exerting its cytotoxic effects (121), and we have previously demonstrated that it is both well-tolerated in mice and effective at treating human HNSCC xenografts (122). These data support that IC-PrAg + LF is a promising candidate for further development to address this unmet clinical need.

We recognize, however, that while xenograft models are a standard in oncology drug development, that there are limitations with extrapolating results from this model system, and there are many examples of agents that exhibited remarkable anti-tumor efficacy in mice with much more modest efficacy in a clinical setting (203). Two of the main weaknesses of xenograft studies are that the disease is induced in an otherwise healthy animal and that the treated tumors are homogenous in nature (204-206). Utilizing a

spontaneous model of cancer in place of an implanted xenograft accounts for both of these deficiencies and may provide data with greater translational relevance (204, 205).

In the case of human HNSCC, a naturally occurring veterinary cancer, feline oral squamous cell carcinoma (OSCC), is ideally suited for this purpose (206, 207).

4.2.1 Feline Oral Squamous Cell Carcinoma

Oral squamous cell carcinoma is the most common oral malignancy occurring in cats, accounting for 61% of all oral lesions, and up to 12% of total cancer diagnoses (207, 208). Prognosis is grave for cats with this disease; and the mean survival time post-diagnosis is only two months (209, 210).

Feline OSCC mimics many aspects of human HNSCC. Both diseases exhibit high levels of local invasiveness characterized by osteolytic lesions (211, 212), they are frequently diagnosed at locally-advanced disease-stages where they are refractory to available treatments (10, 206), and they exhibit high rates of local recurrence directly contributing to patient mortality (213, 214).

The regional distribution of OSCC in cats (51% gingival, 23% sublingual, 11% lingual (211)), is similar to that observed for human OSCC (20% gingival, 19% sublingual, 37% lingual (215)), and it is relevant to note that cats are the only species other than humans that frequently develop SCC of the tongue (206, 216).

The similar regional distribution of OSCCs in cats and humans may be related to shared risk factors between these two populations. In humans, > 75% of cases of OSCC occur in conjunction with oral carcinogen exposure involving substances such as: tobacco, betel quid, areca nut and/or alcohol (217-219). In cats, it is hypothesized that oral carcinogen

exposure is also a key contributor to OSCC development (220). It has been proposed that feline grooming habits may lead to increased exposure of the oral cavity to environmental carcinogens, such as second hand smoke by-products or chemicals from flea collars, spurring malignant transformation (220-222). In support of this hypothesis, a recent study by McNiel et al., demonstrated that cats residing in households with smokers, had higher levels of tobacco-related carcinogens present in their urine (222).

Due to the many commonalities between feline OSCC and human HNSCC, it is likely that advances made in the treatment of the feline disease may be relevant to the human condition As such, testing promising anti-OSCC therapeutic agents in felines may contribute to advances in both human and veterinary medicine.

4.2.2 Phase 0 Clinical Trial

Phase 0 clinical trials were introduced by the FDA in 2006 in response to the dismal success rate observed for oncology drug development (223, 224). This novel step in the drug development pathway allows for early testing of candidates in patients prior to critical investment points, such as full scale GMP production (224). Phase 0 studies rely upon the administration of "microdoses", where a microdose is defined as a concentration that is $1/100^{th}$ of a biologically active dose (223). Using these sub-therapeutic doses, first-in human pharmacokinetics, pharmacodynamics and target localization can be explored prior to initiating Phase I toxicity testing, allowing for early validation of biomarkers and PK/PD assays (225, 226).

Here we have initiated a Phase 0 veterinary clinical trial exploring the use of IC-PrAg + LF in feline OSCC. This trial is on-going, and data from the first completed patient is presented here.

4.2.3 Specific Aims

This Phase 0 veterinary clinical trial was initiated to assess the suitability of IC-PrAg + LF for further clinical development. Specifically, it was designed to address the following, translationally relevant, questions:

1. Is IC-PrAg + LF biologically active in feline OSCC tumors? In order to assess target localization and demonstrate proof-of-mechanism, we plan to monitor LF activity in patient biopsies. LF is a zinc-metalloprotease that cleaves mitogen-activated protein kinase kinases (MAPKK). If IC-PrAg is activated within the tumor microenvironment, and LF is translocated into the cytoplasm, MAPKK cleavage may be increased in treated tumors even in the absence of a measurable anti-tumor effect.

2. Do feline OSCCs express MMPs? and/or uPA? Biopsies will be profiled for MMP expression using gelatin zymography and for uPA expression using plasminogen-casein zymography

3. Does low dose IC-PrAg + LF treatment result in a biologic effect? Pre- and post-treatment biopsies will be analyzed for histological changes, including alterations in necrosis, apoptosis, proliferation and vessel density. Additionally, pre- and post-treatment imaging will be performed to accurately measure tumor volume.

4. Are there any adverse consequences associated with low-dose IC-PrAg + LF treatment? Cats will be monitored by a veterinarian or resident throughout the treatment period in the event that toxin-mediated adverse events are observed.

4.3 Materials and Methods

4.3.1 Animals

This study is being conducted with approval from the Tufts University Cummings School of Veterinary Medicine Clinical Studies Review Committee, with informed owner consent. Eligible patients have: 1) A diagnosis of OSCC confirmed by histology or cytology, 2) No previous chemotherapy or irradiation and 3) A measurable tumor (with or without regional lymph node involvement).

The following factors serve as exclusion criteria for this study: 1) Uncontrolled comorbid conditions likely to compromise the ability of the cat to complete treatment, or 2) Tumors inaccessible to biopsy, intratumoral injections, or other procedures.

4.3.2 Dose Selection

The dual MMP/uPA-activated anthrax lethal toxin, IC-PrAg + LF, has been studied extensively preclinically; however, no data exists regarding the toxicity of this agent in cats, healthy or otherwise. In order to minimize the risk of toxicity to the patient, we therefore elected to use a dose where we were reasonably certain that no harm would occur. We based our initial dose selection off of the preclinical toxicity trials presented in Chapter 2 of this dissertation.

We have selected an absolute dose of 15 µg PrAg-L1-I210A + 15 µg PrAg-U2-R200A + 10 µg LF. C57BL/6J mice treated with 6 I.P. administrations of toxin at this absolute dose had no identifiable gross or histological pathology. In terms of concentration, in mice this is a dose of 0.75 mg/kg PrAg-L1-I210A+ 0.75 mg/kg PrAg-U2-R200A+ 0.5 mg/kg LF. Weight-adjusted for cats, this dose is approximately 0.00375 mg/kg PrAg-L1-I210A + 0.00375 mg/kg PrAg-U2-R200A + 0.0025 mg/kg LF.

Therefore, when body weight-scaled, the dose used in this trial is 200-fold lower than a non-toxic dose used in mice, and meets the FDA's definition of a microdose (223, 227).

4.3.3 Trial Design

Cats will be recruited from the hospital population of the Foster Hospital for Small Animals (FHSA) at the Tufts University Cummings School of Veterinary Medicine, as well as from referring veterinarians. All cats will be examined by a veterinary oncologist, or resident, upon presentation to the FHSA and treatment options and prognosis are discussed. After obtaining informed owner consent, eligible cats will be treated with 3 intratumoral injections of 15 µg PrAg-L1-I210A + 15 µg PrAg-U2-R200A+ 10 µg LF, at timepoints time points indicated in Figure 4.1.

Study Overview:	**Baseline assessment**		**Treatment**					**Final assessment**
	Day 0	**Day 1**	**Day 2**	**Day 3**	**Day 4**	**Day 5**	**Day 6**	**Day 7**
EVALUATION	**F**	**S**	**S**	**M**	**T**	**W**	**Th**	**F**
Physical Exam	**X**	**X**	**X**	**X**	**X**	**X**	**X**	**X**
QOL* assessment	**X**							**X**
Urine collection	**X**							**X**
Thoracic radiograph	**X**							
Blood Draw	**X**				**X**		**X**	**X**
Staging CT	**X**							**X**
Biopsy	**X**							**X**
TREATMENT								
Engineered Anthrax Toxin			**X**		**X**		**X**	
***QOL = quality of life**								

Figure 4.1: Phase 0 clinical trial design.

Pre-/post-treatment biopsy and tumor imaging will be performed for all patients to assess changes in tumor size and composition, as well as to look for evidence of toxin activation within the tumor.

We plan to enroll 5 cats in this initial Phase 0 trial. Two patients have already completed the study, and data from the first patient is presented here.

4.3.4 Calculating Tumor Volume: Patient #1

Transverse and sagittal cross-sectional images of the tumor were obtained using x-ray computed tomography (CT). Images were selected in which the lesion was observed to have maximal size, and the orthogonal diameters were measured. The length and height, as measured from the sagittal view, and width, as measured from the transverse view, were used for calculation. Tumor volume was estimated using an equation describing the volume of an ellipsoid (228):

$$\text{Tumor Volume } (\text{cm}^3) = \frac{4}{3}\pi\left(\frac{\text{length (cm)}}{2}\text{x}\frac{\text{height (cm)}}{2}\text{x}\frac{\text{width (cm)}}{2}\right)$$

4.3.5 Histology: Patient #1

Pre- and post-treatment biopsies were collected, fixed in 4% paraformaldehyde for 24 hours, embedded in paraffin, sectioned, and stained with hematoxylin and eosin (H&E). Slides were reviewed by a certified pathologist blinded as to sample identity.

Unstained sections were stained with a monoclonal rabbit anti-mouse CD31 (Santa Cruz Biotechnology, Inc., Santa Cruz, CA) to examine blood vessel density, and with a monoclonal mouse anti-human Ki67 (Dako, Carpinteria, CA) to assess cellular proliferation. Images were captured using an Aperio T3 Scanscope (Aperio Technologies, Vista, CA) and were reviewed by a blinded investigator using Aperio Imagescope Software (Aperio Technologies, Vista, CA).

4.4 Case Report

The first patient, Ginger, was a female, spayed, domestic shorthair cat who was 14-years old at the time of presentation to the FHSA in October of 2013.

Figure 4.2: Patient #1, Ginger.

Ginger was observed to have a large, sublingual tumor (Figure 4.3) that was rapidly increasing in size. This mass was impeding her ability to eat and drink normally at the time of diagnosis, and was also causing copious drooling.

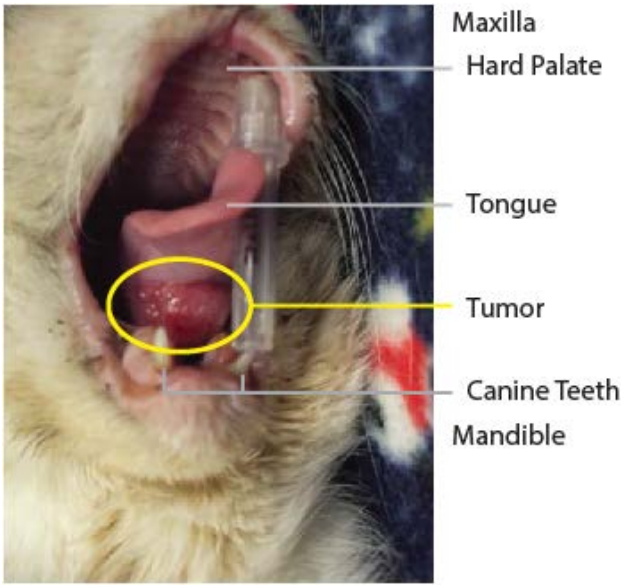

Figure 4.3: Gross photograph of Ginger's OSCC. Selected anatomic structures are highlighted at right for orientation. Note the large size of the tumor mass, as well as its sublingual location.

Tumor biopsy confirmed the diagnosis of OSCC (Figure 4.4). In greater detail, Ginger's tumor was a moderately differentiated squamous cell carcinoma, featuring characteristic irregular cords of pleomorphic, epithelial cells, which were aggressively infiltrating the underlying stroma. Some inflammation was associated with this invasion.

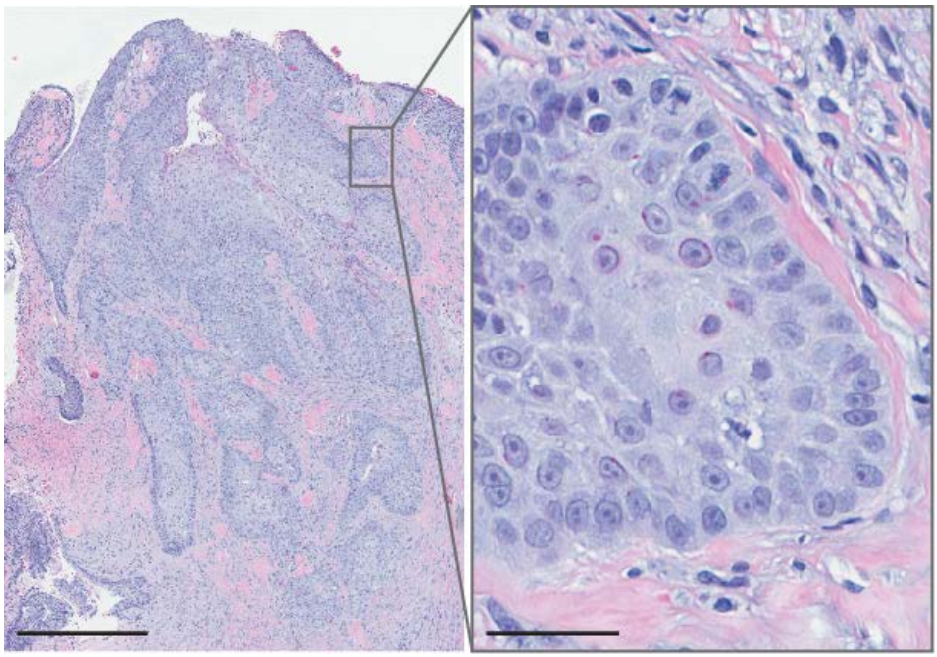

Figure 4.4: Pre-treatment biopsy: H&E. On low magnification, note the presence of cords of epithelial cells invading into the fibrous, pink, stroma. On high magnification, observe pleomorphic cellular morphology and hyperchromatic nuclei within the tumor itself, as well as presence of inflammatory cells in the neighboring stroma. Scale bars are 500 µm (low magnification) and 50 µm (high magnification).

After receiving informed owner consent, Ginger was treated with three intratumoral injections of 15 µg PrAg-L1-I210A + 15 µg PrAg-U2-R200A + 10 µg LF. Over the course of treatment, Ginger's tumor mass was observed to decrease in size. This was visible by gross measurement (data not shown) and was also apparent on CT images (Figure 4.5).

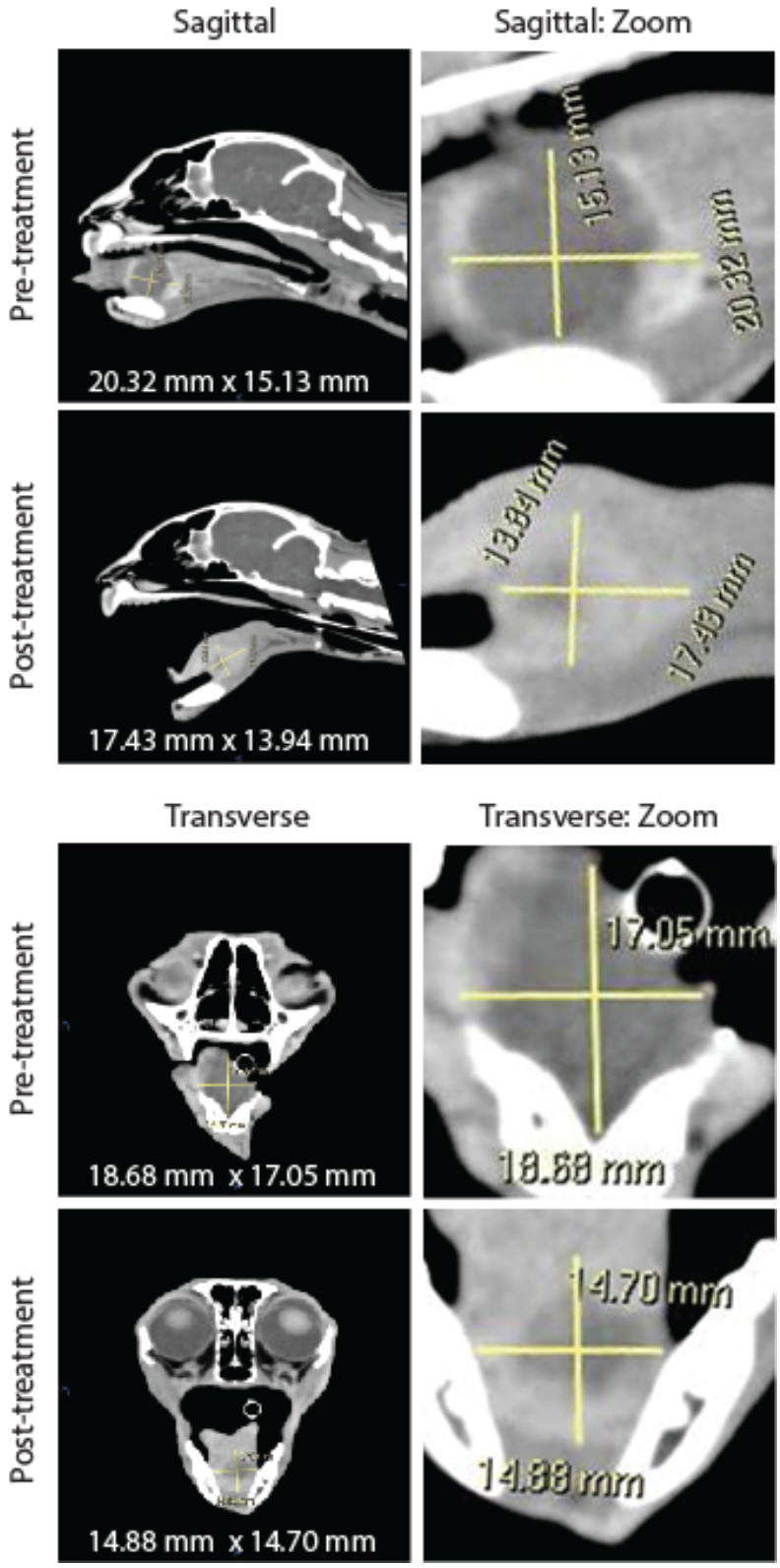

Figure 4.5: X-ray computed tomography (CT) with contrast: sagittal and transverse views. Following treatment with three intratumoral injections of IC-PrAg + LF, tumor mass decreased and contrast distribution was altered.

Tumor volume was calculated from the CT images as described in the Materials and Methods. Ginger's initial tumor volume was 2.7 cm^3, and this decreased to 1.9 cm^3 following treatment, a total reduction of 31%. This reduction in primary tumor mass was associated with an improvement in quality of life as Ginger's drooling resolved and, following administration of subcutaneous fluids, her hydration state was restored.

Interestingly, treatment with IC-PrAg + LF was observed to alter the distribution of contrast agent within the tumor. Relative to the pre-treatment CT, the treated tumor appeared to take up more contrast agent (radiopaque, white) and had a smaller central radiolucent (black) region (Figure 4.5). We hypothesize, that this may be a result of increased vascular leakage in the treated tumors, resulting from direct cytotoxicity to vascular endothelial cells. This hypothesis is supported by previous data, showing that the closely related MMP-activated toxin, PrAg-L1 + LF-HMAGG, has direct anti-vasculature effects (105, 107, 124, 200). An anti-vessel effect was also observed when HN12 HNSCC xenografts were treated with IC-PrAg + LF (122).

Post-treatment biopsy demonstrated that the effect of the toxin treatment was highly localized. Focal regions of necrosis were identified (Figure 4.6D) alongside, regions of proliferating, infiltrating tumor cells (Figure 4.6B, E). Accordingly, this tumor would be expected to re-grow.

Lastly, unlike the pre-treatment biopsy (Figure 4.4), the post-treatment biopsy had an ulcerated surface and contained extensive granulation tissue, featuring proliferating angioblasts in a background of neutrophilic inflammation (Figure 4.6C, F).

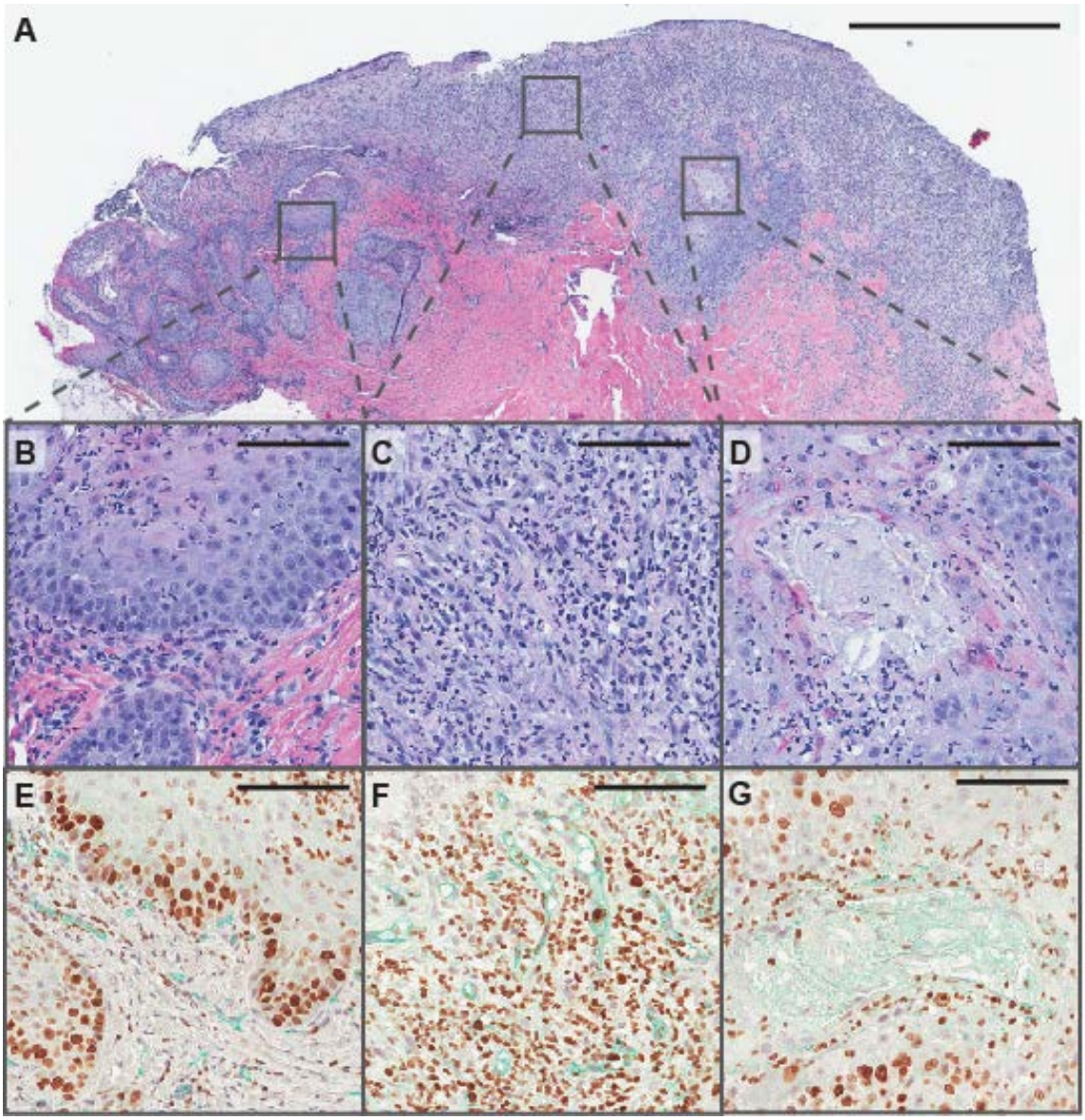

Figure 4.6: Post-treatment biopsy: H&E and immunohistochemistry. Intratumoral IC-PrAg + LF treatment resulted in a localized anti-tumor effect. Regions of viable cancer cells (B), areas of granulation tissue (C), and regions of necrosis (D) were readily identifiable. Widespread neutrophilic inflammation was present throughout the tumor. Note the presence of increased numbers of inflammatory cells in panels B-D. (E-G) Immunohistochemistry was performed to assess proliferation, Ki67 (Brown), and vessel density, CD31 (Green). In sections with viable cancer cells, proliferation was observed in cells at the invasive front (E). (F) Granulation tissue featuring proliferating angioblasts (wispy green cells with brown nuclei) and abundant brown neutrophils (**false positive). Scale bars (A) 1 mm, (B-G) 100 µm.

**When performing this staining, I observed substantial cross-reactivity with neutrophils indicating that their endogenous peroxidase activity was not adequately quenched. Many of the DAB-positive (brown) cells in panels F-G are neutrophils, which can be verified by assessing their cellular morphology on H&E. These cells are not Ki67 positive, and are not proliferating. Instead they are directly cleaving the chromogenic substrate resulting in a false positive signal.

Ginger was euthanized on 12/31/2013, due to advanced local disease progression and diminished quality of life. Time from diagnosis to euthanasia was approximately 2.5 months, which is near average survival for this aggressive, rapidly progressing disease.

4.5 Preliminary Conclusions

Bearing patient safety in mind, a very low microdose was selected for this first-in-patient trial, therefore, the fact that a measurable, 31%, reduction in tumor volume was achieved was quite unexpected and highly encouraging.

This anti-tumor effect was observed to be localized in nature, which is not unexpected given the route of administration and mechanism of action of this toxin system. Following injection, PrAg-L1-I210A and PrAg-U2-R200A will bind to ubiquitously expressed cell-surface receptors. When a small quantity of toxin is administered intratumorally, it is likely that the toxin will be fully bound by receptors near the injection site, limiting its diffusion to a broader area.

Inferring from the observed anti-tumor response, it appears that some feline OSCC tumors express both MMPs and uPA. The MMP and uPA expression status of feline OSCCs has never been reported in the literature, and we plan to explore this further by profiling tumor biopsies for presence of MMP and uPA activities.

Prior to drawing any formal conclusions from this trial, we await the data for the four remaining patients; however, we are cautiously optimistic. We have identified that locally effective doses of IC-PrAg + LF can be administered without adverse effects, and it may be possible that with increasing local concentrations a reduction in primary tumor burden may be achieved that confers a significant survival benefit.

Chapter 5:

Key Findings, Implications & Future Directions

This chapter contains currently unpublished materials and pilot studies in which the dissertation author was a primary contributor to both experimental design and execution.

Specific Experimental Contributions:

Toxicity studies were performed by D.E.P. (Data summarized in Figure 5.1)

Survival studies were performed by D.E.P. (Data in Figure 5.2)

In vitro SCCF1 cytotoxicity assays were performed by D.E.P. (Data in Figure 5.3)

Proteins were expressed and purified by Rasem Fattah.

5.1 Summary of Key Findings

The research in this dissertation was performed in an effort to assess the potential for utilizing tumor-targeted versions of anthrax lethal toxin to treat head and neck squamous cell carcinoma; a disease for which there is unmet clinical need in both veterinary and human patient populations. Previously, three separate engineered variants of anthrax PrAg had been designed, which required activation by tumor-overexpressed proteases. These included: PrAg-L1 (MMP-activated), PrAg-U2 (uPA-activated) and IC-PrAg (dual MMP/uPA-activated) (98, 108, 121). When co-administered with various cytotoxins, each of these engineered PrAgs had been previously demonstrated to exert antitumor activity in multiple preclinical models of cancer (105, 107, 115, 117, 118, 121-123). However, these early efficacy experiments varied not only in cytotoxin identity and treated indication, but also in dose route and treatment schedule, and these differences in experimental design made it difficult to retrospectively assess the suitability of each variant for further development.

In Chapter 2 of this dissertation in-depth toxicity profiling and head-to-head efficacy studies were performed directly comparing PrAg-L1, PrAg-U2 and IC-PrAg, when co-administered systemically with wildtype anthrax lethal factor, LF. IC-PrAg + LF was identified as the optimal lead candidate, as this toxin combination had the highest MTD6, as well as the highest threshold for target-organ toxicity, while it maintained equal effectiveness in treating B16-BL6 melanoma syngrafts.

Expanding upon this finding, in Chapter 3 IC-PrAg + LF was tested for preclinical efficacy using 4 separate human HNSCC cell lines both *in vitro* and *in vivo*. While only 3 of 4 cell lines were toxin sensitive *in vitro,* remarkable toxin sensitivity was observed for

all 4 cell lines when grafted to nude mice. The greatest antitumor response was observed in HN12 xenografts, where 40% of tumor-bearing mice had complete tumor regression following 5 I.P. doses of IC-PrAg + LF; this regression was observed to persist for a one-year follow-up period.

The striking pre-clinical anti-HNSCC efficacy demonstrated in Chapter 3 has now been translated to a veterinary clinical setting. In Chapter 4, a case report is presented for the first feline oral squamous cell carcinoma patient who has completed a Phase 0 veterinary clinical trial exploring the effects of three, low-dose, intratumoral injections of IC-PrAg + LF. While this trial is still in progress, initial findings are highly encouraging. Despite treatment with a microdose selected to minimize risk, this first patient exhibited a measurable 31% reduction in tumor volume.

5.2 Implications of Current Work

The work presented in this dissertation spans from early preclinical toxicology (Chapter 2), to preclinical syngraft and xenograft models of efficacy (Chapters 2 and 3), to initial clinical studies in a veterinary patient population (Chapter 4). All of the findings reported herein support the conclusion that a dual MMP/uPA-activated anthrax lethal toxin, IC-PrAg + LF, is a suitable candidate for further development as an anti-HNSCC agent. Furthermore, the observed antitumor efficacy in a naturally-occurring, heterogeneous, feline OSCC tumor is suggestive that this toxin may also have therapeutic potential in its highly similar human counterpart.

5.3 Future Directions

Our goal is to pursue the clinical development of IC-PrAg + LF as a treatment for human HNSCC. Accordingly, I would suggest that future research be focused in the following three areas: 1. Characterization of mechanisms underlying IC-PrAg + LF toxicities, 2. Continued exploration of IC-PrAg + LF in feline OSCC, and 3. Prediction, and circumvention, of unique challenges facing translation of IC-PrAg + LF to a human clinical setting.

5.3.1 Characterizing Mechanisms Underlying IC-PrAg + LF Toxicity

In the course of performing the comparative toxicity studies reported in Chapter 2, we identified several toxicities associated with systemic IC-PrAg + LF administration. Further exploring the mechanisms underlying these toxicities may be relevant as we attempt to translate this toxin for use in other mammalian species.

5.3.1.1 Identifying the Cellular Target of IC-PrAg + LF GI Toxicity

We first identified that six intraperitoneal (I.P.) or intravenous (I.V.) doses of IC-PrAg + LF resulted in dose-limiting gastrointestinal (GI) toxicity. This toxicity progressed in a dose-dependent manner, as summarized in Figure 5.1.

Interestingly, strikingly similar toxicities have been reported in mice treated with non-lethal doses of PrAg-WT + LF (155, 158).

The GI toxicities observed with either IC-PrAg + LF or PrAg-WT + LF administration have an interesting presentation, including changes suggestive of direct smooth muscle toxicity (155) and/or direct epithelial toxicity (158). (This is discussed in greater detail in Section 2.5, Page 62)

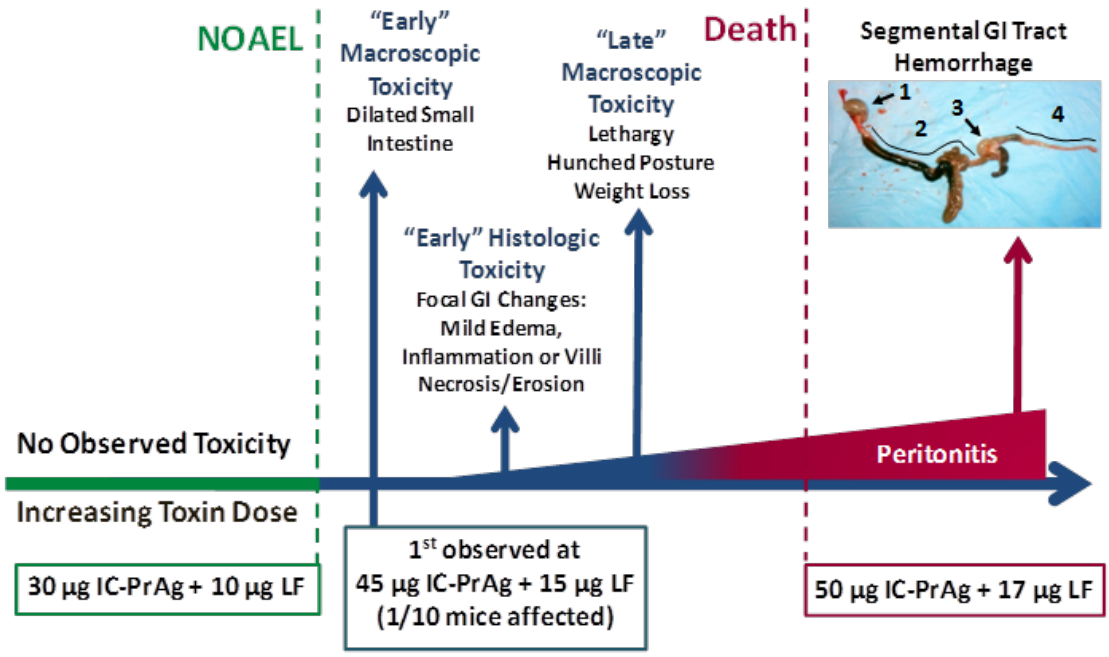

Figure 5.1: Summary of the dose-dependent GI toxicity observed following 6 I.P. administrations of IC-PrAg + LF. 30 µg IC-PrAg + 10 µg LF was the NOAEL (no observed adverse effect level) for the dual MMP/uPA-activated anthrax lethal toxin. As doses were increased above this threshold, the first observed pathology was a mild dilation of the small intestine observed on gross necropsy, with no other abnormalities. Doses exceeding 45 µg IC-PrAg + 15 µg LF were associated with focal to diffuse changes in GI histology as well as dose-dependent peritonitis. At the highest doses, severe fibrinous peritonitis and segmental GI tract hemorrhage (affecting the small intestine (2) and cecum (3)) were routinely identified. Also, note the presence of a full stomach (1) and empty colon (4), suggestive of reduced GI motility.

Identifying the cellular target(s) of IC-PrAg + LF mediated GI toxicity, and the order in which they occur, is relevant. This knowledge could directly contribute to patient monitoring protocols, for example, if GI smooth muscle damage is expected to occur first, addition of procedures such as auscultation of bowel sounds or blood work to detect electrolyte abnormalities and/or muscle injury markers, may allow for the earliest detection of adverse events.

One way to begin to assess the order in which these toxicities arise, would be to look for evidence of functional deficiencies occurring prior to the onset of histological changes in

villous structure. An assay that could be used for this purpose is activated charcoal gavage (229). This is a straightforward functional assay, in which mice are challenged with an oral dose of charcoal followed by euthanasia at a set interval, typically 30-60 minutes following challenge. The distance that the charcoal has traversed through the small intestine can be measured and a GI motility ratio is calculated by comparing the charcoal transit distance to the small intestinal length. If IC-PrAg + LF treatment results in direct smooth muscle toxicity, it may be possible to detect reduced charcoal transit in this functional assay at doses below those where histological changes are first seen.

5.3.1.2 IC-PrAg + LF Thrombocytosis

Complete blood count analysis revealed that mice treated with 6 I.P. doses of IC-PrAg + LF, exhibited a dose-dependent increase in absolute platelet count (Figure 2.12). This thrombocytosis appeared to be relatively mild; at the highest toxin concentration administered there was approximately a 33% increase in absolute platelet count relative to control mice; however, this elevated value still fell within the normal reference range reported for laboratory mice (230). The clinical relevance of this observation is unclear, but it is reasonable to keep this in mind as IC-PrAg + LF is developed further. Platelet count should likely be monitored throughout treatment, and co-administration of a prophylactic anti-coagulant, such as aspirin, may be indicated to reduce risk of blood clots, the primary complication associated with elevated platelet levels.

5.3.1.3 Exploring PrAg-alone Toxicity

Lastly, and unexpectedly, it was observed that high intravenous doses of the engineered PrAgs without cytotoxin, resulted in lethality. Individually, anthrax protective antigen (PrAg) is considered to be a non-toxic entity, functioning primarily as a receptor to

mediate transport of the enzymatically active components, lethal factor (LF) and edema factor (EF), into the cytoplasm. It was therefore surprising to discover that high intravenous doses of PrAg-L1 alone, PrAg-U2 alone or IC-PrAg alone caused 40%, 25% or 20% lethality, respectively (Figure 5.2).

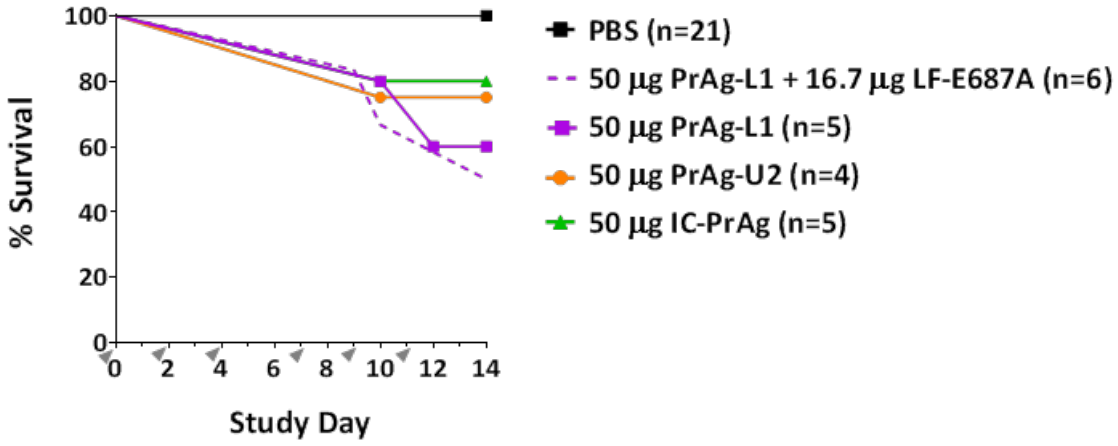

Figure 5.2: Lethality associated with high I.V. doses of engineered PrAgs alone.
Kaplan-Meier survival curves for mice treated with six, high-dose, I.V. injections of engineered PrAg variants alone, or in combination with the enzymatically dead cytotoxin LF-E687A.

5.3.1.3.1 PrAg-alone Toxicity: Implications and Relevance

Importantly, the dose where PrAg-alone toxicity was observed for each of the engineered variants was well-above doses where they would be lethal when combined with LF, thus PrAg-alone toxicity should not be viewed as a limitation for utilizing this technology in its current form.

Additionally, while scarce, occasional reports of PrAg-WT alone toxicity have been made in the literature both in *in vivo* (231) and *in vitro* (232-234). Salles et al., performed extensive characterization on a PrAg-WT alone cytotoxicity that they identified in a mouse macrophage cell line overexpressing ANTXR1 (RAW264.7^{ANTXR1}). When these RAW264.7^{ANTXR1} cells were incubated with PrAg-WT alone, 70% cell death was

observed. Using a variety of ANTXR1 and PrAg mutants, Salles et al. defined the requirements for PrAg-alone toxicity in this system, demonstrating that ANTXR1 receptor binding, PrAg cleavage, PrAg oligomerization and endosomal acidification were all required for this toxicity to occur (232). This suggested that stabilized PrAg pore formation on the endosomal membrane caused cell death, potentially by altering ion conductance, osmolarity and/or cytoplasmic pH, triggering apoptosis.

If the PrAg-alone toxicity incurred with administration of our engineered PrAgs *in vivo* is similar to that reported by Salles and colleagues *in vitro*, proteolytic activation of the engineered PrAgs would be an absolute requirement (232). As such, this "toxicity" would actually still be targeted to the desired cell population, and selective toxicity to cells expressing MMPs and/or uPA would be expected.

5.3.2 Continued Exploration of IC-PrAg + LF in Feline OSCC

In addition to further characterizing the toxicities associated with IC-PrAg + LF, we plan to continue exploring its therapeutic application in feline OSCC.

5.3.2.1 Feline OSCC: Preclinical Studies

As discussed in Chapter 4 of this dissertation, a Phase 0 veterinary clinical trial is currently in progress evaluating low-dose intratumoral administration of IC-PrAg + LF, in spontaneously occurring feline OSCC. Simultaneously, with this initial clinical evaluation, we are performing *in vitro* and preclinical *in vivo* studies to add support to the data obtained in this trial.

SCCF1 is a well-characterized immortalized feline OSCC cell line that was originally derived from a laryngeal SCC (235). A tagged variant of these cells, SCCF110YFPLuc, has been shown to form solid tumors in mice when implanted subcutaneously (207).

We plan to assess both the *in vitro* and *in vivo* sensitivity of the SCCF1 cell line to IC-PrAg + LF. One advantage of using this preclinical model system is that we will be able to assess the sensitivity of transplanted tumors to both local and systemic toxin administration, which is not yet possible in the feline patients due to lack of toxicity data in cats.

5.3.2.1.1 SCCF1 *in vitro* Profiling

5.3.2.1.1.1 Sensitivity of SCCF1 cells to anthrax lethal toxin

I have assessed the *in vitro* sensitivity of SCCF1 cells to IC-PrAg in combination with either wildtype LF or FP59, an engineered fusion protein composed of the N-terminal binding domain of LF coupled to the catalytic domain of *Pseudomonas* aeruginosa exotoxin A (77). Specifically, 50E5 SCCF1 cells were seeded per well in 96 well-plates and cells were allowed to grow overnight. The next day, LF or FP59 was added and plates were incubated at 37ºC for either 3.5 hours (LF) or 48 hours (FP59). Cell viability was then determined using an MTT assay, as described in Appendix AI.7.

I observed that similar to the human HNSCC cell lines described in Chapter 3, Figure 3.3B, the SCCF1 cell line was also resistant to the combination of IC-PrAg + LF *in vitro* (Figure 5.3A) demonstrating that these cells are not reliant upon the MEK/MAPK signaling pathway for survival in culture.

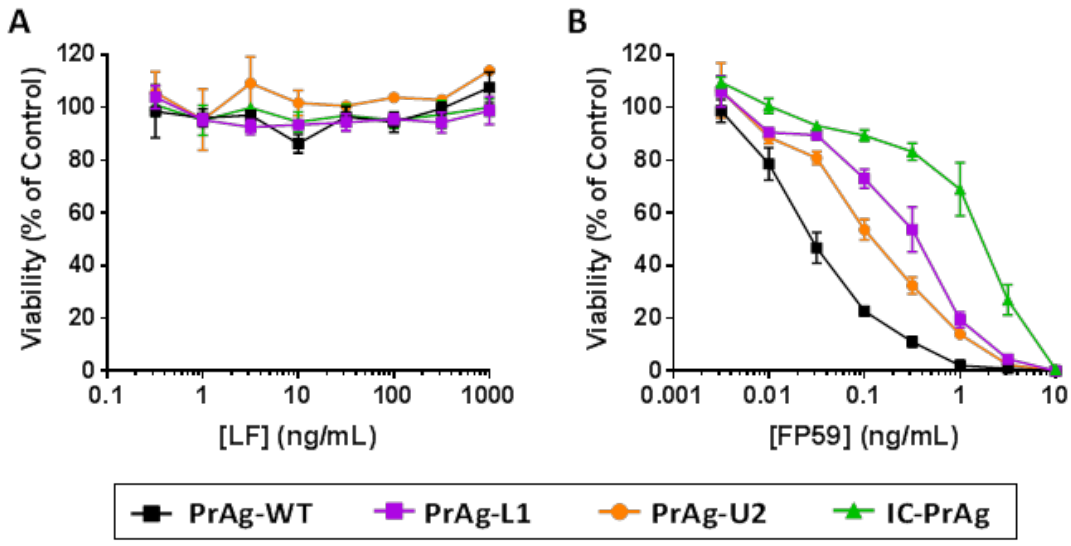

Figure 5.3: Toxin sensitivity of the feline OSCC cell line, SCCF1, *in vitro*. SCCF1 cells were incubated with wildtype PrAg (black), MMP-activated PrAg-L1 (purple), uPA-activated PrAg-U2 (orange) or dual MMP/uPA activated IC-PrAg (green), in combination with varying concentrations of LF (A) or FP59 (B). PrAg-XX and cytotoxin concentrations were optimized to elicit a sigmoidal concentration response curve. For LF assays, a constant concentration of 1000 ng/mL PrAg was used. For FP59 assays, a constant concentration of 50 ng/mL PrAg was used. Mean ± s.d. is plotted.

The SCCF1 cells were sensitive to IC-PrAg when paired with FP59 (Figure 5.3B), demonstrating the presence of anthrax toxin binding receptors and expression of both MMPs and uPA by this cell line. Interestingly, the SCCF1 cells were found to be equally sensitive to MMP-activated PrAg-L1 and uPA-activated PrAg-U2, in combination with FP59, having IC50s of 0.10 ng/mL and 0.34 ng/mL, respectively (Figure 5.3B). This is a somewhat unusual observation, suggesting that the SCCF1 cells have similar levels of MMP and uPA activity.

SCCF1 cells were found to be less sensitive to the combination of IC-PrAg + FP59 than to either PrAg-L1 + FP59 or PrAg-U2 + FP59 (Figure 5.3B). This is consistent with the mechanism of action of these toxins. A native PrAg-WT heptamer can bind and translocate up to 3 molecules of LF/EF/FP59, and it is expected that PrAg-U2 and

PrAg-L1 heptamers would have similar binding and translocation efficiencies (79). However, in order for IC-PrAg to bind and internalize LF/FP59, its two separate constituent proteins PrAg-U2-R200A and PrAg-L1-I210A must form mixed heptamers, and these mixed heptamers are expected to contain some mutated binding sites that will bind to ligand less efficiently, resulting in reduced cytotoxin internalization (121).

Because SCCF1 cells express anthrax toxin receptors and have both MMP and uPA proteolytic activities when grown in culture, I predict that SCCF1 xenografts will be sensitive to IC-PrAg + LF treatment *in vivo*. Every cell line that we have tested to date, that has both expressed anthrax toxin receptors and had activating proteolytic activities *in vitro*, has been found to be sensitive to toxin treatment when grown *in vivo.* Examples of cell lines fitting these criteria include: Colo205 colon carcinoma (105), A549 lung carcinoma (105), HT144 melanoma (105), LL3 Lewis lung carcinoma (105), HeLa cervical adenocarcinoma (unpublished), and HN6, HN12 and Cal27 human HNSCC (122).

Importantly, the expression of functional anthrax toxin receptors and/or activating proteases by tumor cells is not an absolute requirement for *in vivo* sensitivity. This has been shown for Hep2 xenografts (122), which lack an activating protease in culture, and also for CHO PR230 xenografts (105, 198), which are deficient in anthrax toxin receptors. While both of these cell lines were resistant to *in vitro* toxicity, they were still effectively treated *in* vivo, demonstrating that the engineered toxins exert some of their anti-tumor effects by targeting other cells within the tumor microenvironment, possibly proliferating vascular endothelial cells (105).

5.3.2.1.2 SCCF1 *in vivo* Tumor Models

5.3.2.1.2.1 Subcutaneous Xenograft

SCCF1 xenografts will be used to compare local versus systemic administration of IC-PrAg + LF. I am currently performing serial transplants of SCCF1 tumors in nude mice (Method AI.10) to establish a cohort with consistent tumor growth. Following our original xenotransplantation of the SCCF1 cells from culture, tumor growth was slow and 10 months after our initial injection only 10% of mice (4/40) had growing tumors, each of which was smaller than 5 mm in length. Serial transplantation has accelerated this process greatly; and subsequent transplants have required 4 and 2 months, respectively, to achieve tumor sizes exceeding 1 cm.

We plan to establish a xenograft cohort of 40 mice, distributed into the following experimental cohorts: 10 intratumoral (I.T.) PBS, 10 intraperitoneal (I.P.) PBS, 10 I.T IC-PrAg + LF and 10 I.P. IC-PrAg + LF. The absolute dose utilized in this trial will be the same as that employed in our Phase 0 veterinary clinical trial: 30 µg IC-PrAg (15 µg PrAg-L1-I210A + 15 µg PrAg-U2-R200A) + 10 µg LF. We also plan to use the same treatment regimen, 3 total doses on a M,W,F schedule with tumor harvesting 24-48 hours after the third dose. Immunohistochemical and molecular analysis of treated xenografts will be used to support findings from the Phase 0 veterinary clinical trial.

One thing that we are interested in exploring with this xenograft model is the effect of IC-PrAg + LF on tumor vascularization. The first veterinary patient, Ginger, was observed to have changes in the contrast distribution within her tumor following treatment and we speculate that this may have resulted from a toxin-mediated anti-vessel effect and subsequent vascular leakage. It will therefore be interesting to see if the tumor

vasculature is impacted in the SCCF1 model of feline OSCC. We plan to explore this using CD31 immunohistochemistry, which labels all blood vessels, in combination with administration of a dye, such as DiI; a lipophilic carbocyanine dye, that allows for selective visualization of patent blood vessels (236).

5.3.2.1.2.2 Lingual Orthotopic Implant

In parallel with establishing a subcutaneous xenograft cohort, we also plan to generate SCCF1 lingual orthotopic implants. This would be a new model of oral squamous cell carcinoma, which may be particularly relevant as cats are the only species other than humans where lingual OSCCs are frequently observed (206, 216).

5.3.2.2 Feline OSCC: Phase 0 → Phase I/II

Given the anti-tumor response observed in the first treated veterinary patient, we are cautiously optimistic that IC-PrAg + LF has potential for use in the treatment of feline OSCC. Therefore, we are very interested in pursuing further veterinary clinical development.

An appropriate next step may be initiating a trial with local dose-escalation. This strategy may allow us to identify an optimal intratumoral toxin concentration; a concentration where maximal anti-tumor efficacy is achieved in the absence of undesirable features such as rapid necrosis or ulceration. From this target intratumoral concentration, we could then begin to extrapolate the minimum systemic concentrations required to achieve this level of exposure. This type of analysis may assist in selecting doses for initial systemic toxicity testing.

5.3.3 Challenges with Clinical Development

Finally, as with any novel therapeutic agent, IC-PrAg + LF has unique features that will influence the strategy employed during its pre-clinical and clinical development, and it will be important to consider these factors early in order to maximize its potential for success.

5.3.4 Clinical Transition: Logistics

Large-scale production is often a stumbling block for biologic agents; however, in this case full-scale GMP production has already been optimized and implemented to produce the uPA-activated toxin, PrAg-U2 + FP59 (Dr. Arthur Frankel, personal communication). Therefore, scale-up of IC-PrAg + LF is not expected to pose a hurdle for further development.

While production seems readily achievable, perhaps more challenging is the fact that IC-PrAg + LF is composed of three individual proteins. While we predict that each of these component proteins would be non-toxic when used in a therapeutic range, the FDA would likely require full Phase I toxicity testing for each individual component (per the FDA Guidance for Industry “Codevelopment of Two or More New Investigational Drugs for Use in Combination” (237)). If required, this increase in clinical trial costs at an early stage in development may prove to be a hinderance when identifying potential investors. Of course, the increased complexity of this system is balanced by the fact that it enables addition of multiple specificity determinants, and the benefits may be deemed to outweigh the costs for IC-PrAg + LF.

5.3.5 Clinical Transition: Pharmacological Considerations

Specific considerations will need to be made with regard to the pharmacology of IC-PrAg + LF. Since this is a multi-component protein based system there is inherent complexity; however, because the mechanism of action is well understood it should be possible to use this knowledge of the underlying biology to inform experimental design. This is discussed in greater detail below, with specific emphasis on pharmacokinetic analysis, dose scaling and immunogenicity.

5.3.5.1 Nontraditional Pharmacokinetics

When developing biologic agents pharmacokinetic analysis is often challenging, and IC-PrAg + LF is no exception to this trend (238). Following administration, PrAg-L1-I210A and PrAg-U2-R200A will bind to their widely distributed receptors, ANTXR1 and ANTXR2. This is followed by localized activation at the cell-surface by MMPs or uPA, proteases with limited expression on a subset of cells. If PrAg-L1-I210A and PrAg-U2-R200A receptor binding is similar to their parent protein, PrAg-WT, they would be expected to bind to their receptors quickly, with high affinity, and to dissociate at a much slower rate (239). Furthermore, PrAg turnover would be predicted to be fastest in tissues where proteolytic processing occurs, as proteolytic cleavage triggers heptamer formation which in turn initiates complex internalization (240).

Modeling the pharmacokinetics of IC-PrAg + LF, based upon PrAg, would therefore involve a minimum of two turnover rates, slow (non MMP/uPA-expressing cells) and fast (MMP/uPA–expressing cells). These rates would be influenced by both receptor distribution and protease expression. While receptor distribution may be similar across normal persons, tumor burden may alter receptor concentrations in unpredictable and

significant ways. Similarly, protease distribution is known to vary with certain disease conditions, such as with wounds, and presence of these conditions concurrent with the cancerous state would further complicate pharmacokinetic analysis.

For the above reasons, I believe that it will be challenging to estimate either the total quantity of PrAg bound to the cell-surface, or the amount of active PrAg in regions of interest, based upon circulating PrAg levels. Furthermore, if steady-state concentrations of circulating IC-PrAg were to be achieved, this would likely represent a situation where ANTXR1/ANTXR2 receptors are saturated; a state that would likely be associated with unacceptable toxicity as it would be expected to maximize the risk of off-target toxicity to non-tumor tissues. That said, it is possible that blood concentrations of the co-administered cytotoxin, in this case LF, may be an accurate predictor of both biologic activity and clearance rate.

LF is reportedly able to bind to both monomeric and oligomeric forms of PrAg; however, it only binds to PrAg following proteolytic activation (i.e. conversion of PrAg 83 → PrAg 63) (241, 242). Some PrAg-WT can be cleaved within the bloodstream leading to binding and sequestration of LF, and thus a PrAg-dependent reduction in circulating LF levels independent of cellular internalization/biologic activity (243). Importantly, this does not appear to be the case for the PrAg mutants. Neither PrAg-U2 nor PrAg-L1 is cleaved in circulation (105, 243). While IC-PrAg has not yet been tested, if it is also cleaved selectively at the cell-surface, then theoretically all (or most) LF binding will occur at the cell surface, and consequently all LF that is cleared in a PrAg-dependent manner would be internalized by host cells. It is therefore plausible that measurement of

circulating LF levels may be useful to estimate the proportion of IC-PrAg that is activated at the cell surface.

To my knowledge, the pharmacokinetics of LF have not been studied in parallel with administration of the mutant PrAg proteins. In order to explore the predictive capacity of circulating LF levels, it will first be necessary to evaluate the non-PrAg-dependent clearance/degradation of LF from the body. Following, determination of this background clearance level, further studies could be performed evaluating LF clearance in both normal (slow clearance predicted) and tumor-bearing (fast clearance predicted) states. Additionally, preclinical studies evaluating how LF concentrations are impacted with co-morbidities, such as with both a tumor and a wound, would be possible. These types of analyses may be easiest to model in the rat, where xenograft/syngraft tumor models have been increasing in popularity (244), and where serial blood draws are permissible.

With regard to pharmacokinetics and drug distribution, it is important to bear in mind that this dissertation research demonstrated anti-tumor efficacy through use of two separate models of cancer: xenograft models of human HNSCC and syngraft models of murine melanoma. While syngraft modeling is advantageous relative to xenograft modeling, allowing for testing of experimental agents in mice with intact immune systems, both of these model systems are limited in that they involve the growth of externally maintained cells in a non-native environment. The physiologic interactions between the tumor cells and stroma that drive spontaneous cancer formation are not preserved, and differences in tumor cell heterogeneity, tumor vascularization, capillary permeability and tumor interstitial pressure would be expected (245, 246). For these reasons, syngraft and xenograft models are unlikely to accurately model the delivery and distribution of an

experimental agent within a naturally occurring tumor, and these model systems may over-estimate the efficacy of IC-PrAg + LF when administered systemically.

5.3.5.2 Nontraditional Dose Scaling for Systemic Administration

Inter-species dose extrapolation is a critical step when translating an agent from use in early preclinical models to higher species (247, 248). One commonly used method to predict starting doses is allometric dose scaling, which relies upon the basic assumption that many physiologic properties are proportional to body mass (247, 248). Body-weight based dose estimates can then be further improved by incorporating known information regarding relevant species differences in metabolism, transport, clearance, etc. (247, 248).

Due to the widespread receptor binding that occurs when IC-PrAg is first administered, I think it is unlikely that simple allometric scaling will provide an accurate prediction of effective doses. Rather, I propose that an appropriate scaling method would take into account both species variations in ANTXR1/ANTXR2 receptor densities on vascular endothelial cells, as well as the surface area of the vascular tree.

While it is well known that ANTXR1 and ANTXR2 are expressed on vascular endothelial cells (249), to my knowledge, vascular receptor densities have not been estimated for either humans or mice. In mice, this may be a relatively straightforward experiment to perform, as the methodology could be based off of a recently published paper by Dadachova and colleagues (250). Here ^{123}I- and ^{99M}Tc-labeled PrAg-WT were injected intravenously in mice and their tissue distributions were assessed using scintigraphic imaging at 1 and 3 hours, as well as counting of tissue homogenates at 24 hours post-injection (250).

To modify this method to provide a measurement of vascular receptor density, only two small adjustments would be required. First, it would be desirable to use a version of PrAg that is either uncleavable (such as the protease resistant PrAg-U7 (115)), or that requires cell-surface binding prior to cleavage (such as uPA-activated PrAg-U2 (243)). This would minimize signal attributed to the degradation and clearance of PrAg occurring independent of receptor binding.

Second, it would likely be optimal to use a very short time frame between injection of the radiolabeled PrAg and detection. One could likely inject the labeled PrAg into the tail vein of an alert mouse, followed by immediate anesthesia, flush perfusion to remove unbound PrAg from the circulation, blunt dissection of specific lengths of desired vessels, homogenization, scintillation counting and ultimately quantification of receptor density.

It may be possible to estimate human receptor concentrations utilizing a similar binding assay on *ex vivo* vascular tissue, which could, theoretically, be obtained as a by-product from angiectomy; the surgical excision of blood vessels as might be performed to treat conditions such as aneurysm.

5.3.5.3 Immunogenicity: Limited Dosing Window

As introduced above, predicting an effective, and non-toxic dose, for first-in-human use poses some unique challenges. Adding further complexity to this scenario is the fact that administration of a toxin dose that is below an effective range is also undesirable.

As aforementioned, PrAg-L1-I210A and PrAg-U2-R200A bind to widely expressed cell-surface receptors. It is therefore expected that these proteins would bind to cells in the order that they are encountered. With intravenous administration, it is likely that

PrAg-L1-I210A and PrAg-U2-R200A would bind widely to vascular endothelial cells prior to encountering their target tissue, the tumor. If a low dose of IC-PrAg is administered it is possible that all IC-PrAg will be bound prior to achieving effective tumor concentrations. This dose would be ineffective; however, the patient would still be exposed to these novel therapeutic proteins, potentially inciting an immune response.

To maximize the number of effective doses that can be administered prior to development of a neutralizing antibody response by the patient, it is therefore important to reach therapeutic concentrations as quickly as possible. This therapeutic dose must exceed the background IC-PrAg binding requirements (likely to be species specific and dependent upon receptor concentrations), while remaining below the threshold for toxicity.

It is relevant to note that over the past several decades many protein-based biologic agents have been developed, and significant advances have been made in understanding and adapting these biologic agents in order to increase their therapeutic longevity. It is likely, that some of these advances could be directly applied to IC-PrAg + LF in order to extend its treatment window.

In particular, immunotoxins based upon *Pseudomonas* exotoxin A have been widely studied for their immunogenicity. Dr. Ira Pastan is a leader in this field and his group has developed and characterized multiple recombinant immunotoxins with a common backbone structure; these agents are composed of tumor-recognizing Fv antibody fragments coupled to a 38 kDa portion of *Pseudomonas* exotoxin A (PE38) (251). When these immunotoxins are administered to patients in a clinical setting, a neutralizing antibody response typically develops within the first three weeks of treatment (252, 253).

The Pastan group has employed multiple methods to delay this neutralizing response including: conjugating high molecular weight. polyethylene glycol residues to surface peptides, “shielding” the foreign protein from the immune system (254), identifying primary T-cell and B-cell epitopes provoking neutralization and disrupting them with site-directed mutagenesis, a process called “deimmunization” (253, 255-258), and most recently, co-administering an immunosuppressive regimen of pentostatin and cyclophosphamide (259, 260).

This pentostatin and cyclophosphamide immunosuppressive regimen appears to be particularly promising. A Phase 1 trial has recently been performed using this regimen with a recombinant immunotoxin targeting mesothelioma, SS1P (259). When SS1P was administered without immunosuppression 80% of patients (27/34) developed a neutralizing antibody response within the first 22 days of treatment (252). With the addition of immunosuppression, only 20% of patients (2/10) developed a neutralizing antibody response within the first 30 day treatment cycle (259). Furthermore, 2 of the patients received 4 and 6 cycles of treatment respectively, before developing a neutralizing response (259).

This pentostatin and cyclophosphamide immunosuppressive regimen can be administered in an out-patient setting, and it is neither myelosuppressive nor associated with the development of opportunistic infections (259). As such, this may be well-suited for co-administration with many biologic agents, including IC-PrAg + LF.

Lastly, it might also be possible to employ the aforementioned strategy of B-cell “deimmunization” to further reduce the immunogenicity of IC-PrAg + LF. The antigenic B-cell epitopes of LF have recently been mapped (261), and there are several reports of

antigenic B-cell epitopes for PrAg-WT in the literature (262-264). Using this information as a starting point, it may be possible to identify specific antigenic residues that would be candidates for site-directed mutagenesis.

5.4 Concluding Remarks

There is an unmet clinical need for therapeutic agents to treat both feline oral squamous cell carcinoma and human head and neck squamous cell carcinoma. Given the strong similarities between these two diseases it is reasonable to anticipate that a single agent may be efficacious in both conditions. The data presented in this dissertation provides strong support that a dual MMP/uPA-activated anthrax lethal toxin, IC-PrAg + LF, has potential to be a clinically relevant anti-HNSCC agent. As is the case with any novel therapeutic agent, however, there are unique factors that may pose a challenge as further clinical development is pursued, some of which are summarized in Figure 5.4.

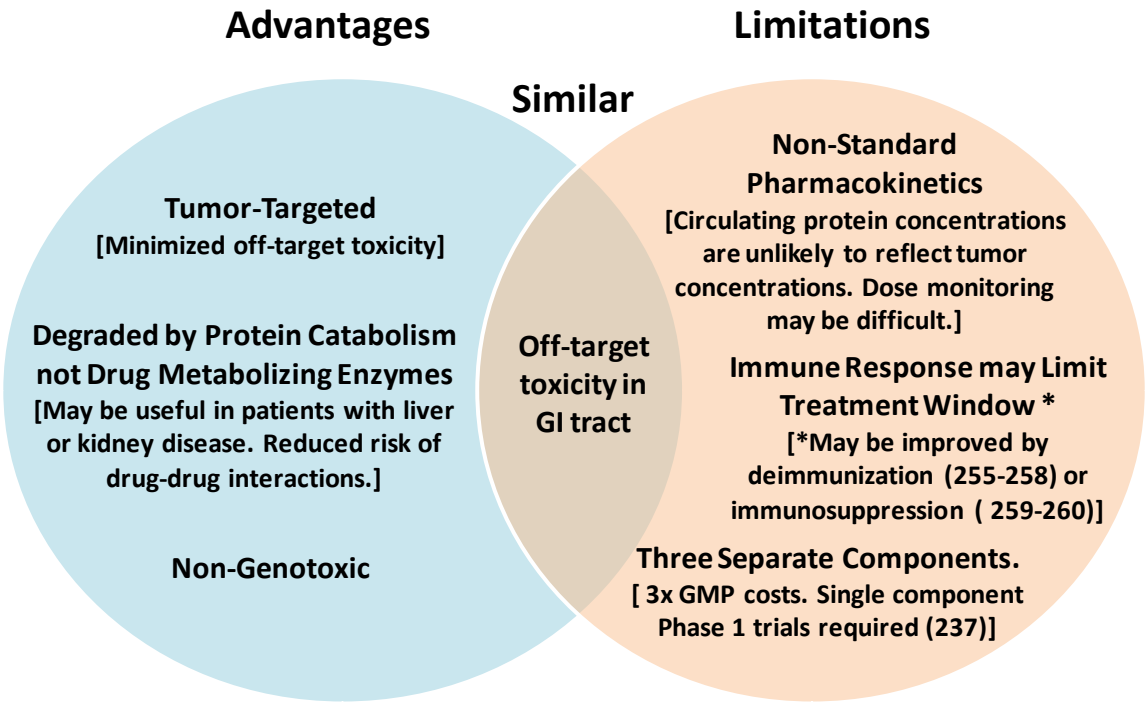

Figure 5.4: Foreseen advantages and limitations of IC-PrAg + LF relative to conventional chemotherapy. Venn diagram illustrating the anticipated advantages and limitations of using a dual MMP/uPA-activated anthrax lethal toxin in place of conventional chemotherapeutic agents in a clinical oncology setting.

In its current form, IC-PrAg + LF is a promising preclinical candidate, and further research to reduce immunogenicity, understand and minimize off-target toxicities, and/or improve tumor selectively will only add to this potential. As future characterization and optimization is performed it will be essential to bear in mind the biology underlying the system, and to use this knowledge to inform all aspects of experimental design. This will be especially critical with regard to pharmacology, where standard practices, such as dose-escalation style toxicity studies or classic pharmacokinetics, may provide misleading information if used in a conventional manner; and where dose scaling and treatment regimen must be carefully optimized to maximize the potential for a successful translation to a clinical setting.

APPENDIX I: PROTOCOLS

AI.1 Cell Culture and Maintenance

Materials:

α-MEM (Gibco 12571-063)

D-MEM (Gibco 11965-092)

FBS (Gibco 26140-079)

Pen Strep Glutamine (100X) (Gibco 1038-016)

PBS pH 7.4 (1X) (Gibco 10010-023) or DPBS (1X) (Gibco 14190-144)

0.05% Trypsin-EDTA (1X) (Gibco 25300-054)

10 cm cell-culture dishes (Corning, 100 mm x 20 mm, 430167)

Hybri-Max™ DMSO (Sigma D2650)

Cryovials (Corning 420487, 1.2 mL or 430488, 2.0 mL)

Freezing Chamber (Nalgene Cryo 1°C Freezing Container, 5100-0001)

0.4% Trypan Blue Stain (BioWhittaker 17-942E)

Complete Growth Media:

α-MEM + 10% FBS + 1% P/S/G [SCCF1]

D-MEM + 10% FBS + 1% P/S/G [Cal27, HeLa, Hep2, HN6, HN12, HN30, B16-BL6, HT1080]

Methods:

Thawing Cells: Direct Culture Method

1. Remove cells from storage and thaw quickly in a 37ºC water bath. Record label information in notebook. Spray vial with EtOH prior to opening in the sterile cell culture hood.
2. Using a pipette, transfer cells to a 10 cm dish containing 10 mL of complete growth medium.
3. Culture cells for 12-24 hours, then refresh the complete growth medium to remove DMSO.

Propagation in a 10 cm Plate (for Cells > 75% Confluent)

1. *Pre-warm complete growth medium to 37ºC.
2. Aspirate media.
3. Rinse plate with 10 mL sterile 1X PBS, aspirate.
4. Add 2 mL 1X Trypsin-EDTA to plate. Swirl to distribute evenly.
5. Incubate plate at 37ºC for 2-3 minutes or until cells have lifted.
6. Quench trypsinization, and resuspend cells, by adding 8 mL of complete growth media.
7. Add 8-10 mL of complete growth media to new 10 cm plates.

8. Seed new plates with aliquots of the cell suspension. (I typically use dilutions of 1:4 – 1:10)
9. Label new plates with initials, date, cell type and passage number.
10. Change media on the plates ~2X weekly, and monitor for confluence.

Counting Cells

1. Prepare the hemocytometer. Ensure that it is clean and debris-free, spray with 70% EtOH and wipe with a Kimwipe. Then place the hemocytometer cover glass.
2. Make sure that the cell suspension to be counted is homogenous. Flick tube or gently pipette up and down.
3. Mix a 100 µL aliquot of cells with 100 µL Trypan blue dye in a microcentrifuge tube. Flick tube to mix. Incubate for 5-15 minutes.
4. Transfer the cell + trypan blue mixture to the hemocytometer via capillary action (15-20 µL).
5. Count viable cells, in all 4 corner; 16 squares per corner. (Viable cells exclude the trypan blue and appear white on a blue background.)
6. Calculate viable cells.

$$\left(\frac{\text{Total Viable Cell Count}}{4}\right) \times \text{Dilution Factor} = \text{Viable Cell \#} \times 10^4 \text{/mL}$$

Freezing Down

1. Prepare freezing media: 90-95% complete growth media + 5-10% DMSO.
2. Label cryovials using an EtOH resistant marker. Include initials, cell line, date and passage #
3. Each confluent 10cm dish can be frozen in two cryovials. (4 x 10 cm plates = 8 cryovials)
4. Rinse plates with 1X PBS.
5. Add 2 mL 1X Trypsin-EDTA.
6. Incubate for 2-3 minutes at 37ºC, or until cells have lifted.
7. Add 10 mL of complete growth media to each plate and resuspend evenly.
8. Transfer cells to a 15 mL or 50 mL Falcon tube. Spin at low speed, 4ºC, for several minutes to pellet cells.
9. Spray outside of tube with 70% EtOH. Aspirate media.
10. Resuspend pellet in an appropriate volume of freezing media: 2 mL freezing media per 10 cm dish.
11. Once evenly resuspended, distribute 1 mL of the cell suspension into each cryovial.
12. Place cryovials in an insulated freezing chamber. Ensure that MeOH level is adequate.
13. Incubate at -80ºC for O/N to 48 hours.
14. Transfer cells to a N_2(l) storage rack.

Submitting Cells for Pathogen Testing

1. Pathogen testing and certification is required prior to using a cell line in vivo. Specific testing requirements vary across facilities, and we routinely use the IMPACT III Profile.
2. IMPACT testing is currently performed by IDEXX BioResearch.
3. Cryovials can be submitted for IMPACT testing as long as they contain 106 – 107 cells/vial, in a minimum volume of 0.5 mL Therefore, prior to freezing down cells for this purpose, an accurate cell count should be determined.

AI.2 Syngraft/Xenograft

Materials:

α-MEM (Gibco 12571-063) or D-MEM (Gibco 11965-092)

FBS (Gibco 26140-079)

Pen Strep Glutamine (100X) (Gibco 1038-016)

PBS pH 7.4 (1X) (Gibco 10010-023)

0.05% Trypsin-EDTA (1X) (Gibco 25300-054)

Cell Strainer, 100 µm (BD Falcon 352360)

1 mL TB Syringes with 27G x ½ Needle (standard injection) (BD 309623)

1 mL TB Syringes without needle (Matrigel injection) (Kendall Monoject 8881501400)

PrecisionGlide™ Needles 21G x 1½ (Matrigel injection) (BD 305167)

Matrigel™ (BD 354262)

Digital Calipers (Fowler 54-100-444-0)

Z-Fix, buffered zinc formalin fixative (Anatech Ltd., Catalog # 170)

Whatman 3mm Chr Filter Paper (Whatman, 3030-861)

80-well microcentrifuge rack (Bio Plas, Inc.)

Complete Growth Media:

α-MEM + 10% FBS + 1% P/S/G [SCCF1]

D-MEM + 10% FBS + 1% P/S/G [Cal27, HeLa, Hep2, HN6, HN12, B16-BL6]

Serum-Free Media:

α-MEM ±1% P/S/G [SCCF1]

D-MEM ±1% P/S/G [Cal27, HeLa, Hep2, HN6, HN12, B16-BL6]

Animals:

Syngraft: C57BL/6J (The Jackson Laboratory, Catalog #: 000664)

Xenograft: Hsd:Athymic Nude-*Foxn1*^{nu} mice (Harlan Laboratories, Inc.)

Notes:

*Prior to beginning ensure that you have sufficient cells in culture. Grow at least 2X as many as you anticipate needing to account for syringe dead volume and/or loss during preparation.

*Cells should be at ~70-80% confluence. If cells are at higher or lower confluence they may not be in an optimal growth phase.

*If using Matrigel, thaw beforehand. (Overnight at 4ºC on ice)

Estimating Required Cell Number

For syngrafts injecting 50E5 cells/mouse is often sufficient for rapid tumor growth. Higher cell concentrations are required for xenografts: 100-300E5 cells/mouse.

Preparing Cells for Injection

1. Aspirate media.
2. Rinse plates with 1X PBS and aspirate.
3. Add 1X Trypsin-EDTA and incubate at 37ºC until cells have lifted.
4. Neutralize with a 4:1 volume of complete growth media.
5. Pipette up and down to reduce clumping and resuspend evenly. Transfer cell solution through a cell strainer into a 50 mL falcon tube to further reduce clumping.
6. Spin cells at low speed, 4ºC, for 5 minutes to pellet. *Have ice ready. Chill serum-free media.
7. Spray falcon tubes with 70% EtOH. *From this point onward cells should be kept on ice at all times. Aspirate media.
8. Resuspend pellet in a small volume of serum-free media (1 mL).
9. Count cells and calculate viable cell concentration. These cells will be at a high concentration and cells should be counted at a 1:10 – 1:100 dilution.
10. Resuspend cells to desired concentration in chilled serum-free media, or Matrigel. Prepare at least 2X the amount of cell suspension that you plan on injecting to account for syringe dead volume, needle clogging, etc.

Subcutaneous Cell Transplant

1. *If injecting with Matrigel, syringes need to be pre-chilled on ice.
2. *For syngraft injections, mice should be shaved one day in advance.
3. Anesthetize mice with Isoflurane.
4. Flick or swirl cell suspension to ensure that it is mixed homogenously and load a syringe with sufficient cell suspension to inject 5 mice. I use an injection volume of between 100 µL to 200 µL per mouse. For Matrigel injections, syringe should be loaded without the needle.
5. Once syringes are filled keep them horizontal so that cells will not distribute preferentially to one end or the other. (If necessary flick syringe between injecting mice to keep the cell suspension homogenous.)
6. With the thumb and pointer finger of the non-injecting hand, tent the mouse skin creating a pouch in the dorsal subcutis, or on the left or right flank.
7. Insert needle, bevel-side-up and in horizontal orientation, through the skin between your fingertips. Take care not to puncture through two surfaces of the skin.

8. Release tent and slowly inject cell suspension. A bubble should form.
9. Remove needle carefully keeping needle horizontal. Minimal to no weeping should occur.
10. Return mouse to home cage and monitor recovery.
11. *With Matrigel injections I return the needle to ice between injections, to reduce the risk that it will gelatinize in the needle hub.

Monitoring Tumor Growth

1. Syngrafts tend to grow more rapidly than xenografts, and it is not unusual to reach the exponential growth phase within 5-7 days following cell injection. Xenografts typically take longer to grow and it would be unusual to see rapid growth within the first 14 days following cell injection. I measure syngrafts every 1-2 days following cell injection, I measure xenografts weekly.
2. Anesthetize mice with Isoflurane.
3. Measure the longest and shortest tumor axes with digital calipers.
4. Calculate tumor volume.
5. Depending upon the specific tumor type, experiments are typically initiated when the mean tumor volumes are between 50-100 mm^3.

A multiple nose-cone apparatus, such as the one pictured here, can be used to enhance the speed for procedures like tumor cell injection, tumor measurement and dosing. This was fabricated at the National Institutes of Health and is not commercially available.

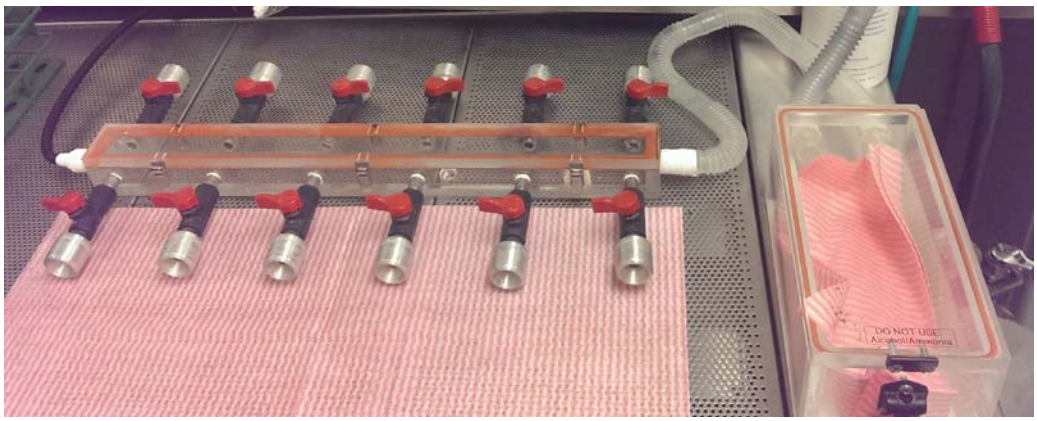

Figure AI-1: Multiple nose-cone apparatus for Isoflurane anesthetic use.

Tumor Harvesting

1. Euthanize mice with CO_2.
2. Excise tumor including a margin of skin.

3. If tumors are small, flatten on filter paper prior to fixing. Filter paper can be kept with specimen for processing and paraffin-embedding, it will not react with stains.
4. If tumors are large, they may need to bisected longitudinally prior to fixation to ensure adequate fixative permeation.
5. Place tissue in ~20 mL of Z-Fix in a glass scintillation vial. Label side and lid with sample identity using an ethanol resistant marker.
6. Fix for 24 hours (optimal) to 48 hours.
7. Bisect tumors longitudinally and transfer to 70% EtOH. The bottom side of an 80-well microcentrifuge rack is an optimal surface for trimming fixed tissues.
8. Samples can be kept in 70% EtOH indefinitely, but I process them as quickly as possible.

AI.3 Intraperitoneal (I.P.) Injection

Materials:

1 mL TB Syringes with 27G x ½ Needle (standard injection) (BD 309623)

Sharp Chute™ Portable Sharps Bin (Heathrow Scientific LLC HS21001A)

PBS pH 7.4 (1X) (Gibco 10010-023)

Notes:

Solutions for intraperitoneal injection should be prepared in a sterile isotonic solution such as PBS or saline. Pure H_2O should not be used as a diluent.

I typically use an injection volume of 400 µL for I.P. injections.

Excess solution must be made to account or syringe dead volume. Prepare at least 100 µL/dose extra.

Methods:

Mouse Restraint and Injection

1. Pre-fill syringes. A new syringe will be used for each injection.
2. Restrain the mouse. Isoflurane can be used if desired. If Isoflurane is not used ensure that you have a grip that will prevent the mouse from kicking the needle with their hind legs. Example grip pictured in Figure AI-2.
3. Tilt the head so that it is facing downward, shifting the abdominal organs cranially.
4. Identify the point of entry for the needle as photographed in Figure AI-2.
5. . Injecting on the right side of the mouse's abdomen reduces the risk of puncturing the cecum.

Figure AI-2: Restraint and needle entry point for intraperitoneal injections.

6. Insert the needle bevel-side-up into the abdomen at approximately a 30-degree angle.
7. Following penetration of the peritoneum, return the needle to a horizontal orientation, resting on the interior surface of the abdomen.
8. Aspirate to ensure that the needle has not punctured the intestines (brown), the urinary bladder (yellow), or a vessel or highly vascularized organ (red).
9. If no fluid is aspirated, inject the solution.* If the needle is positioned subcutaneously, rather than intraperitoneally, a bubble will immediately be observed. In this event, reposition the needle, aspirate again and inject solution. Note the quantity of dose that the mouse received I.P.in its record; ideally the volume will still exceed 90%.
10. Withdraw the needle and discard. Return the mouse to its home cage. If Isoflurane anesthesia was used, monitor for recovery.

AI.4 Intravenous (I.V.) Injection

Materials:

Holding Cage

Restrainer

0.5 mL Insulin Syringe with 29 G ½ Needle (Terumo SS*05M2913)

PBS pH 7.4 (1X) (Gibco 10010-023)

Heat Lamp

Sharp Chute™ Portable Sharps Bin (Heathrow Scientific LLC HS21001A)

Notes:

It is essential to use a syringe with low resistance as this enables you to identify that you are in the tail vein solely by feel. This is extremely important when injecting mice with tail veins that are difficult to visualize.

Use white heat lamp bulb; red bulbs, even at the same voltage are too hot. Animals must be monitored carefully while under the heat lamp to ensure that they do not overheat.

A mouse restrainer, like the one pictured in Figure AI-3, is ideal for tail vein injections. The mouse can be placed in the chamber quickly and is not confined, reducing stress. In addition, the elevation of the chamber allows you to hold the tail at an angle which is helpful to achieve an appropriate angle of entry with the syringe. This restrainer was fabricated at the National Institutes of Health and is not commercially available.

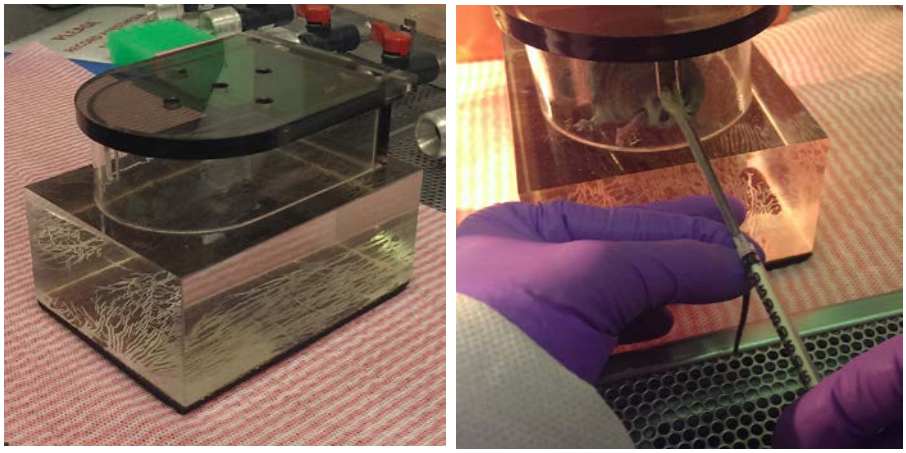

Figure AI-3: Mouse restrainer for tail vein injections.

Methods:

1. Obtain a clean cage to use as a holding cage for mouse warming. Turn on heat lamp and pre-warm cage.
2. Prepare set-up identical to that displayed in Figure AI-4.
3. Pre-fill syringes. I use an injection volume of 50 – 100 µL. Fill with a slightly larger so that a small volume can be ejected immediately prior to injection. Remove all air bubbles..

Figure AI-4: Optimal set-up for performing tail vein injections.

I.V. Injection

1. Transfer pre-warmed mouse to restrainer.
2. Check that syringe is not clogged by ejecting extra volume.
3. Hold tail taut at a comfortable angle.
4. Roll tail slightly so that lateral tail vein is visible, Injection can be performed on either the right or left side.
5. Initial injection attempts should be made as distal as possible, allowing for multiple attempts in a distal to cranial manner.
6. Insert needle, bevel side up, initially at an 15-20º angle. The tail vein is at a depth of approximately ¾ the length of the bevel, dependent upon the position on the tail.
7. Adjust needle angle so that it is horizontal to the lateral tail vein and advance slightly.
8. Inject solution. There should be no resistance on the plunger. If any resistance is felt, or if the tissue swells at the injection site. Remove needle and try again at a cranial position. Using a needle with low resistance, a volume of 1-10 µL would be lost with each missed injection.
9. Discard syringe.
10. Apply light pressure on tail until bleeding has stopped. Return mouse to home cage.

AI.5 Cardiac Puncture Blood Collection

Materials:

CO_2 Euthanasia Chamber

Ice

1 mL TB Syringes with 27G x ½ Needle (standard injection) (BD 309623)

Tubes with EDTA, Lavender Top (CBC) (BD Microtainer 365973)

Tubes, Red Top or Gold Top (Blood Chemistry):(BD Microtainer 365957 or 365959)

Notes:

Up to 1 mL of blood can be obtained.

Syringe grip is important. The syringe must be held such that constant back pressure can be applied throughout the procedure. Additionally, you must be able to extend the plunger to full volume capacity without adjusting your hand (Figure AI-5).

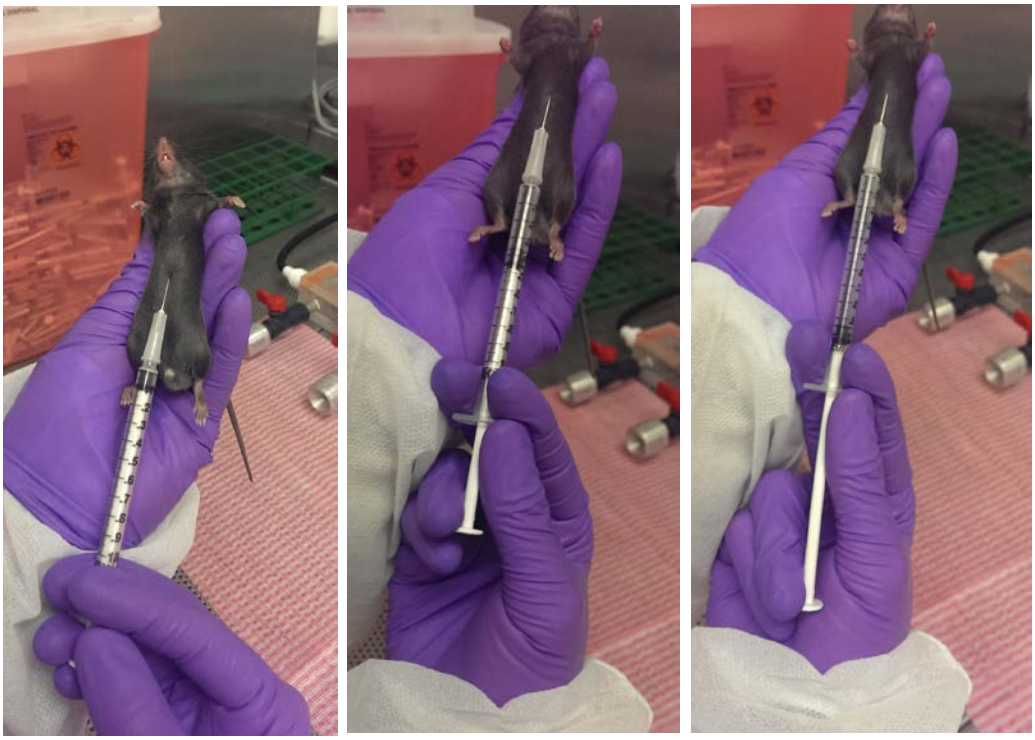

Figure AI-5: Syringe grip for cardiac puncture.

Methods:

Cardiac Puncture

1. Label collection tubes and place on ice.
2. Euthanize mouse by CO_2 asphyxiation.

3. Monitor mouse closely. Perform procedure as closely as possible to the time of death.
4. Restrain mouse as shown in Figure AI-5.
5. Insert needle slightly to the left of the xiphoid process of the sternum, pointed cranially, at a 20-30º angle.
6. Apply slow, steady back pressure. (Too much back pressure can cause the heart to collapse). Make small manipulations with the needle. When the needle is appropriately placed it will fill rapidly with blood. Hold the syringe steady at this point, while continuing to apply back-pressure. Even small movements may cause you to lose blood flow.
7. Carefully detach needle from syringe. Expel blood into pre-labeled tubes. Invert each tube, for ~30 seconds. If samples are not adequately mixed the blood may clot even if anti-coagulants are present in the collection tube.

AI.6 Immunohistochemistry (IHC)

Materials:

Safeclear II (Fisher Scientific 23-044-192)

30% H_2O_2 (Fisher Scientific H325-500)

PBS, pH 7.4 (10X), dilute 1:10 with DI H_2O (Gibco 70011-044)

10X TBS pH 7.4, dilute 1:10 with DI H_2O (Quality Biological Inc. 351-086-101)

Albumin Bovine, Fraction V (MP Biomedical 160069)

Whatman 3mm Chr Filter Paper (Whatman, 3030-861)

Blotting Tray

DAB (Sigma D4168-50SET)

ABC (Vectastain Elite ABC Kit, Standard* PK-6100)

ABC-AP (VectostainABC-AP Kit, Standard* AK-5000)

Vulcan Fast Red Chromagen Kit 2 (Biocare Medical FR805H)

Vina Green (Biocare Medical BRR807AH)

Hematoxylin (Sigma 51275)

Mounting Media (VectaMount™, Vector Laboratories H-5000)

24 x 50 Microscope Cover Glass (Thermo Scientific 24X50-1)

Notes:

When using alkaline phosphatase based detection systems, always use TBS instead of PBS.

When performing a double stain, it is necessary to use 1º Antibodies that were raised in different species. Also, it is optimal to use DAB first, as it is a very persistent dye that will not fade with alcohol, acid or xylene treatment.

Methods:

Day 1

1. Deparaffinize slides by incubating in Safeclear II, 3 x 5 min.
2. Hydrate with graded alcohol (100%, 95%, 70%), 2 x 5 min.
3. Block endogenous peroxidase activity by incubating in 3% H_2O_2 in 70% EtOH or 20-30 min.
   - H_2O_2 should be fresh, ideally replaced monthly. Using old H_2O_2 can increase background signal.
   - Extended incubation in the H_2O_2 solution will damage tissue. Do not leave longer than 30 min.
   - This step should be performed even when using alkaline phosphatase detection.
4. Wash extensively with DI H_2O, 3 x 5 min.

5. Perform antigen retrieval. Cover slides with a 10 mM citric acid solution. Heat in a microwave for 2-3 minutes at 100% power until boiling. Then reduce power to 10-20% and continue heating for 18 minutes.
    - Times and power levels may vary with different microwaves.
    - Be careful not to boil slides too vigorously, as tissue may detach.
6. Allow to cool.
7. Wash with DI H_2O, 3 x 5 min. While washing, prepare blocking solution: 2.5% BSA in PBS. Also prepare a humidified chamber, by moistening a piece of filter paper and placing it in a blotting tray.
8. Wash with PBS, 3 x 5 min.
9. Remove slides from PBS. Tap on paper towel to remove excess liquid. Place in humidified chamber. Add 50 – 200 µL blocking solution per slide. Ensure that tissue is covered and that slides are laying flat. Incubate at room temperature, covered, for 30-60 min. While slides are incubating prepare1º antibody solution (1º Ab in Blocking Solution at desired dilution).
10. Without rinsing, tap slides on paper towel to remove excess liquid. Return to humidified chamber. Add 100-200 µL of 1º antibody solution per slide.
11. Incubate at 4ºC overnight, covered.

Day 2

1. Wash with PBS, 3 x 5 min. While slides are rinsing, prepare2º antibody solution (2º Ab in Blocking Solution at desired dilution).
2. Tap slides on paper towel to remove excess liquid. Return to humidified chamber. Add 100-200 µL of 2º antibody solution per slide. Incubate at room temperature for 30-60 min. While slides are incubating prepare ABC, or ABC-AP, detection reagent; 1:50 Reagent A + 1:50 Reagent B in 2.5% BSA in PBS. ABC solutions must be prepared at least 30 min before use.
3. Wash with PBS, 3 x 5 min.
4. Incubate with ABC complex at room temperature for 30 minutes.
5. Wash with PBS, 3 x 5 min.
6. Prepare detection reagents as indicated by manufacturer. I use DAB, Vulcan FastRed and/or VinaGreen.
7. Incubate with the appropriate developing solution under microscopic control.
8. When stain has reached the desired intensity stop the reaction by immersing in DI H_2O.
9. Wash thoroughly with DI H_2O.
10. Proceed to Double Staining instructions below OR counterstain with hematoxylin for 30 seconds to 2 minutes.
11. Stabilize the hematoxylin by washing for 15 minutes in running *tap* water. Verify change in color from purple to blue.

12. Dehydrate in graded alcohols (70%, 95%, 100%) and Safeclear II, approximately 30 sec. x 2. Then mount slides with a permanent mounting media. Slides must be allowed to dry overnight before scanning or viewing under the microscope.

Day 2: Double Staining

1. Ensure that slides have been thoroughly rinsed in DI H_2O.
2. Elute Igs with 50 µM Citric Acid, 3 x 5 min.
3. Wash with DI H_2O, 3 x 5 min.
4. Incubate in 3% H_2O_2 in 70% EtOH for 30 min to quench exogenous peroxidase activity.
5. Wash with DI H_2O, 3 x 5 min.
6. Wash with PBS, 3 x 5 min.
7. Remove slides from PBS. Tap on paper towel to remove excess liquid. Place in humidified chamber. Add 50 – 200 µL blocking solution per slide. Ensure that tissue is covered and that slides are laying flat. Incubate at room temperature, covered, for 30-60 min. While slides are incubating prepare the second 1º antibody solution.
8. Without rinsing, tap slides on paper towel to remove excess liquid. Return to humidified chamber. Add 100-200 µL of 1º antibody solution per slide.
9. Incubate at 4ºC overnight, covered.

Day 3: Double Staining

1. Wash with PBS, 3 x 5 min. While slides are rinsing, prepare2º antibody solution.
2. Tap slides on paper towel to remove excess liquid. Return to humidified chamber. Add 100-200 µL of 2º antibody solution per slide. Incubate at room temperature for 30-60 min. While slides are incubating prepare ABC, or ABC-AP, detection reagent; 1:50 Reagent A + 1:50 Reagent B in 2.5% BSA in PBS. ABC solutions must be prepared at least 30 min before use.
3. Wash with PBS, 3 x 5 min.
4. Incubate with ABC complex at room temperature for 30 minutes.
5. Wash with PBS, 3 x 5 min.
6. Prepare detection reagent as indicated by manufacturer. DAB should have been used for the first stain, VinaGreen should be used for the second stain. (Visually, it is easier to distinguish Brown/Green than it is to distinguish Brown/Red.)
7. Incubate with the appropriate developing solution under microscopic control.
8. When stain has reached the desired intensity stop the reaction by immersing in DI H_2O.
9. Wash thoroughly with DI H_2O.
10. Counterstain with hematoxylin for 30 seconds to 2 minutes.
11. Stabilize the hematoxylin by washing for 15 minutes in running *tap* water. Verify change in color from purple to blue.

12. Dehydrate in graded alcohols (70%, 95%, 100%) approximately 30 sec. x 2.
13. Clear in SafeClear II.
14. Mount slides with a permanent mounting media. Slides must be allowed to dry overnight before scanning or viewing under the microscope.

AI.7 MTT Cytotoxicity Assay

Materials:

α-MEM Gibco 12571-063) or D-MEM (Gibco 11965-092)

FBS (Gibco 26140-079)

Pen Strep Glutamine (100X) (Gibco 1038-016)

PBS pH 7.4 (1X) (Gibco 10010-023)

96-well Cell Culture Plates (Corning 3596)

Sterile Reagent Reservoirs (Thermo Scientific 8093-11)

MTT (Sigma M2128-1G)

Isopropanol (Sigma 190764-500mL)

10% SDS (KD Medical RGE-3230)

12.1 M HCl (Mallinckrodt Baker 9535-02)

Multi-channel Pipette

Multi-channel Aspirator

Complete Growth Media:

α-MEM + 10% FBS + 1% P/S/G [SCCF1]

D-MEM + 10% FBS + 1% P/S/G [Cal27, HeLa, Hep2, HN6, HN12, HN30, B16-BL6, HT1080]

Methods:

Assay in a 96-well Format

1. Aspirate media, rinse with PBS, and add 200 µL fresh complete growth medium.
2. Add 30 µL MTT Solution: 5 mg/mL in complete growth medium.
3. Incubate for 1-2 hours at 37°C (optimal time is cell line dependent).
4. Aspirate, or pour, medium off.
5. Add 50 µL formazan solubilizer per well.
6. Shake for 30 seconds.
7. Measure absorbance @ 570 – 630 nm.

Formazan Solubilizer

205 mL Isopropanol
25 mL 10% SDS
1.65 mL 12.1 M HCl
36.7 mL DI H_2O

Use fresh SDS (No precipitate): SDS quality can affect the MTT color

AI.8 Gelatin Zymography

Materials:

Gelatin Gel (Novex 10% Zymogram (Gelatin) Gel, 1.0 mm x 10 well. EC6175BOX)

Sample Loading Buffer (Novex Tris-Glycine SDS Sample Buffer (2X). LC2676)

Running Buffer (Novex Tris-Glycine SDS Running Buffer (10X). LC2675)

Renaturing Buffer (Novex Zymogram Renaturing Buffer (10X). LC2670)

Developing Buffer (Novex Zymogram Developing Buffer (10X). LC2671)

EDTA (Quality Biological, Inc. 0.5M EDTA, pH 8.0 Molecular Biology Grade)

Protein Ladder (Novex SeeBlue Plus2 Prestained Standard. LC5925)

Coomassie Brilliant Blue R-250 (Bio-Rad 1610400)

Notes:

When performing gelatin-zymography to detect MMPs, prepare and run 2 identical gels. One will be washed and developed in buffers containing EDTA (a known MMP inhibitor) the other will be developed without EDTA. Bands specific for MMPs will be found only in the gel without EDTA.

Methods:

Running Gel, Staining and De-Staining

1. Mix samples with Sample Loading Buffer 1:2. *Do not boil or reduce. Samples can contain protease inhibitors. We use: Sigma P8340)*
2. Prepare Chamber. [Ensure that the tape at the bottom the gels has been removed and that gels are inserted in chamber such that the comb faces inward.]
3. Rinse wells with Running Buffer and load samples.
4. Run gel at a constant voltage of **100V,** on ice, for **3-4 hours**. [This will allow for separation of pro-/intermediate/active forms of MMP-2/9.]
5. After electrophoresis, remove the gel and incubate in 1X Zymogram Renaturing Buffer (+/- 100 mM EDTA) for 30 minutes at RT with gentle agitation.
6. Decant the Zymogram Renaturing Buffer and add 1X Zymogram Developing Buffer (+/- 100 mM EDTA) and equilibrate the gel for30 minutes at RT with gentle agitation.
7. Decant the buffer and add fresh 1X Zymogram Developing Buffer (+/- 100 mM EDTA). Incubate O/N to 24 hr at 37C. Cover container with Parafilm.
8. The next day, decant the Zymogram Developing Buffer and rinse with De-Stain Solution.

De-Stain Solution

20% MeOH (20-30% of either MeOH or EtOH OK)*
10 % Acetic Acid

*Composition should match the Coomassie Brilliant Blue Stain Solution.

9. Add Coomassie Brilliant Blue Stain Solution. Leave O/N (minimum), RT, covered with gentle agitation.

Coomassie Brilliant Blue Stain Solution

0.2% Coomassie Brilliant Blue R-250 (0.1-0.5% OK)
20% MeOH (20-30% of either MeOH or EtOH OK)
10 % Acetic Acid

When preparing the stain solution dissolve CBB directly in the MeOH of EtOH. Add acetic acid, and then q.s. to desired volume with DI H_2O. Stain can be re-used.

10. Following staining, de-stain with 10% Acetic Acid, 30% MeOH.
11. When stain has reached desired intensity, remove de-stain, obtain image. *Optional, incubate with 10-20% Acetic Acid O/N. (This treatment makes bands “pop”).
12. Photograph or scan gel. Clear sheet protectors are easier to manipulate than saran wrap for imaging purposes.
13. Dry gel if desired.

AI.9 Plasminogen/Casein Zymography

Materials:

Protogel (National Diagnostics. EC-890)

4X Protogel Resolving Buffer. (National Diagnostics. EC-892)

Protogel Stacking Buffer. (National Diagnostics. EC-893)

TEMED (Biorad. 161-0800)

Ammonium Persulfate (APS). (Biorad. 161-0700)

Non-Fat Dry Milk (LabScientific, Inc. M0842)

Plasminogen, Lys-Type, Human Plasma (Calbiochem 528185)

Sample Loading Buffer (Novex Tris-Glycine SDS Sample Buffer (2X). LC2676)

Running Buffer (Novex Tris-Glycine SDS Running Buffer (10X). LC2675)

Triton X-100 (Sigma. T-9284)

UltraPure Glycine (Invitrogen. 15527-013)

EDTA (Quality Biological, Inc. 0.5M EDTA, pH 8.0 Molecular Biology Grade)

Protein Ladder (Novex SeeBlue Plus2 Prestained Standard. LC5925)

Coomassie Brilliant Blue R-250 (Bio-Rad 1610400)

Notes:

When performing Plasminogen/Casein-zymography for detection of uPA activity, 2 separate gels should be prepared (+/- plasminogen). Additionally, control samples such as urine collected from uPA+/+ and uPA-/- mice can be run alongside samples as positive and negative controls.

Methods:

Gel

1. Pour 10.5% Acrylamide/0.1% SDS gels containing 1% Nonfat Dry Milk, ± 20 µg/mL Human Plasminogen. (Milk solution should be boiled, cooled and filtered before each use.)

Resolving Gel (10 mL)	**Stacking Gel (5 mL)**
4.1 mL Nonfat Dry Milk Solution. [0.024 g/mL milk in DI H_2O. Milk solution should be boiled, cooled, and filtered before each use.] 2.5 mL 4X ProtoGel Resolving Buffer 3.3 mL ProtoGel 100 µL 10% APS 4 µL TEMED +/- 20 µg/mL Human Plasminogen (200 µL of 1 mg/mL solution)	3 mL DI water 1.2 mL ProtoGel Stacking Buffer 0.65 mL ProtoGel 25 µL 10% APS 5 µL TEMED

Running Gel, Staining and De-Staining

1. Mix samples with Sample Loading Buffer 1:2. *Do not boil or reduce. Samples must not contain protease inhibitors.*
2. Include 1-5 µL $uPA^{+/+}$ and $uPA^{-/-}$ urine as control samples.
3. Rinse wells with Running Buffer and load samples.
4. Run gel for desired length of time.
5. After electrophoresis, remove the gels and wash 2x 30 min with 2.5% Triton X-100, 10 mM EDTA to remove SDS.
6. Add developing buffer [100 mM Glycine, 10 mM EDTA, pH 8.3]. Incubate O/N to 24 hr at 37C. Cover container with Parafilm.
7. The next day, decant the Developing Buffer and rinse with De-Stain (10% Acetic Acid, 30% Methanol)
8. Add Coomassie Stain Solution. Leave O/N (minimum), RT, covered with gentle agitation.

Coomassie Brilliant Blue Stain Solution

0.2% Coomassie Brilliant Blue R-250 (0.1-0.5% OK)
20% MeOH (20-30% of either MeOH or EtOH OK)
10 % Acetic Acid

When preparing the stain solution dissolve CBB directly in the MeOH of EtOH. Add acetic acid, and then q.s. to desired volume with DI H_2O. Stain can be re-used.

9. Following staining, de-stain with 10% Acetic Acid, 30% MeOH.
10. *Optional, incubate with 10-20% Acetic Acid O/N. (This treatment makes bands “pop”).
11. Photograph or scan gel. Clear sheet protectors are easier to manipulate than saran wrap for imaging purposes.
12. Dry gel if desired.

AI.10 Tumor Transplantation

Materials:

α-MEM Gibco 12571-063)

FBS (Gibco 26140-079)

Pen Strep Glutamine (100X) (Gibco 1038-016)

0.05% Trypsin-EDTA (1X) (Gibco 25300-054)

10 cm cell-culture dishes (Corning, 100 mm x 20 mm, 430167)

1 mL TB Syringes without needle (Matrigel injection) (Kendall Monoject 8881501400)

PrecisionGlide™ Needles 21G x 1½ (Matrigel injection) (BD 305167)

Matrigel™ (BD 354262)

Razor Blades, Single Edge (GEM Blue Star)

Complete Growth Media:

α-MEM + 10% FBS + 1% P/S/G [SCCF1]

Serum-Free Media:

α-MEM ±1% P/S/G [SCCF1]

Animals:

Hsd:Athymic Nude-*Foxn1*^{nu} mice (Harlan Laboratories, Inc.)

Notes:

Matrigel needs to be thawed one day in advance. Thaw overnight at 4°C, on ice.

When you transplant a tumor you lose at least 50% of the cell mass.

With some slow growing tumors, if you increase the Matrigel concentration to can increase the chance that the transplant will be successful.

Transplanting tumor pieces will result in heterogeneous tumor growth, which is less consistent than the cell suspension method described here.

Methods:

Tumor Harvesting and Cell Preparation

1. CO_2 euthanize mice.
2. Spray mouse, and instruments, with 70% EtOH to sanitize.
3. Remove tumor. Trim away from skin. Cut into large pieces (do not chop, just increase the surface area)
4. Place tumor pieces in a sterile 10 cm dish containing 1X trypsin.
5. Incubate for 30 min at 37°C. You can also incubate overnight at 4°C.

6. One at a time, transfer tissue pieces to a clean 10 cm dish and mince with a razor blade. Return to Trypsin containing plate.
7. Rinse plate where tissues were minced with trypsin.
8. Incubate for 5 min at 37 °C.
9. Pass contents through a cell strainer into a 50 mL Falcon tube. Use pipette action to break up clumps.
10. Rinse dish with complete growth media, this will also neutralize trypsin. (Use a 4:1 volume)
11. Connective tissue will remain in the filter and can be discarded. Cancer cells will be in the flow-through.
12. Spin at low speed, 4°C, for 5 minutes to pellet cells. While cells are spinning chill syringes on ice.
13. Place Cell Pellet on ice. Aspirate media. Resuspend in a small volume of serum-free media. Count.
14. Add serum free media and Matrigel to achieve the desired cell concentration. I have been injecting the SCCF1 cells in Matrigel only since it appears to help their growth. With other cell lines a 1:1 mixture is often used.

Subcutaneous Cell Transplant with Matrigel

1. Syringes need to be pre-chilled.
2. Anesthetize mice with Isoflurane.
3. Fill syringe (no needle) with 200 µL cell suspension per mouse.
4. Add 21 g needle and remove air bubbles.
5. Keep syringe in a horizontal orientation, and keep it cold. Matrigel will polymerize rapidly when it warms. To prevent this from occurring (especially in the needle bore or hub) the syringe can be laid flat on the ice in between injections.
6. With the thumb and pointer finger of the non-injecting hand, tent the mouse skin creating a pouch in the dorsal subcutis, or on the left or right flank.
7. Insert needle, bevel-side-up and in horizontal orientation, through the skin between your fingertips
8. Inject the cell suspension while releasing grip on the skin. A bubble should form.
9. Remove needle carefully keeping needle horizontal. Minimal to no weeping should occur.
10. Return needle to ice, and return mouse to home cage and monitor recovery.

REFERENCES

1. Jemal A, Bray F, Center MM, Ferlay J, Ward E, Forman D. Global cancer statistics. CA Cancer J Clin. 2011;61:69-90.

2. Ferlay J, Shin HR, Bray F, Forman D, Mathers C, Parkin DM. Estimates of worldwide burden of cancer in 2008: GLOBOCAN 2008. Int J Cancer. 2010;127:2893-917.

3. Cancer facts and figures, 2014. *American Cancer Society*.

4. Barnes L. Pathology and genetics of head and neck tumours: IARC; 2005.

5. Pazdur R, Hoskins WJ. Cancer management: a multidisciplinary approach: medical, surgical & radiation oncology, 9th edition: Oncology Group; 2005.

6. Ries LAG EM, Kosary CL, Hankey BF, Miller BA, Clegg L, Mariotto A, Feuer EJ, Edwards BK SEER Cancer Statistics Review, 1975-2002. http://seer.cancer.gov/csr/1975_2002/.

7. Howlader N NA, Krapcho M, Garshell J, Neyman N, Altekruse SF, Kosary CL, Yu M, Ruhl J, Tatalovich Z, Cho H, Mariotto A, Lewis DR, Chen HS, Feuer EJ, Cronin KA SEER Cancer Statistics Review, 1975-2010. http://seer.cancer.gov/csr/1975_2010/.

8. NCCN Clinical Practice Guidelines in Oncology (NCCN Guidelines): Head and Neck Cancers. Version 2.2013. http://oralcancerfoundation.org/treatment/pdf/head-and-neck.pdf.

9. Head and Neck Cancer: Multidisciplinary Management Guidelines, 4th edition. London; 2011.

10. Carvalho AL, Nishimoto IN, Califano JA, Kowalski LP. Trends in incidence and prognosis for head and neck cancer in the United States: A site-specific analysis of the SEER database. Int J Cancer. 2005;114:806-16.

11. Bjordal K, Kaasa S, Mastekaasa A. Quality of life in patients treated for head and neck cancer: A follow-up study 7 to 11 years after radiotherapy. Int J Radiat Oncol Biol Phys. 1994;28:847-56.

12. Klein J, Livergant J, Ringash J. Health related quality of life in head and neck cancer treated with radiation therapy with or without chemotherapy: A systematic review. Oral Oncol. 2014;50:254-62.

13. Grundmann O, Mitchell GC, Limesand KH. Sensitivity of salivary glands to radiation: from animal models to therapies. J Dent Res. 2009;88:894-903.

14. Nelson GM. Biology of taste buds and the clinical problem of taste loss. Anat Rec. 1998;253:70-8.

15. Garcia-Serra A, Amdur RJ, Morris CG, Mazzaferri E, Mendenhall WM. Thyroid function should be monitored following radiotherapy to the low neck. Am J Clin Oncol. 2005;28:255-8.

16. Vergeer MR, Doornaert PA, Rietveld DH, Leemans CR, Slotman BJ, Langendijk JA. Intensity-modulated radiotherapy reduces radiation-induced morbidity and improves health-related quality of life: results of a nonrandomized prospective study using a standardized follow-up program. Int J Radiat Oncol Biol Phys. 2009;74:1-8.

17. Pow EH, Kwong DL, McMillan AS, Wong MC, Sham JS, Leung LH, et al. Xerostomia and quality of life after intensity-modulated radiotherapy vs. conventional radiotherapy for early-stage nasopharyngeal carcinoma: initial report on a randomized controlled clinical trial. Int J Radiat Oncol Biol Phys. 2006;66:981-91.

18. Chambers MS, Garden AS, Kies MS, Martin JW. Radiation-induced xerostomia in patients with head and neck cancer: pathogenesis, impact on quality of life, and management. Head Neck. 2004;26:796-807.

19. Slootweg PJ, Bolle CW, Koole R, Hordijk GJ. Cause of death in squamous cell carcinoma of the head and neck. An autopsy study on 31 patients. J Craniomaxillofac Surg. 1992;20:225-7.

20. Coatesworth AP, Tsikoudas A, MacLennan K. The cause of death in patients with head and neck squamous cell carcinoma. J Laryngol Otol. 2002;116:269-71.

21. Adelstein DJ. Systemic chemotherapy for squamous cell head and neck cancer. Expert Opin Pharmacother. 2003;4:2151-63.

22. Forastiere A, Koch W, Trotti A, Sidransky D. Head and Neck Cancer. N Engl J Med. 2001;345:1890-900.

23. Pignon JP, le Maitre A, Maillard E, Bourhis J, Group M-NC. Meta-analysis of chemotherapy in head and neck cancer (MACH-NC): an update on 93 randomised trials and 17,346 patients. Radiother Oncol. 2009;92:4-14.

24. Cooper JS, Pajak TF, Forastiere AA, Jacobs J, Campbell BH, Saxman SB, et al. Postoperative concurrent radiotherapy and chemotherapy for high-risk squamous-cell carcinoma of the head and neck. N Engl J Med. 2004;350:1937-44.

25. Mehra R, Cohen RB, Harari PM. EGFR inhibitors for the treatment of squamous cell carcinoma of the head and neck. Curr Oncol Rep. 2008;10:176-84.

26. Kalyankrishna S, Grandis JR. Epidermal Growth Factor Receptor Biology in Head and Neck Cancer. J Clin Oncol. 2006;24:2666-72.

27. Rubin Grandis J, Melhem MF, Gooding WE, Day R, Holst VA, Wagener MM, et al. Levels of TGF-alpha and EGFR protein in head and neck squamous cell carcinoma and patient survival. J Natl Cancer Inst. 1998;90:824-32.

28. Dassonville O, Formento JL, Francoual M, Ramaioli A, Santini J, Schneider M, et al. Expression of epidermal growth factor receptor and survival in upper aerodigestive tract cancer. J Clin Oncol. 1993;11:1873-8.

29. Mehra R, Cohen RB, Burtness BA. The role of cetuximab for the treatment of squamous cell carcinoma of the head and neck. Clin Adv Hematol Oncol. 2008;6:742-50.

30. Ang KK, Berkey BA, Tu X, Zhang HZ, Katz R, Hammond EH, et al. Impact of epidermal growth factor receptor expression on survival and pattern of relapse in patients with advanced head and neck carcinoma. Cancer Res. 2002;62:7350-6.

31. Pollack VA, Savage DM, Baker DA, Tsaparikos KE, Sloan DE, Moyer JD, et al. Inhibition of epidermal growth factor receptor-associated tyrosine phosphorylation in human carcinomas with CP-358,774: dynamics of receptor inhibition in situ and antitumor effects in athymic mice. J Pharmacol Exp Ther. 1999;291:739-48.

32. Niu G, Sun X, Cao Q, Courter D, Koong A, Le Q-T, et al. Cetuximab-Based Immunotherapy and Radioimmunotherapy of Head and Neck Squamous Cell Carcinoma. Clin Cancer Res. 2010;16:2095-105.

33. Bonner JA, Harari PM, Giralt J, Azarnia N, Shin DM, Cohen RB, et al. Radiotherapy plus cetuximab for squamous-cell carcinoma of the head and neck. N Engl J Med. 2006;354:567-78.

34. Levy A, Blanchard P, Bellefqih S, Brahimi N, Guigay J, Janot F, et al. Concurrent use of cisplatin or cetuximab with definitive radiotherapy for locally advanced head and neck squamous cell carcinomas. Strahlenther Onkol. 2014.

35. Ye AY, Hay JH, Laskin JJ, Wu JS, Ho CC. Toxicity and outcomes in combined modality treatment of head and neck squamous cell carcinoma: cisplatin versus cetuximab. J Cancer Res Ther. 2013;9:607-12.

36. Koutcher L, Sherman E, Fury M, Wolden S, Zhang Z, Mo Q, et al. Concurrent cisplatin and radiation versus cetuximab and radiation for locally advanced head-and-neck cancer. Int J Radiat Oncol Biol Phys. 2011;81:915-22.

37. Caudell JJ, Sawrie SM, Spencer SA, Desmond RA, Carroll WR, Peters GE, et al. Locoregionally advanced head and neck cancer treated with primary radiotherapy: a comparison of the addition of cetuximab or chemotherapy and the impact of protocol treatment. Int J Radiat Oncol Biol Phys. 2008;71:676-81.

38. Walsh L, Gillham C, Dunne M, Fraser I, Hollywood D, Armstrong J, et al. Toxicity of cetuximab versus cisplatin concurrent with radiotherapy in locally advanced head and neck squamous cell cancer (LAHNSCC). Radiother Oncol. 2011;98:38-41.

39. Dragon DC, Rennie RP. The ecology of anthrax spores: tough but not invincible. Can Vet J. 1995;36:295-301.

40. Gould GW. Recent Advances in the Understanding of Resistance and Dormancy in Bacterial Spores. J Appl Bacteriol. 1977;42:297-309.

41. Watson A, Keir D. Information on which to base assessments of risk from environments contaminated with anthrax spores. Epidemiol Infect. 1994;113:479-90.

42. Dixon TC, Meselson M, Guillemin J, Hanna PC. Anthrax. N Engl J Med. 1999;341:815-26.

43. Organization WH. Guidelines for the Surveillance and Control of Anthrax in Humans and Animals. In: Diseases WDoEOC, editor.: World Heath Organization; 1998.

44. Riedel S. Anthrax: a continuing concern in the era of bioterrorism. Proc (Bayl Univ Med Cent). 2005;18:234-43.

45. Turell MJ, Knudson GB. Mechanical transmission of Bacillus anthracis by stable flies (Stomoxys calcitrans) and mosquitoes (Aedes aegypti and Aedes taeniorhynchus). Infect Immun. 1987;55:1859-61.

46. Bradaric N, Punda-Polic V. Cutaneous anthrax due to penicillin-resistant Bacillus anthracis transmitted by an insect bite. Lancet. 1992;340:306-7.

47. Hendricks KA, Wright ME, Shadomy SV, Bradley JS, Morrow MG, Pavia AT, et al. Centers for disease control and prevention expert panel meetings on prevention and treatment of anthrax in adults. Emerg Infect Dis. 2014;20.

48. Beatty ME, Ashford DA, Griffin PM, Tauxe RV, Sobel J. Gastrointestinal anthrax: review of the literature. Arch Intern Med. 2003;163:2527-31.

49. From the Centers for Disease Control and Prevention. Human ingestion of Bacillus anthracis-contaminated meat--Minnesota, August 2000. J Am Med Assoc. 2000;284:1644-6.

50. MacDonald WD. Anthrax: Report of a Fatal Case Involving the Cutaneous and Gastrointestinal Systems. N Engl J Med. 1942;226:949-51.

51. Gastrointestinal anthrax after an animal-hide drumming event - New Hampshire and Massachusetts, 2009. MMWR Morb Mortal Wkly Rep. 2010;59:872-7.

52. Jernigan JA, Stephens DS, Ashford DA, Omenaca C, Topiel MS, Galbraith M, et al. Bioterrorism-related inhalational anthrax: the first 10 cases reported in the United States. Emerg Infect Dis. 2001;7:933-44.

53. Metcalfe N. The history of woolsorters' disease: a Yorkshire beginning with an international future? Occup Med (Lond). 2004;54:489-93.

54. Cohen HW, Gould RM, Sidel VW. The pitfalls of bioterrorism preparedness: the anthrax and smallpox experiences. Am J Public Health. 2004;94:1667-71.

55. Hanczaruk M RU, Holzmann T, Frangoulidis D, Wagner DM, Keim PS, et al. Injectional anthrax in heroin users, Europe, 2000–2012 [letter]. Emerg Infect Dis. 2014.

56. Grunow R, Verbeek L, Jacob D, Holzmann T, Birkenfeld G, Wiens D, et al. Injection anthrax--a new outbreak in heroin users. Dtsch Arztebl Int. 2012;109:843-8.

57. Ringertz SH, Hoiby EA, Jensenius M, Maehlen J, Caugant DA, Myklebust A, et al. Injectional anthrax in a heroin skin-popper. Lancet. 2000;356:1574-5.

58. An Outbreak of Anthrax Among Drug Users in Scotland, December 2009 to December 2010. A report on behalf of the National Anthrax Outbreak Control Team. Health Protection Scotland (HPS). 2011.

59. Veitch J, Kansara A, Bailey D, Kustos I. Severe systemic Bacillus anthracis infection in an intravenous drug user. BMJ Case Rep. 2014;2014.

60. Russell L, Pedersen M, Jensen AV, Soes LM, Hansen AB. Two anthrax cases with soft tissue infection, severe oedema and sepsis in Danish heroin users. BMC Infect Dis. 2013;13:408.

61. Holzmann T, Frangoulidis D, Simon M, Noll P, Schmoldt S, Hanczaruk M, et al. Fatal anthrax infection in a heroin user from southern Germany, June 2012. Euro Surveill. 2012;17.

62. Ruckert C, Licht K, Kalinowski J, Espirito Santo C, Antwerpen M, Hanczaruk M, et al. Draft genome sequence of Bacillus anthracis UR-1, isolated from a German heroin user. J Bacteriol. 2012;194:5997-8.

63. Organization WH. Anthrax in Humans and Animals, 4th Edition; 2007.

64. Moayeri M, Leppla SH. The roles of anthrax toxin in pathogenesis. Curr Opin Microbiol. 2004;7:19-24.

65. Welkos SL, Vietri NJ, Gibbs PH. Non-toxigenic derivatives of the Ames strain of Bacillus anthracis are fully virulent for mice: role of plasmid pX02 and chromosome in strain-dependent virulence. Microb Pathog. 1993;14:381-8.

66. Welkos SL. Plasmid-associated virulence factors of non-toxigenic (pX01-) Bacillus anthracis. Microb Pathog. 1991;10:183-98.

67. Ezzell JW, Welkos SL. The capsule of bacillus anthracis, a review. J Appl Microbiol. 1999;87:250.

68. Okinaka RT, Cloud K, Hampton O, Hoffmaster AR, Hill KK, Keim P, et al. Sequence and organization of pXO1, the large Bacillus anthracis plasmid harboring the anthrax toxin genes. J Bacteriol. 1999;181:6509-15.

69. Loving CL, Khurana T, Osorio M, Lee GM, Kelly VK, Stibitz S, et al. Role of anthrax toxins in dissemination, disease progression, and induction of protective adaptive immunity in the mouse aerosol challenge model. Infect Immun. 2009;77:255-65.

70. Bradley KA, Mogridge J, Mourez M, Collier RJ, Young JA. Identification of the cellular receptor for anthrax toxin. Nature. 2001;414:225-9.

71. Scobie HM, Rainey GJ, Bradley KA, Young JA. Human capillary morphogenesis protein 2 functions as an anthrax toxin receptor. Proc Natl Acad Sci U S A. 2003;100:5170-4.

72. Liu S, Crown D, Miller-Randolph S, Moayeri M, Wang H, Hu H, et al. Capillary morphogenesis protein-2 is the major receptor mediating lethality of anthrax toxin in vivo. Proc Natl Acad Sci U S A. 2009;106:12424-9.

73. Klimpel KR, Molloy SS, Thomas G, Leppla SH. Anthrax toxin protective antigen is activated by a cell surface protease with the sequence specificity and catalytic properties of furin. Proc Natl Acad Sci U S A. 1992;89:10277-81.

74. Milne JC, Furlong D, Hanna PC, Wall JS, Collier RJ. Anthrax protective antigen forms oligomers during intoxication of mammalian cells. J Biol Chem. 1994;269:20607-12.

75. Kintzer AF, Thoren KL, Sterling HJ, Dong KC, Feld GK, Tang, II, et al. The protective antigen component of anthrax toxin forms functional octameric complexes. J Mol Biol. 2009;392:614-29.

76. Quinn CP, Singh Y, Klimpel KR, Leppla SH. Functional mapping of anthrax toxin lethal factor by in-frame insertion mutagenesis. J Biol Chem. 1991;266:20124-30.

77. Arora N, Klimpel KR, Singh Y, Leppla SH. Fusions of anthrax toxin lethal factor to the ADP-ribosylation domain of Pseudomonas exotoxin A are potent cytotoxins which are translocated to the cytosol of mammalian cells. J Biol Chem. 1992;267:15542-8.

78. Pimental RA, Christensen KA, Krantz BA, Collier RJ. Anthrax toxin complexes: heptameric protective antigen can bind lethal factor and edema factor simultaneously. Biochem Biophys Res Commun. 2004;322:258-62.

79. Mogridge J, Cunningham K, Collier RJ. Stoichiometry of anthrax toxin complexes. Biochemistry. 2002;41:1079-82.

80. Abrami L, Liu S, Cosson P, Leppla SH, van der Goot FG. Anthrax toxin triggers endocytosis of its receptor via a lipid raft-mediated clathrin-dependent process. J Cell Biol. 2003;160:321-8.

81. Miller CJ, Elliott JL, Collier RJ. Anthrax protective antigen: prepore-to-pore conversion. Biochemistry. 1999;38:10432-41.

82. Lacy DB, Wigelsworth DJ, Melnyk RA, Harrison SC, Collier RJ. Structure of heptameric protective antigen bound to an anthrax toxin receptor: a role for receptor in pH-dependent pore formation. Proc Natl Acad Sci U S A. 2004;101:13147-51.

83. Blaustein RO, Koehler TM, Collier RJ, Finkelstein A. Anthrax toxin: channel-forming activity of protective antigen in planar phospholipid bilayers. Proc Natl Acad Sci U S A. 1989;86:2209-13.

84. Wesche J, Elliott JL, Falnes PO, Olsnes S, Collier RJ. Characterization of membrane translocation by anthrax protective antigen. Biochemistry. 1998;37:15737-46.

85. Collier RJ. Membrane translocation by anthrax toxin. Mol Aspects Med. 2009;30:413-22.

86. Duesbery NS, Webb CP, Leppla SH, Gordon VM, Klimpel KR, Copeland TD, et al. Proteolytic inactivation of MAP-kinase-kinase by anthrax lethal factor. Science. 1998;280:734-7.

87. Vitale G, Pellizzari R, Recchi C, Napolitani G, Mock M, Montecucco C. Anthrax lethal factor cleaves the N-terminus of MAPKKs and induces tyrosine/threonine phosphorylation of MAPKs in cultured macrophages. Biochem Biophys Res Commun. 1998;248:706-11.

88. Vitale G, Bernardi L, Napolitani G, Mock M, Montecucco C. Susceptibility of mitogen-activated protein kinase kinase family members to proteolysis by anthrax lethal factor. Biochem J. 2000;352 Pt 3:739-45.

89. Klimpel KR, Arora N, Leppla SH. Anthrax toxin lethal factor contains a zinc metalloprotease consensus sequence which is required for lethal toxin activity. Mol Microbiol. 1994;13:1093-100.

90. Leppla SH. Anthrax toxin edema factor: a bacterial adenylate cyclase that increases cyclic AMP concentrations of eukaryotic cells. Proc Natl Acad Sci U S A. 1982;79:3162-6.

91. Yeager LA, Chopra AK, Peterson JW. Bacillus anthracis edema toxin suppresses human macrophage phagocytosis and cytoskeletal remodeling via the protein kinase A and exchange protein activated by cyclic AMP pathways. Infect Immun. 2009;77:2530-43.

92. Liu S, Schubert RL, Bugge TH, Leppla SH. Anthrax toxin: structures, functions and tumour targeting. Expert Opin Biol Ther. 2003;3:843-53.

93. Gupta PK, Moayeri M, Crown D, Fattah RJ, Leppla SH. Role of N-terminal amino acids in the potency of anthrax lethal factor. PloS one. 2008;3:e3130.

94. Arora N, Leppla SH. Residues 1-254 of anthrax toxin lethal factor are sufficient to cause cellular uptake of fused polypeptides. J Biol Chem. 1993;268:3334-41.

95. Collier RJ, Gilliland DG, Lory S. Structure-activity relationships in diphtheria toxin and exotoxin A from Pseudomonas aeruginosa. Prog Clin Biol Res. 1979;31:751-9.

96. Yamaizumi M, Mekada E, Uchida T, Okada Y. One molecule of diphtheria toxin fragment A introduced into a cell can kill the cell. Cell. 1978;15:245-50.

97. Gupta PK, Liu S, Leppla SH. Characterization of a Chinese hamster ovary cell mutant having a mutation in elongation factor-2. PloS one. 2010;5:e9078.

98. Liu S, Netzel-Arnett S, Birkedal-Hansen H, Leppla SH. Tumor cell-selective cytotoxicity of matrix metalloproteinase-activated anthrax toxin. Cancer Res. 2000;60:6061-7.

99. Nelson AR, Fingleton B, Rothenberg ML, Matrisian LM. Matrix Metalloproteinases: Biologic Activity and Clinical Implications. JCO. 2000;18:1135.

100. Stetler-Stevenson WG, Aznavoorian S, Liotta LA. Tumor cell interactions with the extracellular matrix during invasion and metastasis. Annu Rev Cell Biol. 1993;9:541-73.

101. Netzel-Arnett S, Fields GB, Birkedal-Hansen H, Van Wart HE. Sequence specificities of human fibroblast and neutrophil collagenases. J Biol Chem. 1991;266:6747-55.

102. Netzel-Arnett S, Sang QX, Moore WG, Navre M, Birkedal-Hansen H, Van Wart HE. Comparative sequence specificities of human 72- and 92-kDa gelatinases (type IV collagenases) and PUMP (matrilysin). Biochemistry. 1993;32:6427-32.

103. Will H, Atkinson SJ, Butler GS, Smith B, Murphy G. The soluble catalytic domain of membrane type 1 matrix metalloproteinase cleaves the propeptide of progelatinase A and initiates autoproteolytic activation. Regulation by TIMP-2 and TIMP-3. J Biol Chem. 1996;271:17119-23.

104. Alfano RW, Leppla SH, Liu S, Bugge TH, Herlyn M, Smalley KS, et al. Cytotoxicity of the matrix metalloproteinase-activated anthrax lethal toxin is dependent on gelatinase expression and B-RAF status in human melanoma cells. Mol Cancer Ther. 2008;7:1218-26.

105. Liu S, Wang H, Currie BM, Molinolo A, Leung HJ, Moayeri M, et al. Matrix metalloproteinase-activated anthrax lethal toxin demonstrates high potency in targeting tumor vasculature. J Biol Chem. 2008;283:529-40.

106. Guedez L, Rivera AM, Salloum R, Miller ML, Diegmueller JJ, Bungay PM, et al. Quantitative assessment of angiogenic responses by the directed in vivo angiogenesis assay. Am J Pathol. 2003;162:1431-9.

107. Alfano RW, Leppla SH, Liu S, Bugge TH, Ortiz JM, Lairmore TC, et al. Inhibition of tumor angiogenesis by the matrix metalloproteinase-activated anthrax lethal toxin in an orthotopic model of anaplastic thyroid carcinoma. Mol Cancer Ther. 2010;9:190-201.

108. Liu S, Bugge TH, Leppla SH. Targeting of tumor cells by cell surface urokinase plasminogen activator-dependent anthrax toxin. J Biol Chem. 2001;276:17976-84.

109. Sidenius N, Blasi F. The urokinase plasminogen activator system in cancer: recent advances and implication for prognosis and therapy. Cancer Metast Rev. 2003;22:205-22.

110. Andreasen PA, Kjoller L, Christensen L, Duffy MJ. The urokinase-type plasminogen activator system in cancer metastasis: a review. Int J Cancer. 1997;72:1-22.

111. Dass K, Ahmad A, Azmi AS, Sarkar SH, Sarkar FH. Evolving role of uPA/uPAR system in human cancers. Cancer Treat Rev. 2008;34:122-36.

112. Ke SH, Coombs GS, Tachias K, Navre M, Corey DR, Madison EL. Distinguishing the specificities of closely related proteases. Role of P3 in substrate and inhibitor discrimination between tissue-type plasminogen activator and urokinase. J Biol Chem. 1997;272:16603-9.

113. Ke SH, Coombs GS, Tachias K, Corey DR, Madison EL. Optimal subsite occupancy and design of a selective inhibitor of urokinase. J Biol Chem. 1997;272:20456-62.

114. Abi-Habib RJ, Singh R, Liu S, Bugge TH, Leppla SH, Frankel AE. A urokinase-activated recombinant anthrax toxin is selectively cytotoxic to many human tumor cell types. Mol Cancer Ther. 2006;5:2556-62.

115. Liu S, Aaronson H, Mitola DJ, Leppla SH, Bugge TH. Potent antitumor activity of a urokinase-activated engineered anthrax toxin. Proc Natl Acad Sci U S A. 2003;100:657-62.

116. Liu S, Bugge TH, Frankel AE, Leppla SH. Dissecting the urokinase activation pathway using urokinase-activated anthrax toxin. Methods Mol Biol. 2009;539:175-90.

117. Su Y, Ortiz J, Liu S, Bugge TH, Singh R, Leppla SH, et al. Systematic urokinase-activated anthrax toxin therapy produces regressions of subcutaneous human non-small cell lung tumor in athymic nude mice. Cancer Res. 2007;67:3329-36.

118. Rono B, Romer J, Liu S, Bugge TH, Leppla SH, Kristjansen PE. Antitumor efficacy of a urokinase activation-dependent anthrax toxin. Mol Cancer Ther. 2006;5:89-96.

119. Mogridge J, Cunningham K, Lacy DB, Mourez M, Collier RJ. The lethal and edema factors of anthrax toxin bind only to oligomeric forms of the protective antigen. Proc Natl Acad Sci U S A. 2002;99:7045-8.

120. Cunningham K, Lacy DB, Mogridge J, Collier RJ. Mapping the lethal factor and edema factor binding sites on oligomeric anthrax protective antigen. Proc Natl Acad Sci U S A. 2002;99:7049-53.

121. Liu S, Redeye V, Kuremsky JG, Kuhnen M, Molinolo A, Bugge TH, et al. Intermolecular complementation achieves high-specificity tumor targeting by anthrax toxin. Nat Biotechnol. 2005;23:725-30.

122. Schafer JM, Peters DE, Morley T, Liu S, Molinolo AA, Leppla SH, et al. Efficient targeting of head and neck squamous cell carcinoma by systemic administration of a dual uPA and MMP-activated engineered anthrax toxin. PloS one. 2011;6:e20532.

123. Wein AN, Liu S, Zhang Y, McKenzie AT, Leppla SH. Tumor therapy with a urokinase plasminogen activator-activated anthrax lethal toxin alone and in combination with paclitaxel. Invest New Drugs. 2013;31:206-12.

124. Alfano RW, Leppla SH, Liu S, Bugge TH, Duesbery NS, Frankel AE. Potent inhibition of tumor angiogenesis by the matrix metalloproteinase-activated anthrax lethal toxin: implications for broad anti-tumor efficacy. Cell Cycle. 2008;7:745-9.

125. Bugge TH. Proteolysis in carcinogenesis. In: Ensley JF, Gutkind, J.S., Jacob, J.R., Lippman, S.M., editor. Head and Neck Cancer. San Diego: Academic Press; 2003. p. 137-49.

126. Roy R, Yang J, Moses MA. Matrix metalloproteinases as novel biomarkers and potential therapeutic targets in human cancer. J Clin Oncol. 2009;27:5287-97.

127. Duffy MJ, Mullooly M, O'Donovan N, Sukor S, Crown J, Pierce A, et al. The ADAMs family of proteases: new biomarkers and therapeutic targets for cancer? Clin Proteomics. 2011;8:9.

128. Kontos CK, Scorilas A. Kallikrein-related peptidases (KLKs): a gene family of novel cancer biomarkers. Clin Chem Lab Med. 2012;50:1877-91.

129. Park S, Leppla SH. Optimized production and purification of Bacillus anthracis lethal factor. Protein Expr Purif. 2000;18:293-302.

130. Tomayko MM, Reynolds CP. Determination of subcutaneous tumor size in athymic (nude) mice. Cancer Chemother Pharmacol. 1989;24:148-54.

131. Knight K, Wade S, Balducci L. Prevalence and outcomes of anemia in cancer: a systematic review of the literature. Am J Med. 2004;116 Suppl 7A:11S-26S.

132. Ludwig H, Van Belle S, Barrett-Lee P, Birgegard G, Bokemeyer C, Gascon P, et al. The European Cancer Anaemia Survey (ECAS): a large, multinational, prospective survey defining the prevalence, incidence, and treatment of anaemia in cancer patients. Eur J Cancer. 2004;40:2293-306.

133. Spivak JL. Cancer-related anemia: its causes and characteristics. Semin Oncol. 1994;21:3-8.

134. Spivak JL. The anaemia of cancer: death by a thousand cuts. Nat Rev Cancer. 2005;5:543-55.

135. Dicato M, Plawny L, Diederich M. Anemia in cancer. Ann Oncol. 2010;21 Suppl 7:vii167-72.

136. Rodgers GM, 3rd, Becker PS, Blinder M, Cella D, Chanan-Khan A, Cleeland C, et al. Cancer- and chemotherapy-induced anemia. J Natl Compr Canc Netw. 2012;10:628-53.

137. Miyayama H, Doellgast GJ, Memoli V, Gandbhir L, Fishman WH. Direct immunoperoxidase staining for Regan isoenzyme of alkaline phosphatase in human tumor tissues. Cancer. 1976;38:1237-46.

138. Benham FJ, Fogh J, Harris H. Alkaline phosphatase expression in human cell lines derived from various malignancies. Int J Cancer. 1981;27:637-44.

139. Fishman WH, Inglis NR, Green S, Anstiss CL, Gosh NK, Reif AE, et al. Immunology and biochemistry of Regan isoenzyme of alkaline phosphatase in human cancer. Nature. 1968;219:697-9.

140. Harris H. The human alkaline phosphatases: what we know and what we don't know. Clinica chimica acta. 1990;186:133-50.

141. Saif MW, Alexander D, Wicox CM. Serum Alkaline Phosphatase Level as a Prognostic Tool in Colorectal Cancer: A Study of 105 patients. J Appl Res. 2005;5:88-95.

142. Mayne PD, Thakrar S, Rosalki SB, Foo AY, Parbhoo S. Identification of bone and liver metastases from breast cancer by measurement of plasma alkaline phosphatase isoenzyme activity. J Clin Pathol. 1987;40:398-403.

143. Tartter PI, Slater G, Gelernt I, Aufses AH, Jr. Screening for liver metastases from colorectal cancer with carcinoembryonic antigen and alkaline phosphatase. Ann Surg. 1981;193:357-60.

144. Lum G. Significance of low serum alkaline phosphatase activity in a predominantly adult male population. Clin Chem. 1995;41:515-8.

145. Van D, Klaassen CH. Cyanocobalamin-Dependent Depression of the Serum Alkaline Phosphatase Level in Patients with Pernicious Anemia. N Engl J Med. 1964;271:541-4.

146. Shaver WA, Bhatt H, Combes B. Low serum alkaline phosphatase activity in Wilson's disease. Hepatology. 1986;6:859-63.

147. Vander Heiden MG, Cantley LC, Thompson CB. Understanding the Warburg effect: the metabolic requirements of cell proliferation. Science. 2009;324:1029-33.

148. DiPersio L, Kyriazis AP, Michael JG, Pesce AJ. Monitoring the therapy of human tumor xenografts in nude mice by the use of lactate dehydrogenase. J Natl Cancer Inst. 1979;62:375-9.

149. Yang RZ, Park S, Reagan WJ, Goldstein R, Zhong S, Lawton M, et al. Alanine aminotransferase isoenzymes: molecular cloning and quantitative analysis of tissue expression in rats and serum elevation in liver toxicity. Hepatology. 2009;49:598-607.

150. Johnsen M, Lund LR, Romer J, Almholt K, Dano K. Cancer invasion and tissue remodeling: common themes in proteolytic matrix degradation. Curr Opin Cell Biol. 1998;10:667-71.

151. Cui X, Moayeri M, Li Y, Li X, Haley M, Fitz Y, et al. Lethality during continuous anthrax lethal toxin infusion is associated with circulatory shock but not inflammatory cytokine or nitric oxide release in rats. Am J Physiol Regul Integr Comp Physiol. 2004;286:R699-709.

152. Golden HB, Watson LE, Lal H, Verma SK, Foster DM, Kuo SR, et al. Anthrax toxin: pathologic effects on the cardiovascular system. Front Biosci (Landmark Ed). 2009;14:2335-57.

153. Liu S, Zhang Y, Moayeri M, Liu J, Crown D, Fattah RJ, et al. Key tissue targets responsible for anthrax-toxin-induced lethality. Nature. 2013;501:63-8.

154. Moayeri M, Haines D, Young HA, Leppla SH. Bacillus anthracis lethal toxin induces TNF-alpha-independent hypoxia-mediated toxicity in mice. J Clin Invest. 2003;112:670-82.

155. Abi-Habib RJ, Singh R, Leppla SH, Greene JJ, Ding Y, Berghuis B, et al. Systemic anthrax lethal toxin therapy produces regressions of subcutaneous human melanoma tumors in athymic nude mice. Clin Cancer Res. 2006;12:7437-43.

156. Fang H, Sun C, Xu L, Owen RJ, Auth RD, Snoy PJ, et al. Neutrophil elastase mediates pathogenic effects of anthrax lethal toxin in the murine intestinal tract. J Immunol. 2010;185:5463-7.

157. Okugawa S, Moayeri M, Eckhaus MA, Crown D, Miller-Randolph S, Liu S, et al. MyD88-dependent signaling protects against anthrax lethal toxin-induced impairment of intestinal barrier function. Infect Immun. 2011;79:118-24.

158. Sun C, Fang H, Xie T, Auth RD, Patel N, Murray PR, et al. Anthrax lethal toxin disrupts intestinal barrier function and causes systemic infections with enteric bacteria. PloS one. 2012;7:e33583.

159. Parkin DM, Bray F, Ferlay J, Pisani P. Global cancer statistics, 2002. CA Cancer J Clin. 2005;55:74-108.

160. Jemal A, Siegel R, Ward E, Hao Y, Xu J, Murray T, et al. Cancer statistics, 2008. CA Cancer J Clin. 2008;58:71-96.

161. Mao L, Hong WK, Papadimitrakopoulou VA. Focus on head and neck cancer. Cancer Cell. 2004;5:311-6.

162. Molinolo AA, Amornphimoltham P, Squarize CH, Castilho RM, Patel V, Gutkind JS. Dysregulated molecular networks in head and neck carcinogenesis. Oral Oncol. 2009;45:324-34.

163. Leemans CR, Braakhuis BJ, Brakenhoff RH. The molecular biology of head and neck cancer. Nat Rev Cancer. 2010;In press.

164. Emami N, Diamandis EP. Utility of kallikrein-related peptidases (KLKs) as cancer biomarkers. Clin Chem. 2008;54:1600-7.

165. Rosenthal EL, Matrisian LM. Matrix metalloproteases in head and neck cancer. Head Neck. 2006;28:639-48.

166. Shi Z, Stack MS. Urinary-type plasminogen activator (uPA) and its receptor (uPAR) in squamous cell carcinoma of the oral cavity. Biochem J. 2007;407:153-9.

167. Szabo R, Rasmussen AL, Moyer AB, Kosa P, Schafer JM, Molinolo AA, et al. c-Met-induced epithelial carcinogenesis is initiated by the serine protease matriptase. Oncogene. 2011;30:2003-16.

168. Pettus JR, Johnson JJ, Shi Z, Davis JW, Koblinski J, Ghosh S, et al. Multiple kallikrein (KLK 5, 7, 8, and 10) expression in squamous cell carcinoma of the oral cavity. Histol Histopathol. 2009;24:197-207.

169. Franchi A, Santucci M, Masini E, Sardi I, Paglierani M, Gallo O. Expression of matrix metalloproteinase 1, matrix metalloproteinase 2, and matrix metalloproteinase 9 in carcinoma of the head and neck. Cancer. 2002;95:1902-10.

170. Schmidt M, Schler G, Gruensfelder P, Muller J, Hoppe F. Urokinase receptor up-regulation in head and neck squamous cell carcinoma. Head Neck. 2000;22:498-504.

171. Curino A, Patel V, Nielsen BS, Iskander AJ, Ensley JF, Yoo GH, et al. Detection of plasminogen activators in oral cancer by laser capture microdissection combined with zymography. Oral Oncol. 2004;40:1026-32.

172. Romer J, Pyke C, Lund LR, Ralfkiaer E, Dano K. Cancer cell expression of urokinase-type plasminogen activator receptor mRNA in squamous cell carcinomas of the skin. J Invest Dermatol. 2001;116:353-8.

173. Okada A, Bellocq JP, Rouyer N, Chenard MP, Rio MC, Chambon P, et al. Membrane-type matrix metalloproteinase (MT-MMP) gene is expressed in stromal cells of human colon, breast, and head and neck carcinomas. Proc Natl Acad Sci U S A. 1995;92:2730-4.

174. Miyajima Y, Nakano R, Morimatsu M. Analysis of expression of matrix metalloproteinases-2 and -9 in hypopharyngeal squamous cell carcinoma by in situ hybridization. Ann Otol Rhinol Laryngol. 1995;104:678-84.

175. Bjorlin G, Ljungner H, Wennerberg J, Astedt B. Plasminogen activators in human xenografted oro-pharyngeal squamous cell carcinomas. Acta Otolaryngol. 1987;104:568-72.

176. Itaya T, Suzuki K, Takagi I, Motai H, Baba S. Relationship between head and neck squamous cell carcinomas and fibrinolytic factors. Immunohistological study. Acta Otolaryngol Suppl. 1996;525:113-9.

177. Yasuda T, Sakata Y, Kitamura K, Morita M, Ishida T. Localization of plasminogen activators and their inhibitor in squamous cell carcinomas of the head and neck. Head Neck. 1997;19:611-6.

178. Schmidt M, Hoppe F. Increased levels of urokinase receptor in plasma of head and neck squamous cell carcinoma patients. Acta Otolaryngol. 1999;119:949-53.

179. Johansson N, Airola K, Grenman R, Kariniemi AL, Saarialho-Kere U, Kahari VM. Expression of collagenase-3 (matrix metalloproteinase-13) in squamous cell carcinomas of the head and neck. Am J Pathol. 1997;151:499-508.

180. Budihna M, Strojan P, Smid L, Skrk J, Vrhovec I, Zupevc A, et al. Prognostic value of cathepsins B, H, L, D and their endogenous inhibitors stefins A and B in head and neck carcinoma. Biol Chem Hoppe Seyler. 1996;377:385-90.

181. Muller D, Wolf C, Abecassis J, Millon R, Engelmann A, Bronner G, et al. Increased stromelysin 3 gene expression is associated with increased local invasiveness in head and neck squamous cell carcinomas. Cancer Res. 1993;53:165-9.

182. Kusukawa J, Sasaguri Y, Shima I, Kameyama T, Morimatsu M. Expression of matrix metalloproteinase-2 related to lymph node metastasis of oral squamous cell carcinoma. A clinicopathologic study. Am J Clin Pathol. 1993;99:18-23.

183. Birkedal-Hansen B, Pavelic ZP, Gluckman JL, Stambrook P, Li YQ, Stetler-Stevenson WG. MMP and TIMP gene expression in head and neck squamous cell carcinomas and adjacent tissues. Oral Dis. 2000;6:376-82.

184. Imanishi Y, Fujii M, Tokumaru Y, Tomita T, Kanke M, Kanzaki J, et al. Clinical significance of expression of membrane type 1 matrix metalloproteinase and matrix metalloproteinase-2 in human head and neck squamous cell carcinoma. Hum Pathol. 2000;31:895-904.

185. Strojan P, Budihna M, Smid L, Vrhovec I, Skrk J. Urokinase-type plasminogen activator, plasminogen activator inhibitor type 1 and cathepsin D: analysis of their prognostic significance in squamous cell carcinoma of the head and neck. Anticancer Res. 2000;20:3975-81.

186. Yoshizaki T, Maruyama Y, Sato H, Furukawa M. Expression of tissue inhibitor of matrix metalloproteinase-2 correlates with activation of matrix metalloproteinase-2 and predicts poor prognosis in tongue squamous cell carcinoma. Int J Cancer. 2001;95:44-50.

187. Kos J, Smid A, Krasovec M, Svetic B, Lenarcic B, Vrhovec I, et al. Lysosomal proteases cathepsins D, B, H, L and their inhibitors stefins A and B in head and neck cancer. Biol Chem Hoppe Seyler. 1995;376:401-5.

188. Kawada A, Hara K, Kominami E, Kobayashi T, Hiruma M, Ishibashi A. Cathepsin B and D expression in squamous cell carcinoma. Br J Dermatol. 1996;135:905-10.

189. Coussens LM, Fingleton B, Matrisian LM. Matrix metalloproteinase inhibitors and cancer: trials and tribulations. Science. 2002;295:2387-92.

190. Mohamed MM, Sloane BF. Cysteine cathepsins: multifunctional enzymes in cancer. Nat Rev Cancer. 2006;6:764-75.

191. Wong L, Suh DY, Frankel AE. Toxin conjugate therapy of cancer. Semin Oncol. 2005;32:591-5.

192. Williams SA, Merchant RF, Garrett-Mayer E, Isaacs JT, Buckley JT, Denmeade SR. A prostate-specific antigen-activated channel-forming toxin as therapy for prostatic disease. J Natl Cancer Inst. 2007;99:376-85.

193. Olson ES, Aguilera TA, Jiang T, Ellies LG, Nguyen QT, Wong EH, et al. In vivo characterization of activatable cell penetrating peptides for targeting protease activity in cancer. Integr Biol (Camb). 2009;1:382-93.

194. Liu S, Leung HJ, Leppla SH. Characterization of the interaction between anthrax toxin and its cellular receptors. Cell Microbiol. 2007;9:977-87.

195. Gioanni J, Fischel JL, Lambert JC, Demard F, Mazeau C, Zanghellini E, et al. Two new human tumor cell lines derived from squamous cell carcinomas of the tongue: establishment, characterization and response to cytotoxic treatment. Eur J Cancer Clin Oncol. 1988;24:1445-55.

196. Cardinali M, Pietraszkiewicz H, Ensley JF, Robbins KC. Tyrosine phosphorylation as a marker for aberrantly regulated growth-promoting pathways in cell lines derived from head and neck malignancies. Int J Cancer. 1995;61:98-103.

197. Moore AE, Sabachewsky L, Toolan HW. Culture characteristics of four permanent lines of human cancer cells. Cancer Res. 1955;15:598-602.

198. Liu S, Leppla SH. Cell surface tumor endothelium marker 8 cytoplasmic tail-independent anthrax toxin binding, proteolytic processing, oligomer formation, and internalization. J Biol Chem. 2003;278:5227-34.

199. Alfano RW, Leppla SH, Liu S, Bugge TH, Ortiz JM, Lairmore TC, et al. Inhibition of tumor angiogenesis by the matrix metalloproteinase-activated anthrax lethal toxin in an orthotopic model of anaplastic thyroid carcinoma. Mol Cancer Ther.9:190-201.

200. Alfano RW, Leppla SH, Liu S, Bugge TH, Meininger CJ, Lairmore TC, et al. Matrix metalloproteinase-activated anthrax lethal toxin inhibits endothelial invasion and neovasculature formation during in vitro morphogenesis. Mol Cancer Res. 2009;7:452-61.

201. Liotta LA, Kohn EC. The microenvironment of the tumour-host interface. Nature. 2001;411:375-9.

202. Bettendorf O, Piffko J, Bankfalvi A. Prognostic and predictive factors in oral squamous cell cancer: important tools for planning individual therapy? Oral Oncol. 2004;40:110-9.

203. Kerbel RS. Human tumor xenografts as predictive preclinical models for anticancer drug activity in humans: better than commonly perceived-but they can be improved. Cancer Biol Ther. 2003;2:S134-9.

204. Sausville EA, Burger AM. Contributions of Human Tumor Xenografts to Anticancer Drug Development. Cancer Res. 2006;66:3351-4.

205. Troiani T, Schettino C, Martinelli E, Morgillo F, Tortora G, Ciardiello F. The use of xenograft models for the selection of cancer treatments with the EGFR as an example. Crit Rev Oncol Hematol. 2008;65:200-11.

206. Wypij JM. A naturally occurring feline model of head and neck squamous cell carcinoma. Patholog Res Int. 2013;2013:502197.

207. Tannehill-Gregg SH, Levine AL, Rosol TJ. Feline head and neck squamous cell carcinoma: a natural model for the human disease and development of a mouse model. Vet Comp Oncol. 2006;4:84-97.

208. Stebbins KE, Morse CC, Goldschmidt MH. Feline Oral Neoplasia: A Ten-Year Survey. Vet Path. 1989;26:121-8.

209. Bregazzi VS, LaRue SM, Powers BE, Fettman MJ, Ogilvie GK, Withrow SJ. Response of feline oral squamous cell carcinoma to palliative radiation therapy. Vet Radiol Ultrasoun. 2001;42:77-9.

210. Marretta JJ, Garrett LD, Marretta SM. Feline oral squamous cell carcinoma: An overview. Vet Med. 2007;102:392-406.

211. Martin CK, Tannehill-Gregg SH, Wolfe TD, Rosol TJ. Bone-invasive oral squamous cell carcinoma in cats: pathology and expression of parathyroid hormone-related protein. Vet Pathol. 2011;48:302-12.

212. Zhang X, Junior CR, Liu M, Li F, D'Silva NJ, Kirkwood KL. Oral squamous carcinoma cells secrete RANKL directly supporting osteolytic bone loss. Oral Oncol. 2013;49:119-28.

213. Evans SM, LaCreta F, Helfand S, VanWinkle T, Curran WJ, Jr., Brown DQ, et al. Technique, pharmacokinetics, toxicity, and efficacy of intratumoral etanidazole and radiotherapy for treatment of spontaneous feline oral squamous cell carcinoma. Int J Radiat Oncol Biol Phys. 1991;20:703-8.

214. de Aguiar A, Jr., Kowalski LP, de Almeida OP. Clinicopathological and immunohistochemical evaluation of oral squamous cell carcinoma in patients with early local recurrence. Oral Oncol. 2007;43:593-601.

215. Pires FR, Ramos AB, Oliveira JB, Tavares AS, Luz PS, Santos TC. Oral squamous cell carcinoma: clinicopathological features from 346 cases from a single oral pathology service during an 8-year period. J Appl Oral Sci. 2013;21:460-7.

216. Gardner DG. Spontaneous squamous cell carcinomas of the oral region in domestic animals: a review and consideration of their relevance to human research. Oral Dis. 1996;2:148-54.

217. Vargas-Ferreira F, Nedel F, Etges A, Gomes APN, Furuse C, Tarquinio SBC. Etiologic factors associated with oral squamous cell carcinoma in non-smokers and non-alcoholic drinkers: a brief approach. Braz Dent J. 2012;23:586-90.

218. Zhu C, Ling Y, Dong C, Zhou X, Wang F. The relationship between oral squamous cell carcinoma and human papillomavirus: a meta-analysis of a Chinese population (1994-2011). PloS one. 2012;7:e36294.

219. Subapriya R, Thangavelu A, Mathavan B, Ramachandran CR, Nagini S. Assessment of risk factors for oral squamous cell carcinoma in Chidambaram, Southern India: a case-control study. Eur J Cancer Prev. 2007;16:251-6.

220. Bertone ER, Snyder LA, Moore AS. Environmental and lifestyle risk factors for oral squamous cell carcinoma in domestic cats. J Vet Intern Med. 2003;17:557-62.

221. Snyder LA, Bertone ER, Jakowski RM, Dooner MS, Jennings-Ritchie J, Moore AS. p53 expression and environmental tobacco smoke exposure in feline oral squamous cell carcinoma. Vet Pathol. 2004;41:209-14.

222. McNiel EA, Carmella SG, Heath LA, Bliss RL, Le KA, Hecht SS. Urinary biomarkers to assess exposure of cats to environmental tobacco smoke. Am J Vet Res. 2007;68:349-53.

223. FDA Guidance for Industry, Investigators, and Reviewers: Exploratory IND Studies. 2006.

224. Kummar S, Rubinstein L, Kinders R, Parchment RE, Gutierrez ME, Murgo AJ, et al. Phase 0 clinical trials: conceptions and misconceptions. Cancer J. 2008;14:133-7.

225. Murgo AJ, Kummar S, Rubinstein L, Gutierrez M, Collins J, Kinders R, et al. Designing phase 0 cancer clinical trials. Clin Cancer Res. 2008;14:3675-82.

226. Kummar S, Doroshow JH, Tomaszewski JE, Calvert AH, Lobbezoo M, Giaccone G, et al. Phase 0 clinical trials: recommendations from the Task Force on Methodology for the Development of Innovative Cancer Therapies. Eur J Cancer. 2009;45:741-6.

227. Lappin G, Noveck R, Burt T. Microdosing and drug development: past, present and future. Expert Opin Drug Metab Toxicol. 2013;9:817-34.

228. Sorensen AG, Patel S, Harmath C, Bridges S, Synnott J, Sievers A, et al. Comparison of Diameter and Perimeter Methods for Tumor Volume Calculation. J Clin Oncol. 2001;19:551-7.

229. Guillaume P, Provost D, Lacroix P. Gastrointestinal models: Intestinal transit, gastric emptying, and ulcerogenic activity in the rat. Current Protocols in Pharmacology. 2008:5.3.1-5.3.12.

230. Dingle JH, Green L, Snell GD. Biology of the Laboratory Mouse; 1966.

231. Vick JA, Lincoln RE, Klein F, Mahlandt BG, Walker JS, Fish DC. Neurological and physiological responses of the primate to anthrax toxin. J Infect Dis. 1968;118:85-96.

232. Salles, II, Voth DE, Ward SC, Averette KM, Tweten RK, Bradley KA, et al. Cytotoxic activity of Bacillus anthracis protective antigen observed in a macrophage cell line overexpressing ANTXR1. Cell Microbiol. 2006;8:1272-81.

233. Taft SC, Weiss AA. Toxicity of anthrax toxin is influenced by receptor expression. Clin Vaccine Immunol. 2008;15:1330-6.

234. Backer MV, Patel V, Jehning BT, Claffey KP, Karginov VA, Backer JM. Inhibition of anthrax protective antigen outside and inside the cell. Antimicrob Agents Chemother. 2007;51:245-51.

235. Tannehill-Gregg S, Kergosien E, Rosol TJ. Feline head and neck squamous cell carcinoma cell line: characterization, production of parathyroid hormone-related protein, and regulation by transforming growth factor-beta. In Vitro Cell Dev Biol Anim. 2001;37:676-83.

236. Li Y, Song Y, Zhao L, Gaidosh G, Laties AM, Wen R. Direct labeling and visualization of blood vessels with lipophilic carbocyanine dye DiI. Nat Protocols. 2008;3:1703-8.

237. FDA Guidance for Industry: Codevelopment of Two or More New Investigational Drugs for Use in Combination. 2010.

238. Mould DR, Frame B. Population pharmacokinetic-pharmacodynamic modeling of biological agents: when modeling meets reality. J Clin Pharmacol. 2010;50:91s-100s.

239. Wigelsworth DJ, Krantz BA, Christensen KA, Lacy DB, Juris SJ, Collier RJ. Binding stoichiometry and kinetics of the interaction of a human anthrax toxin receptor, CMG2, with protective antigen. J Biol Chem. 2004;279:23349-56.

240. Young JAT, Collier RJ. Anthrax Toxin: Receptor Binding, Internalization, Pore Formation, and Translocation. Annu Rev Biochem. 2007;76:243-65.

241. Singh Y, Klimpel KR, Goel S, Swain PK, Leppla SH. Oligomerization of anthrax toxin protective antigen and binding of lethal factor during endocytic uptake into mammalian cells. Infect Immun. 1999;67:1853-9.

242. Chvyrkova I, Zhang XC, Terzyan S. Lethal factor of anthrax toxin binds monomeric form of protective antigen. Biochem Biophys Res Commun. 2007;360:690-5.

243. Moayeri M, Wiggins JF, Leppla SH. Anthrax protective antigen cleavage and clearance from the blood of mice and rats. Infect Immun. 2007;75:5175-84.

244. Szpirer C. Cancer research in rat models. Methods Mol Biol. 2010;597:445-58.

245. Cespedes MV, Casanova I, Parreno M, Mangues R. Mouse models in oncogenesis and cancer therapy. Clinical & translational oncology : official publication of the Federation of Spanish Oncology Societies and of the National Cancer Institute of Mexico. 2006;8:318-29.

246. Dong Z, Imai A, Krishnamurthy S, Zhang Z, Zeitlin BD, Nor JE. Xenograft tumors vascularized with murine blood vessels may overestimate the effect of anti-tumor drugs: a pilot study. PloS one. 2013;8:e84236.

247. Mahmood I. Application of allometric principles for the prediction of pharmacokinetics in human and veterinary drug development. Adv Drug Delivery Rev. 2007;59:1177-92.

248. Sharma V, McNeill JH. To scale or not to scale: the principles of dose extrapolation. Br J Pharmacol. 2009;157:907-21.

249. Reeves C, Charles-Horvath P, Kitajewski J. Studies in mice reveal a role for anthrax toxin receptors in matrix metalloproteinase function and extracellular matrix homeostasis. Toxins (Basel). 2013;5:315-26.

250. Dadachova E, Rivera J, Revskaya E, Nakouzi A, Cahill SM, Blumenstein M, et al. In vitro evaluation, biodistribution and scintigraphic imaging in mice of radiolabeled anthrax toxins. Nucl Med Biol. 2008;35:755-61.

251. Pastan I, Hassan R, FitzGerald DJ, Kreitman RJ. Immunotoxin therapy of cancer. Nat Rev Cancer. 2006;6:559-65.

252. Hassan R, Bullock S, Premkumar A, Kreitman RJ, Kindler H, Willingham MC, et al. Phase I study of SS1P, a recombinant anti-mesothelin immunotoxin given as a bolus I.V. infusion to patients with mesothelin-expressing mesothelioma, ovarian, and pancreatic cancers. Clin Cancer Res. 2007;13:5144-9.

253. Nagata S, Pastan I. Removal of B cell epitopes as a practical approach for reducing the immunogenicity of foreign protein-based therapeutics. Adv Drug Deliv Rev. 2009;61:977-85.

254. Benhar I, Wang QC, FitzGerald D, Pastan I. Pseudomonas exotoxin A mutants. Replacement of surface-exposed residues in domain III with cysteine residues that can be modified with polyethylene glycol in a site-specific manner. J Biol Chem. 1994;269:13398-404.

255. Onda M, Nagata S, FitzGerald DJ, Beers R, Fisher RJ, Vincent JJ, et al. Characterization of the B Cell Epitopes Associated with a Truncated Form of Pseudomonas Exotoxin (PE38) Used to Make Immunotoxins for the Treatment of Cancer Patients. J Immunol. 2006;177:8822-34.

256. Onda M, Beers R, Xiang L, Nagata S, Wang QC, Pastan I. An immunotoxin with greatly reduced immunogenicity by identification and removal of B cell epitopes. Proc Natl Acad Sci U S A. 2008;105:11311-6.

257. Liu W, Onda M, Lee B, Kreitman RJ, Hassan R, Xiang L, et al. Recombinant immunotoxin engineered for low immunogenicity and antigenicity by identifying and silencing human B-cell epitopes. Proc Natl Acad Sci U S A. 2012;109:11782-7.

258. Mazor R, Vassall AN, Eberle JA, Beers R, Weldon JE, Venzon DJ, et al. Identification and elimination of an immunodominant T-cell epitope in recombinant immunotoxins based on Pseudomonas exotoxin A. Proc Natl Acad Sci U S A. 2012;109:E3597-603.

259. Hassan R, Miller AC, Sharon E, Thomas A, Reynolds JC, Ling A, et al. Major cancer regressions in mesothelioma after treatment with an anti-mesothelin immunotoxin and immune suppression. Sci Transl Med. 2013;5:208ra147.

260. Mossoba ME, Onda M, Taylor J, Massey PR, Treadwell S, Sharon E, et al. Pentostatin plus cyclophosphamide safely and effectively prevents immunotoxin immunogenicity in murine hosts. Clin Cancer Res. 2011;17:3697-705.

261. Nguyen ML, Crowe SR, Kurella S, Teryzan S, Cao B, Ballard JD, et al. Sequential B-cell epitopes of Bacillus anthracis lethal factor bind lethal toxin-neutralizing antibodies. Infect Immun. 2009;77:162-9.

262. Kaur M, Chug H, Singh H, Chandra S, Mishra M, Sharma M, et al. Identification and characterization of immunodominant B-cell epitope of the C-terminus of protective antigen of Bacillus anthracis. Mol Immunol. 2009;46:2107-15.

263. Abboud N, De Jesus M, Nakouzi A, Cordero RJ, Pujato M, Fiser A, et al. Identification of linear epitopes in Bacillus anthracis protective antigen bound by neutralizing antibodies. J Biol Chem. 2009;284:25077-86.

264. Crowe SR, Ash LL, Engler RJ, Ballard JD, Harley JB, Farris AD, et al. Select human anthrax protective antigen epitope-specific antibodies provide protection from lethal toxin challenge. J Infect Dis. 2010;202:251-60.